NOTICE

AVIS

The quality of this microform is heavily dependent upon the quality of the original thesis submitted for microfilming. Every effort has been made to ensure the highest quality of reproduction possible.

La qualité de cette microforme dépend grandement de la qualité de la thèse soumise au microfilmage. Nous avons tout fait pour assurer une qualité supérieure de reproduction.

If pages are missing, contact the university which granted the degree.

S'il manque des pages, veuillez communiquer avec l'université qui a conféré le grade.

Some pages may have indistinct print especially if the original pages were typed with a poor typewriter ribbon or if the university sent us an inferior photocopy.

La qualité d'impression de certaines pages peut laisser à désirer, surtout si les pages originales ont été dactylographiées à l'aide d'un ruban usé ou si l'université nous a fait parvenir une photocopie de qualité inférieure.

Canada

UNIVERSITY OF ALBERTA

$THE\ ^{76}Se(n,p)^{76}As\ REACTION\ AT\ E_n = 198$ MeV

BY

MUNASINGHE ARACHCHIGE PUNYASENA

A thesis
submitted to the Faculty of Graduate Studies and Research
in partial fulfillment of the requirements for the degree of

MASTER OF SCIENCE

IN

NUCLEAR PHYSICS

DEPARTMENT OF PHYSICS

EDMONTON, ALBERTA

FALL 1993

The author has granted an irrevocable non-exclusive licence allowing the National Library of Canada to reproduce, loan, distribute or sell copies of his/her thesis by any means and in any form or format, making this thesis available to interested persons.

L'auteur a accordé une licence irrévocable et non exclusive permettant à la Bibliothèque nationale du Canada de reproduire, prêter, distribuer ou vendre des copies de sa thèse de quelque manière et sous quelque forme que ce soit pour mettre des exemplaires de cette thèse à la disposition des personnes intéressées.

The author retains ownership of the copyright in his/her thesis. Neither the thesis nor substantial extracts from it may be printed or otherwise reproduced without his/her permission.

L'auteur conserve la propriété du droit d'auteur qui protège sa thèse. Ni la thèse ni des extraits substantiels de celle-ci ne doivent être imprimés ou autrement reproduits sans son autorisation.

Canada

UNIVERSITY OF ALBERTA

RELEASE FORM

NAME OF THE AUTHOR : Munasinghe Arachchige Punyasena

TITLE OF THE THESIS : *The $^{76}Se(n,p)^{76}As$ Reaction*
at $E_n = 198 MeV$

DEGREE : Master of Science

YEAR THIS DEGREE GRANTED : Fall 1993

Department of Physics,
University of Kelaniya,
Kelaniya,
Shri Lanka.

Date : 26th August, 1993
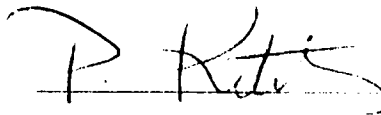
THE UNIVERSITY OF ALBERTA

FACULTY OF GRADUATE STUDIES AND RESEARCH

The undersigned certify that they have read, and recommend to the Faculty of Graduate Studies and Research for acceptance, a thesis entitled THE $^{76}Se(n,p)^{76}As$ REACTION AT E_n=198 MeV submitted by Munasinghe Arachchige Punyasena in partial fulfillment of the requirements for the degree of MASTER OF SCIENCE in nuclear physics.

Dr. W. C. Olsen (Supervisor)
Professor of Physics

Dr. P. Kitching
Professor of Physics

Dr. L. G. Greeniaus
Professor of Physics

Dr. E. Korkmaz
Research Scientist

Dr. R. Fedosejevs (External Examiner)
Professor of Electrical Engineering
University of Alberta

Date : August 26, 1993

This thesis is dedicated
to my teachers

ABSTRACT

The $^{76}Se(n,p)^{76}As$ reaction has been investigated at an incident neutron energy of 198 MeV using the TRIUMF charge exchange facility. Outgoing protons were observed using the medium resolution spectrometer up to excitation energies of 25 MeV in ^{76}As.

Cross sections for the reaction were measured at center of mass angles of 1.8^0, 3.6^0, 6.2^0, 9.9^0, and 14.8^0. A multipole decomposition was carried out by fitting the experimental data to theoretical cross section angular distributions calculated using th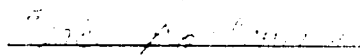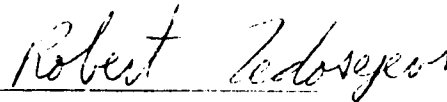e distorted wave impulse approximation. The Gamow-Teller strength, $B(GT^+)$, was extracted up to 10 MeV excitation, and was compared with theoretical predictions from a quasi-particle random phase approximation calculation. The predicted Gamow-Teller strengths at two values of the g^{pp} (particle particle coupling strength) are underestimated compared to those extracted from the experiment.

Hall probes of all the quadrupoles were recalibrated for the beamline 4B, and the results were compared with the old calibration done in 1985. Calibrations of the Hall probes in the cyclotron vault were found to have changed due to the high radiation levels. A software programme was developed to activate a Rawson-Lush gauss meter for monitoring the magnetic field inside the dipole of the second arm spectrometer.

ACKNOWLEDGEMENTS

Contents

List of Tables

List of Figures

Chapter 1

Introduction

The $^{76}Se(n,p)^{76}As$ reaction was investigated using the charge exchange facility at the TRIUMF laboratory. The experiment was carried out using 198 MeV incident neutrons, and double differential cross sections for excitation energies up to 25 MeV in ^{76}As were measured for five proton angles between 0^0 and 15^0 in the laboratory frame. These distributions are used to extract the Gamow-Teller strengths, $B(GT^+)$, for the β^+ decay of ^{76}Se to states in ^{76}As, which are then compared to calculated strengths. These measurements provide a test of model calculations of some of the matrix elements involved in the transition amplitudes for the double beta decay ($\beta\beta$-decay) of ^{76}Ge. It is important to test these calculations because the interpretation of lifetime measurements of $\beta\beta$-decay in terms of extensions to the Standard Model depend on their reliability. In addition to the specific application to the problem of $\beta\beta$-decay of ^{76}Ge, these results are of general interest in connection with the problem of establishing appropriate approximations for large scale shell model calculations in this mass region.

1.1 Charge Exchange Reactions

A number of years ago, it was shown that the charge exchange reactions, (p,n) and (n,p), could be related to the Gamow-Teller strengths, $B(GT^-)$ and $B(GT^+)$, in ordinary β^- and β^+ decay, respectively [1,2]. The pioneering studies of the (n,p) reaction for 152 MeV neutrons [3] were limited by low counting rates and poor energy resolution (6 MeV). Another (n,p) facility was developed by Brady et al. [4] utilizing a collimated

1

neutron beam for neutron energies up to 65 MeV. The TRIUMF charge exchange facility (CHARGEX) was developed to exploit both the (p,n) and the (n,p) reactions as a probe of nuclear structure in the intermediate energy range of 190 to 500 MeV [5-9]. At energies above 100 MeV, the forward-angle (p, n) cross section, extrapolated to zero momentum transfer, was shown to be proportional to the strength of the allowed Gamow-Teller beta transition between the same states [10-12]. Although some deviations from this strict proportionality have been reported in later studies [13], (p, n) cross section measurements still provide useful estimates of GT strength, especially for transitions energetically forbidden in beta decay. Studies in the other charge exchange reaction mode, (n, p), have revealed a similar proportionality between cross sections at zero momentum transfer and Gamow-Teller (GT) transition strengths for β^+ decay [14,9].

In the intermediate energy range, the Isobaric Analog Resonance (IAR), which dominates the (p, n) spectrum at low energy, is suppressed, while in (n, p) reactions, the IAR is not present because of isospin selection rules. Furthermore, because the third component of isospin is changed, these reactions involve purely isovector interactions; the isoscalar amplitudes which dominate (p, p') reactions are forbidden. It is therefore possible to study the Gamow-Teller states relatively free of background.

The study of these GT transitions may provide useful information relating to the $\beta\beta$ -decay process [15-17]. Before making this connection, a brief review of $\beta\beta$-decay is presented.

1.2   History of the Neutrino

Several decades ago, Pauli postulated the existence of a new particle, the neutrino or "little neutron" as it was called at that time [18]. With this new particle, it was possible to explain energy conservation in beta decay, $n \rightarrow p + e^- + \bar{\nu}_e$. However, direct observation of neutrinos did not occur until 25 years after Pauli's original proposal [19]. The neutrino has little or no mass, spin $\frac{1}{2}$ and no charge. With the development of particle physics, it is believed that neutrinos come in three flavors associated with three charged partners: the electron, the muon, and the tauon. As is the case in beta decay, neutrinos participate in a variety of charge-changing weak interactions together with their charged partners. We restrict ourselves to a discussion of nuclear double beta decay, since our experimental

2

program is related to this process.

1.3 A Brief Survey of $\beta\beta$-decay

1.3.1 Two-Neutrino Mode

Double beta decay was suggested by Wigner in the 1930's as a second-order weak interaction between isobars differing by two units in atomic number so that a nucleus with neutron and proton numbers (N, Z) undergoes a transition to the nucleus $(N - 2, Z + 2)$. It can occur whenever a given even-even nucleus has a larger mass than the next higher or lower even-even isobar. When the transition to the intermediate nucleus $(N - 1, Z + 1)$ is energetically forbidden, it is the only decay process possible.

By defining the electron neutrino and the anti-neutrino by the following two reactions,

$$n \rightarrow p + e^- + \bar{\nu}_e \tag{1.1}$$

and

$$\nu_e + n \rightarrow p + e^- , \tag{1.2}$$

the second-order weak interaction

$$2n \rightarrow n + p + e^- + \bar{\nu}_e \rightarrow 2p + 2e^- + 2\bar{\nu}_e \tag{1.3}$$

is allowed (see fig. 1.1a). This two-neutrino mode of $\beta\beta$-decay is generally denoted as

$$(A, Z) \rightarrow (A, Z + 2) + 2e^- + 2\bar{\nu}_e \tag{1.4}$$

where the nucleus (A,Z) transforms into the daughter nucleus (A,Z+2) by emitting two electrons and two electron-type anti-neutrinos. Two-neutrino $\beta\beta$-decay is one of the rarest processes in nature, with a half life of the order of 10^{20} yrs [20,21]. It has been observed in the laboratory for only two elements, ^{82}Se and ^{76}Ge, with measured lifetimes of $(1.1^{+0.8}_{-0.3}) \times 10^{20}$ yrs [22] and 6.3×10^{20} yrs [23], respectively. Another recent experimental study [24,25] also provides strong evidence for two-neutrino $\beta\beta$-decay of ^{76}Ge, with an observed lifetime that is in agreement with [23]. These are the rarest natural processes that have ever been observed directly in a laboratory.

3
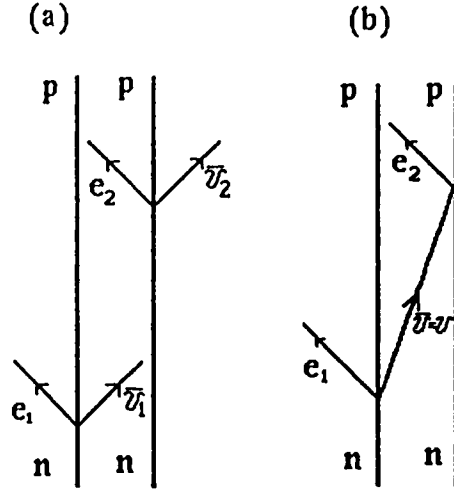
Figure 1.1: Two nucleon mechanisms for (a) two-neutrino and (b) neutrinoless $\beta\beta$-decay.

1.3.2 Zero-Neutrino Mode

If the neutrino is a Majorana particle (ie. identical to its antiparticle), a second $\beta\beta$-decay mode is possible with the emission of two electrons but no neutrinos in the final state. As first suggested by Furry [26], this process can occur when the antineutrino emitted at one vertex is absorbed as a neutrino at the other vertex (see fig. 1.1b). In this case, the reaction can be written as

$$2n \rightarrow n + p + e^- + \bar{\nu}_e = n + p + e^- + \nu_e \rightarrow 2p + 2e^- \tag{1.5}$$

and, is generally denoted by

$$(A, Z) \rightarrow (A, Z + 2) + 2e^-. \tag{1.6}$$

Although zero-neutrino $\beta\beta$-decay has never been seen, its observation would have profound implications for particle physics. For example, two electrons appearing in the final state constitute a violation of lepton number conservation in contradiction with the Standard Model. This type of symmetry breakdown is expected in some theories of grand unification. Also, observation of this decay process would imply that at least one neutrino must be a Majorana particle with non-vanishing mass [27,28]. Observation of a non-zero

mass of the order of a few electron volts has profound implications for cosmology and astrophysics. The total mass of the universe might be dominated by a neutrino mass of 1 eV, and that of 10 eV is enough to account for the apparent large excess of dark matter in the universe [29]. Massive neutrinos could also be important in galaxy formation [30].

1.3.3 Decay Rates for $\beta\beta$-decay

Fig. 1.1b shows a schematic diagram of the neutrinoless $\beta\beta$-decay mode according to the two-nucleon mechanism. At one vertex, an anti-neutrino is created by $n \rightarrow p + e^- + \bar{\nu}_e$, and a neutrino is absorbed at the other vertex, $\nu_e + n \rightarrow p + e^-$. This decay mode is forbidden in the Standard Model with massless neutrinos because the anti-neutrino emitted at the first vertex is right handed, and so has the wrong helicity to be absorbed at the second vertex. If the neutrino has a small Majorana mass, however, the decay is allowed, and the rate can be related to the mass term in the following way [31].

$$[T_{1/2}^{0\nu}]^{-1} = G^{0\nu} M_{0\nu}^2 \langle m_\nu \rangle \tag{1.7}$$

In this expression, $G^{0\nu}$ is a phase space factor, $M_{0\nu}$ is the nuclear matrix element for 0ν $\beta\beta$-decay, and m_ν is the presumed neutrino mass. Therefore measurements of the lifetime can be related to the mass, but it is clearly necessary to have reliable estimates of the nuclear matrix element.

In the case of 2ν decay, the rate can be expressed as

$$[T_{1/2}^{2\nu}]^{-1} = G^{2\nu} M_{2\nu}^2 \tag{1.8}$$

where again $G^{2\nu}$ is a phase space factor and $M_{2\nu}$ is given by

$$M_{2\nu} = \sum_m \frac{\langle 0_f^+ | \Theta_{GT} | 1_m^+ \rangle \langle 1_m^+ | \Theta_{GT} | 0_i^+ \rangle}{E_m - (M_i + M_f)/2} \tag{1.9}$$

In eq. (1.9), Θ_{GT} is the Gamow-Teller operator which converts a neutron into a proton and takes the initial $| 0_i^+ \rangle$ state (mass M_i) into a virtual intermediate state $| 1_m^+ \rangle$ (energy E_m), and from $| 1_m^+ \rangle$ into the final state $| 0_f^+ \rangle$ (mass M_f). It is therefore possible, in the case of 2ν decay, to check whether calculated values of the nuclear matrix elements agree with values derived from measured rates. Many early calculations gave values for the matrix elements that were often several orders of magnitude too large [32]. More recently, calculations

based on the quasi-particle random phase approximation (QRPA) [33,44] have shown that inclusion of particle-particle interactions can dramatically suppress these matrix elements and thereby bring calculated rates more into line with the measured values.

A critical test of these calculations can be provided by measuring directly the matrix elements and comparing the observed strength with that predicted. Good agreement would provide some confidence that the neutrino mass deduced from 0ν decay is reliable. In the case studied here, the $^{76}Se(n,p)^{76}As$ reaction can be related to the second leg of the 2ν $\beta\beta$-decay of ^{76}Ge, and hence provides a test of lifetime calculations for this decay.

Chapter 2

Data Analysis

The analysis of the data is discussed in this chapter, but a brief description of the way the data were collected is presented first.

2.1 (n,p) Measurements at TRIUMF

The experiment was carried out using the charge exchange (CHARGEX) facility [5,6] on beamline 4B at the TRIUMF cyclotron facility. The accelerator, a sector-focused isochronous cyclotron, can provide proton beams of variable energy between 180 and 520 MeV. The cyclotron actually accelerates H^- ions, and the proton beam is obtained by passing these ions through a thin stripping foil located at a radius that is appropriate for the desired energy of the proton beam. The same magnetic field that keeps the H^- ions circulating then bends the oppositely charged protons out of the accelerator. In this experiment, the primary proton beam energy was 200 MeV. Fig. 2.1 shows the general layout of the TRIUMF laboratory, a schematic view of the CHARGEX facility is given in fig. 2.2, and a more detailed view is presented in fig. 2.3.

The primary proton beam from the cyclotron is directed onto the neutron production target, T_{pn} (usually ^7Li), and is then bent by a dipole magnet into a shielded beam dump. The nearly monoenergetic neutron beam from T_{pn} impinges on the target being studied, T_{np}. Protons from the resulting (n,p) reactions are then analysed with the Medium Resolution Spectrometer (MRS). A thick (6 inch) absorber prevents protons scattered from T_{pn} from reaching the secondary target chamber.

7
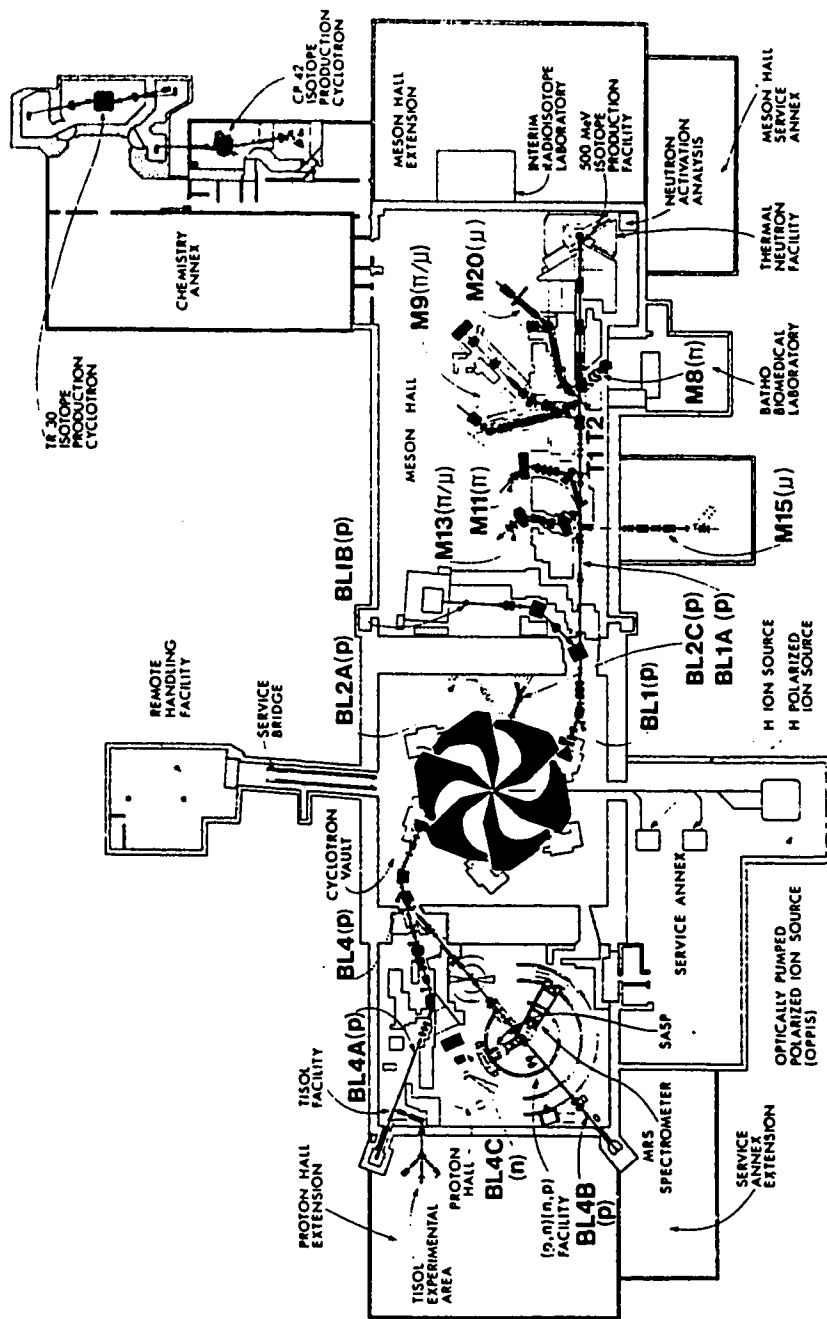
Figure 2.1: General layout of the TRIUMF nuclear laboratory.

The secondary target, T_{np}, consists of a stack of six target layers alternating with detecting wire planes as shown in fig. 2.3. The target layers are labelled as $T_a - T_f$, and the wire planes $Y_v, Y_v', Y_a - Y_f$. The wire planes $Y_a - Y_f$ make it possible to determine from which target the reaction proton originated. Target layer T_c is centered over the MRS pivot, and is 92 cm downstream from the primary target. The two wire planes Y_v, Y_v', in front of the target stack are used to veto incident charged particles. A scintillator (VS) in front of the target box is also used to veto these particles.

There is a provision for three separate stacks of targets which can be remotely rotated into the reaction plane. The last target in each stack is normally polyethelene (CH_2); the cross section for the reaction of interest can then be normalized to the known $^1H(n,p)$ cross section. The two front-end multi-wire chambers between T_{np} and the MRS, FEC0 and FECM (see fig. 2.2), are used to trace back accurately to the interaction point in the secondary target (T_{np}). More complete descriptions of the overall facility and the segmented target chamber can be found in references [5,6].

The MRS spectrometer used to detect the reaction protons consists of a quadrupole-dipole configuration which provides point-to-point focusing in the non-bend (Y) plane. The momentum bite of the MRS is $\pm 15\%$, and the solid angle subtended at the pivot is 2.5 msr. A schematic side view of the MRS including CHARGEX is illustrated in fig. 2.3. The detector system just above the focal plane of the MRS consists of two large multi-wire vertical drift chambers (VDC's) for traceback to the focal plane, and a scintillator array, SP(0-9), for trigger purposes and particle identification. There are also two large scintillators, S1 and S2, which can be used in the trigger to reduce backgrounds. A more complete description of the MRS facility can be found elsewhere [34].

2.2 Configuration for $^{76}Se(n,p)^{76}As$ Measurements

The ^{76}Se targets consisted of a powder sandwiched between thin mylar foils. The thickness of each target was chosen so that its contribution to the overall resolution was comparable with the other contributions. Four targets were mounted in positions b through e. The thickness of each target is listed in table 2.1.

The observed overall energy resolution depended mainly on the following factors,

MRS Dipole Magnet →

MRS Quadrupole Magnet →

FECO →

FECM →

Secondary Target Chamber →

Veto Scintillator →

(p,n) Neutrons →

Proton Beam Blocker →

To Beam Dump

(p,n) Target

Sweeping Magnet

Primary Proton Beam
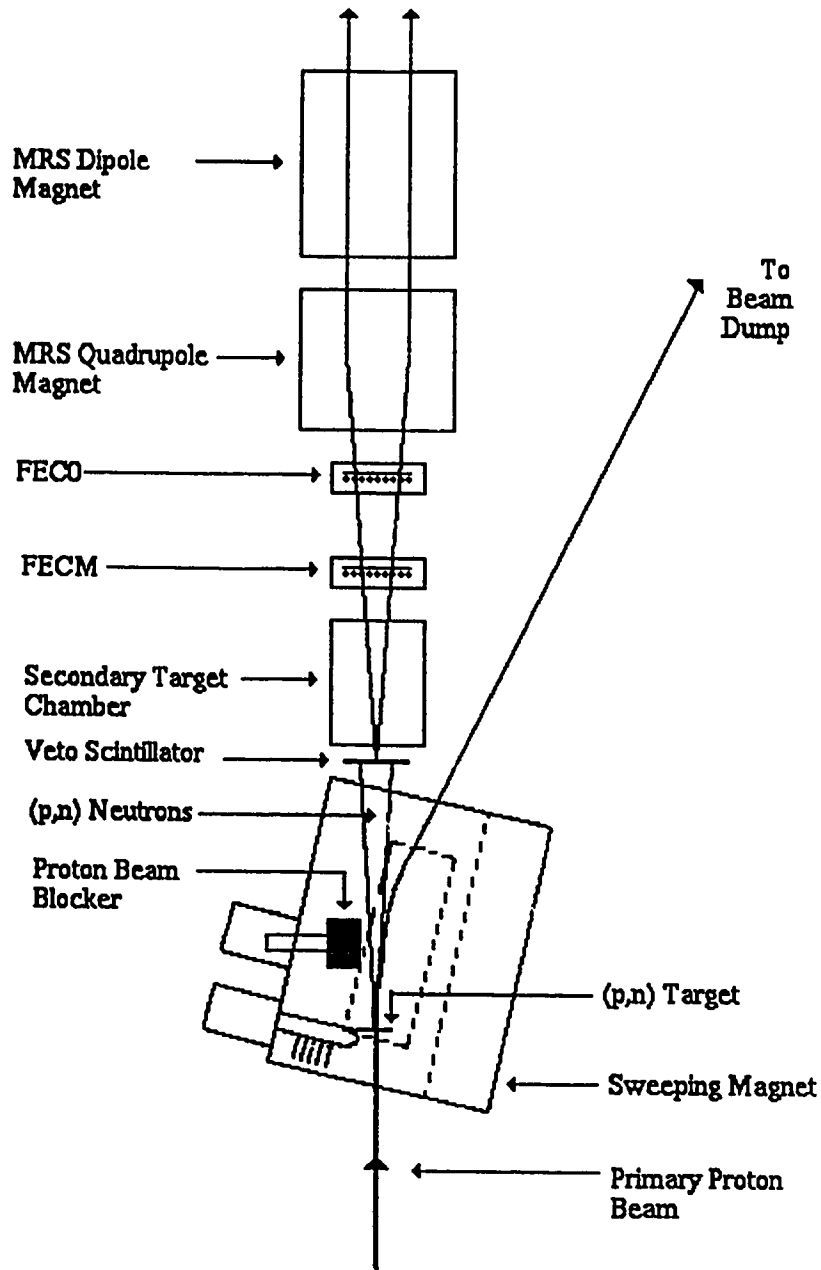
Figure 2.2: Plan view of the CHARGEX facility at TRIUMF in (n,p) mode.

10

S1 S2

SP (0-9)

VDC2 VDC1

MRS dipole ⟶

MRS quad ⟶

Xó, Yó
FEC0 ⟶   Xo, Yo

Xm, Ym
FECM ⟶   Xm, Ym

Yf ⟶   ⟵ Tf
Ye ⟶   ⟵ Te
Yd ⟶   ⟵ Td
Tnp ⟶   Yc ⟶   ⟵ Tc
Yb ⟶   ⟵ Tb
Ya ⟶   ⟵ Ta
Yv,Yv ⟶

⟵ VS

sweeping   n
magnet ⟶

Tpn ⟶   'Li

p
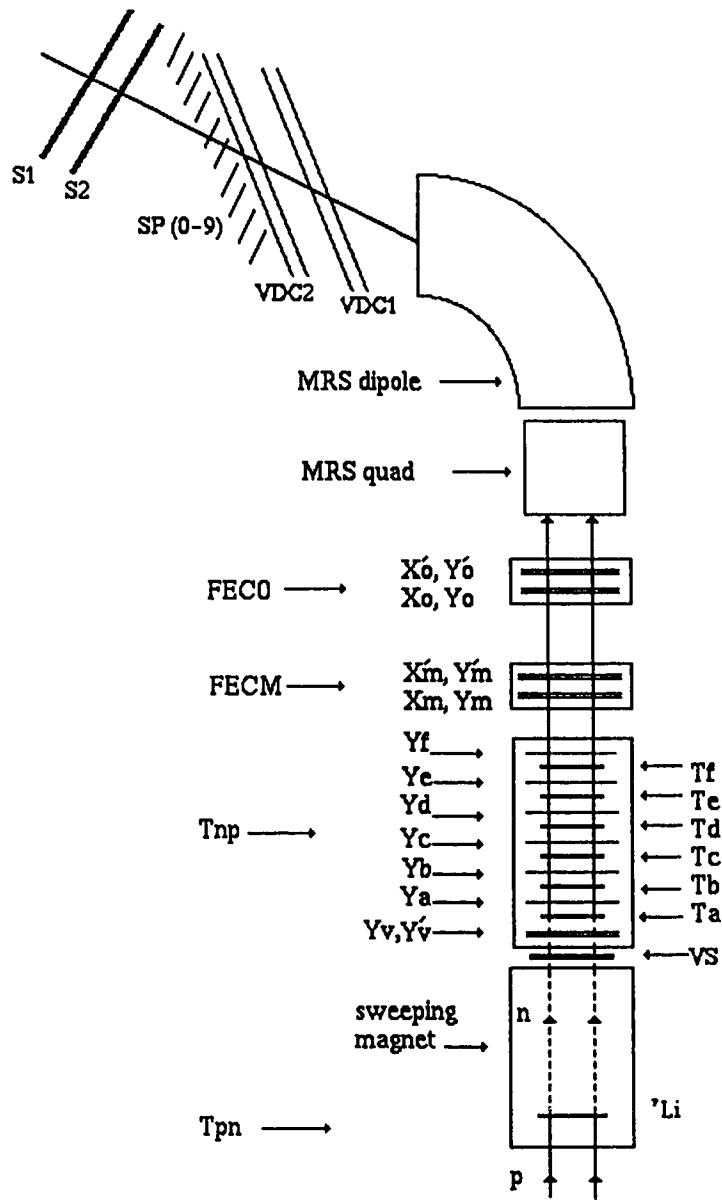
Figure 2.3: An schematic side view of the CHARGEX facility with MRS for (n,p) experiments.

1. the energy spread of the incident proton beam, $\sim$ 700 keV,

2. energy loss in the 240 mg/cm^2 ^7Li target, $\sim$ 869 keV,

3. the $^7Li(p,n)$ reaction populating both the g.s. and 430 keV states in ^7Be, and

4. energy loss and straggling in both the selenium targets and the polyethelene target in the target stack. The energy losses in these targets were calculated to be 831, 807, 792, 841, and 224 keV, respectively.

A second stack of targets consisted of a similar arrangement as above but with the ^{76}Se powder not present. In principle, this stack can be used for background subtraction. However, in practice the count rate was too low to accumulate spectra with good statistics in a reasonable time. This stack was then used just to check that there was no unexpected, large source of background.

Finally, the third target stack refered to as the $(CH_2)^6$ consisted of six CH_2 foils. These were used to determine the acceptance along the focal plane via the $^1H(n,p)$ reaction. This measurement is described in section 2.5.

A valid trigger consisted of no hit in the veto scintillator, hits in both planes of FEC0 and in VDC1, and signals present in S1, S2, and any of the focal plane scintillator paddles. Data were taken at five spectrometer angles: 0^0, 3^0, 6^0, 10^0, and 15^0. The data were recorded event by event and stored on magnetic tape for later off-line analysis. Various parameters to monitor the experiment were also scaled and written to tape at five second intervals.

2.3   Analysis of the $^{76}Se(n,p)$ Reaction Data

All the data analysis work was carried out using one of the TRIUMF data analysis programs, LISA, which performs LISt mode Analysis [35].

2.3.1   Particle Identification

Protons were identified by a combination of their time-of-flight (TTB) from the front-end wire chamber, FEC0, to whichever of the focal plane scintillators, SP0 to SP9,

Chamber position	Target position	Target material	Thickness (mg/cm^2)	Brief description
	a	empty	-	
	b	^{76}Se	286.60	^{76}Se powder between mylar foils
stack	c	^{76}Se	278.30	^{76}Se powder between mylar foils
number	d	^{76}Se	273.20	^{76}Se powder between mylar foils
(1)	e	^{76}Se	290.10	^{76}Se powder between mylar foils
	f	CH_2	46.70	solid material
	a	empty	-	two mylar foils only
	b	empty	-	two mylar foils only
stack	c	empty	-	two mylar foils only
number	d	empty	-	two mylar foils only
(2)	e	empty	·	two mylar foils only
	f	CH_2	092.39	solid material
	a	CH_2	142.98	solid material
	b	CH_2	143.27	solid material
stack	c	CH_2	142.73	solid material
number	d	CH_2	143.17	solid material
(3)	e	CH_2	143.07	solid material
	f	CH_2	143.06	solid material

Table 2.1: Description of target configurations in each stack placed in the secondary target chamber.

they passed through, and the energy deposited (ESUM) in that scintillator. Figs. 2.4a and 2.4b show three-dimensional spectra of ESUM vs TTB which clearly distinguish the identified proton peak by the density boxes and the surface variations. Cuts were applied to both parameters (ESUM and TTB) to ensure that all further analysis was carried out on protons only.
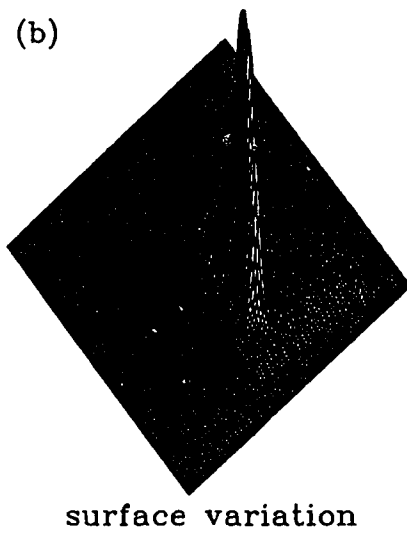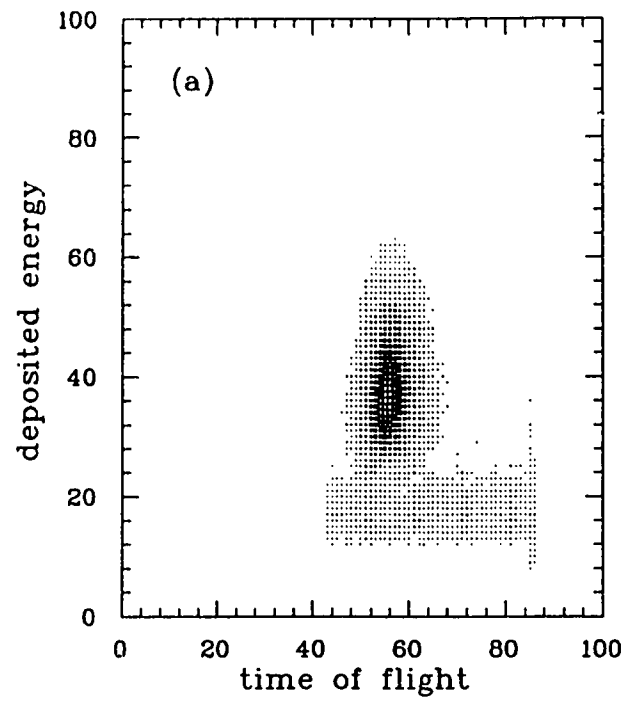
Figure 2.4: Particle identification is illustrated as (a) density boxes and (b) surface variations.

14

2.3.2 Multi-Wire Drift Chamber Decoding and Target Identification

Reaction protons first encounter the front-end chambers, FECM and FEC0. Multiple hits are rejected, and only those events with a hit in one wire or two adjacent wires in each of the wire planes are accepted. Multiple hits in the focal plane wire chambers, VDC1 and VDC2, are also rejected, and only those events with 3-7 adjacent wires hit in each plane are accepted.

The front-end chamber information is used to trace back to the event position in the target plane (the front-end coordinate system is illustrated in fig. 2.5). This is done by calculating the point of interaction, (X_I, Y_I) in the target plane with the two trajectory coordinates, (X_0, Y_0) and (X_M, Y_M), in FEC0 and FECM, respectively. The sum of events builds up an outline of the target; an example is shown in fig. 2.10.

It is convenient to determine the cosine of the scattering angle of each event as the dot product between the unit vectors of the incoming neutron and outgoing proton. For this calculation, the neutron is presumed to originate from a point source centered on the production target. This is a reasonable assumption because the proton beam on the primary target was about 3 mm in diameter, and this target was 92 cm upstream from the secondary targets.

The Z-coordinate for each target layer with respect to the neutron source can be calculated using the information from the target box wire planes and knowledge of the target separation in the stack, thus improving the scattering angle calculation. In order to improve the efficiency of detection of the target box wire planes, only the wires immediately on either side of the trajectory calculated from FEC0 and FECM are checked for hits; all other wires are ignored. The distribution of scattering angles calculated for each event at each spectrometer angle is shown in fig. 2.6. Since the MRS spectrometer has a range of angular acceptance of 4.2^0, it is clearly indicated in the figure that there is a substantial overlap of the data at each spectrometer angle.

2.3.3 Reconstruction of the Focal Plane Coordinate

The position (X_F) of a reaction proton in the spectrometer focal plane is determined using the trajectory information from VDC1 and VDC2. In order to improve the resolution, the raw focal plane position has to be corrected for aberrations due to particle

15
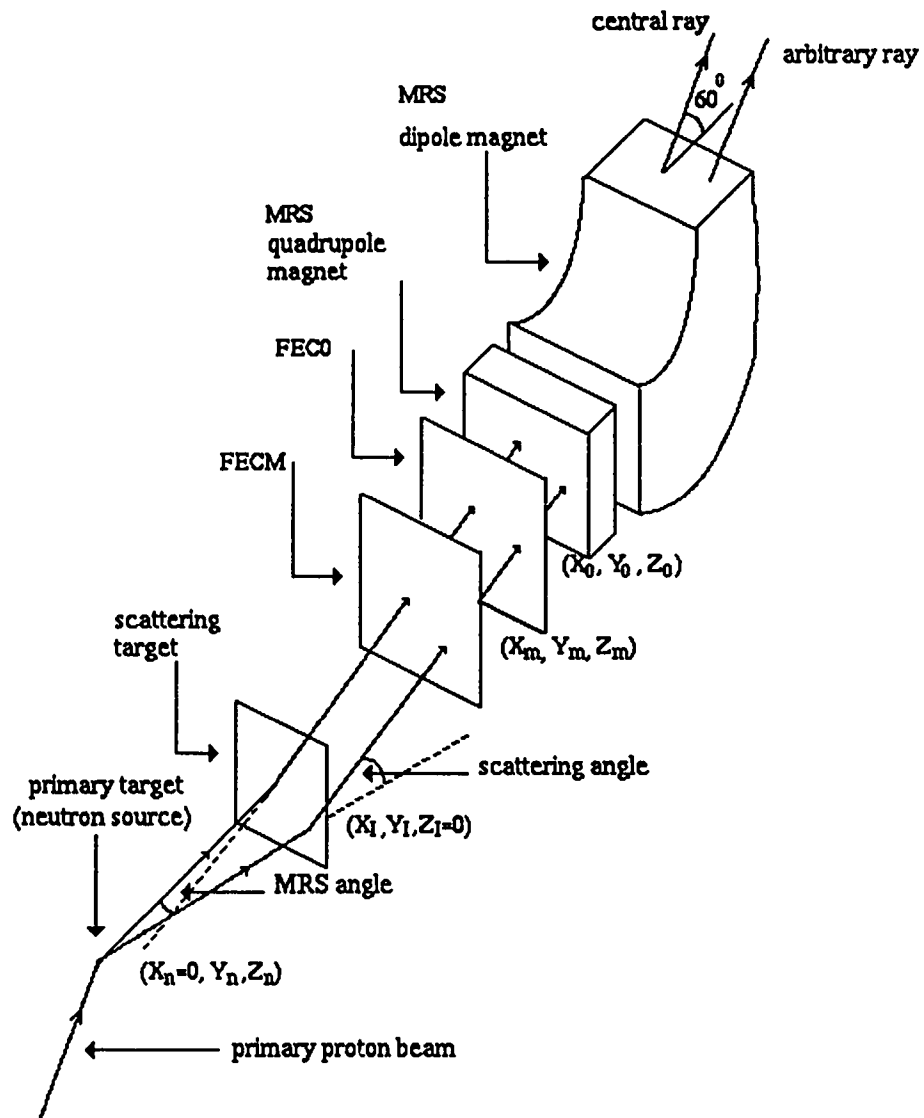
Figure 2.5: Coordinate system at the front-end of the MRS spectrometer for CHARGEX experiments.
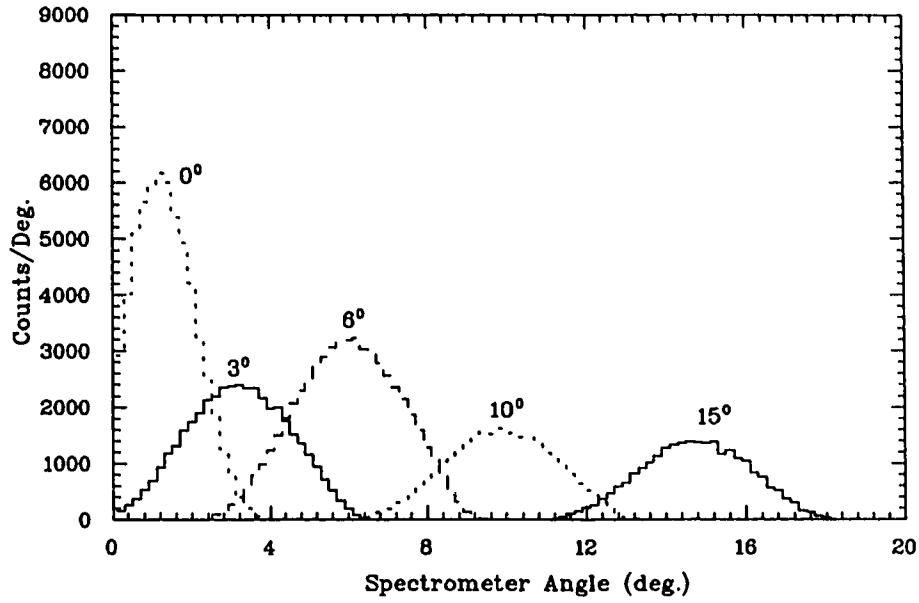
Figure 2.6: Histograms of the scattering angles for each spectrometer angle (θ_{MRS}) at 200 MeV proton beam energy. Data were taken with a $(CH_2)^6$ target stack.

trajectories which pass through non-homogeneous regions of the MRS magnetic field.

It was found empirically that these corrections to the focal plane position depend on the (n,p) reaction position (X_I, Y_I), and angle $(\Theta_{FEC}, \Phi_{FEC})$, where $(\Theta_{FEC}, \Phi_{FEC})$ are the trajectory angles of a particle through the front-end chambers. The only other dependence of the focal plane coordinate was found to be the momentum-corrected angle, Θ_{pc}, through the VDC's. The final, corrected focal plane coordinate was calculated as

$$X_{FK} = n_1 X_F + n_2 X_I + n_3 Y_I + n_4 Y_I^2 + n_5 \Theta_{pc} + n_6 \Theta_{pc}^2 + n_7 \Theta_{FEC} + n_8 \Phi_{FEC} + n_9 \Phi_{FEC}^2 \quad (2.1)$$

where X_F is the raw focal plane position and the n_i coefficients are empirically adjusted correction constants. The independence of X_{FK} on the various variables is indicated by the vertically concentrated bands in figs. 2.7 and 2.8.

Shown in fig. 2.7 are the two-dimensional density plots which demonstrate that the aberration corrected focal plane position (X_{FK}) is independent of all the quantities, X_I, Y_I (the positions in the bend and non-bend planes in the target) in (a) and (b); Θ_{FEC}, Φ_{FEC} (the polar angles at the front-end chambers) in (c) and (d). In order to demonstrate the

17

correction effects for these quantities for the focal plane position (X_{FK}), fig. 2.9 shows the uncorrected focal plane position as a function of X_I. The tilt of the vertical band indicates that X_F is not completely independent of X_I without those corrections.

Fig. 2.8a shows a three-dimensional spectrum of the corrected focal plane position (X_{FK}) for exit particle angles (Θ_{pc}) at the focal plane VDCs. The spectra were shifted for the calculated energy loss through the targets downstream from the struck target. This is indicated by the straight vertical band of counts in fig. 2.8c. Similarly, fig. 2.8b shows a kinematic correction included in the spectra to correct for the energy loss due to the angle variation. These spectra, constructed using data with the $(CH_2)^6$ target stack, include only the proton events that originated from within the target dimensions, see fig. 2.10 which shows the point of interaction (X_I, Y_I) in the target. Initially, cuts were placed to exclude all events outside the denser region, but further analysis required tighter cuts to ensure that events did not originate in the target frames. For example, the vertical band above $Y_I=50$ comes from events striking the frame.

The initial data sorting was thus completed to end up with $^{76}Se(n,p)$ spectra corrected for the effects discussed above. Background subtraction, spectrometer acceptance correction and energy calibration, and cross section calculations are discussed in the following sections.

2.4   Background Subtraction

The background is mainly due to the events from the mylar foils used in the secondary target chamber. It was found that a satisfactory estimation of the background could be made by using the last (CH_2) target in the selenium stack. The normalization was set by subtracting the $^1H(n,p)$ reaction peak in the zero degree data. The Q-value for the $^{76}Se(n,p)$ reaction is -2.185 MeV so that the minimum X_{FK} value for the selenium events is clearly separated right to the $^1H(p,n)$ background peak at $0°$, thus leaving no events of interest under the $^1H(n,p)$ peak.

The background subtractions for the other angles $(3°, 6°, 10°, 15°)$ were performed in the same way, but using the zero-degree normalization because, at the larger angles, background is mixed with selenium data. The analysed data and the corresponding background subtractions are shown in figs. 2.11, 2.12, and 2.13 which represent the number of
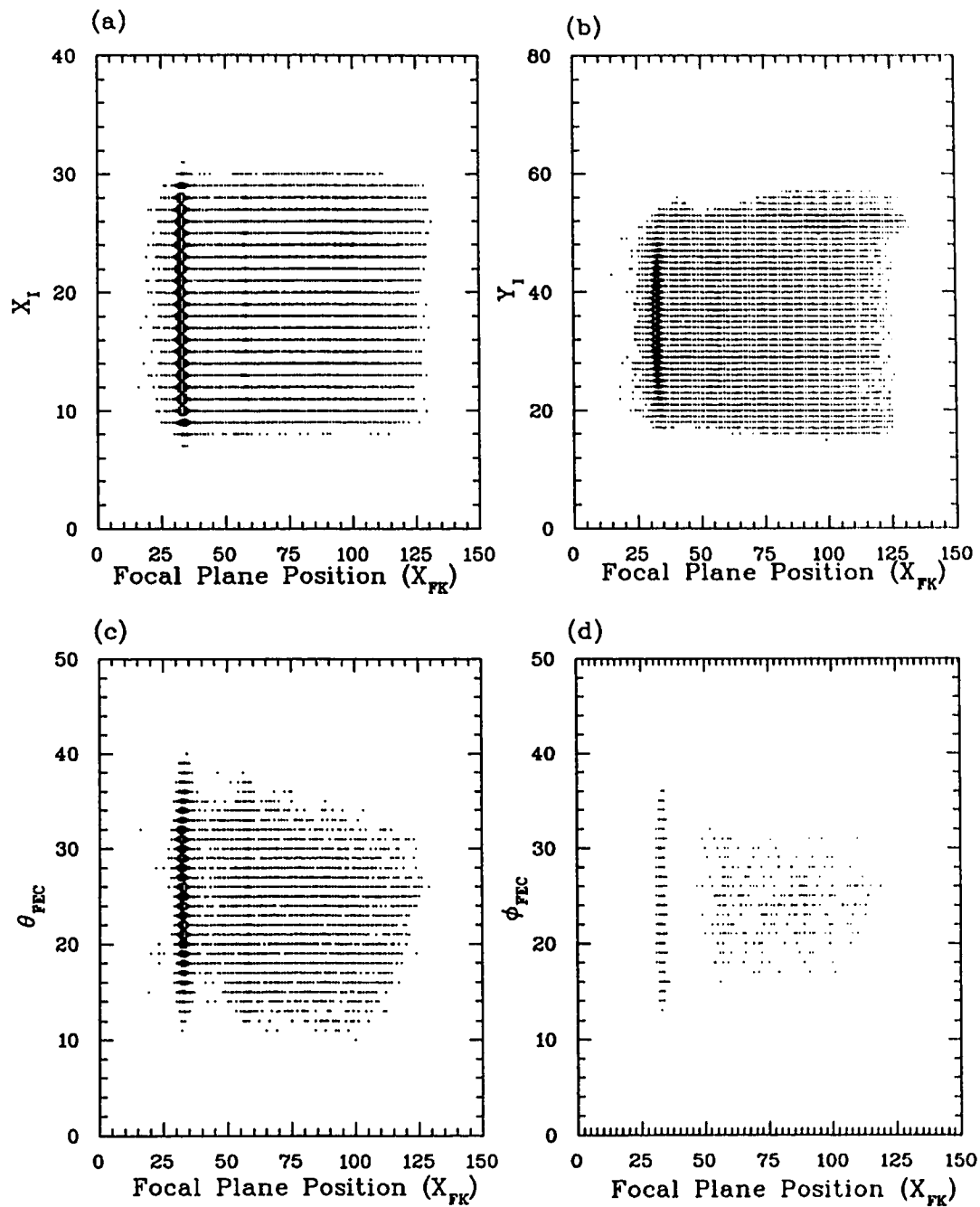
Figure 2.7: (a), (b), (c), and (d) Two-dimensional density plots show the corrected X_{FK} as a function of X_I, Y_I, Θ_{FEC}, and Φ_{FEC}, respectively. The data were taken with the $(CH_2)^6$ stack.
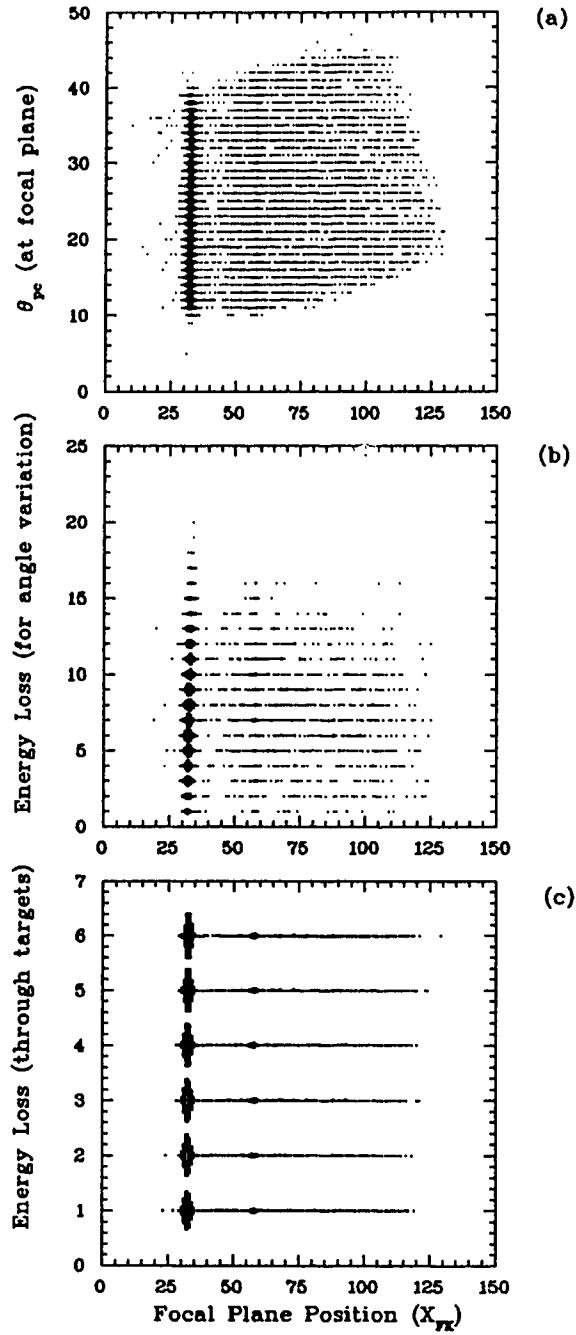
Figure 2.8: (a), (b), and (c) two-dimensional density plots show the corrected X_{FK} as a function of Θ_{pc}, Θ_{scatt}, and energy loss through the targets, respectively. Data were taken with the $(CH_2)^6$ stack.

20
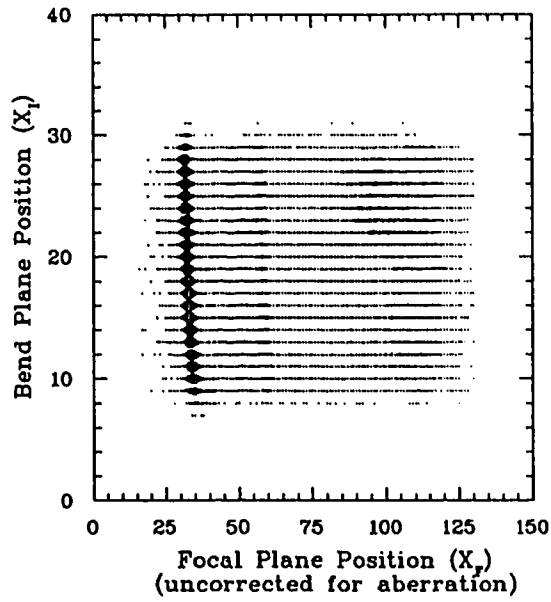
Figure 2.9: A two-dimensional box density plot to demonstrate the X_F dependence on X_I without corrections for the aberration.
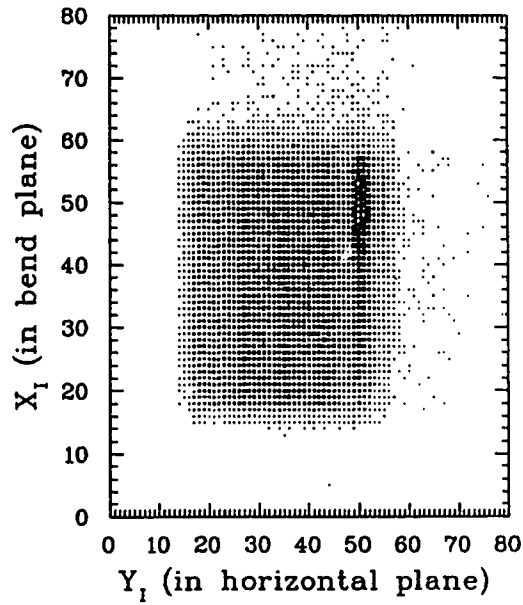
Figure 2.10: A two-dimensional box density plot to illustrate the distribution of proton event interaction points (Y_I, X_I) in the target.

counts per channel as a function of the corrected focal plane position.

2.5 The Spectrometer Acceptance

The spectra were also corrected for the variation of spectrometer acceptance across the focal plane. The acceptance scan data were taken using the third stack, $(CH_2)^6$, in the secondary target, by varying the magnetic field of the spectrometer. The acceptance corrections were determined by measuring the relative intensity of the proton peak from the $^1H(n,p)$ reaction as the peak was stepped across the focal plane. The data at the various magnetic field settings were normalized to the integrated charge collected at the beam-stop.

Fig. 2.14 shows this acceptance calibration obtained by fitting the H peak area for each magnetic field setting to a cubic function. The resulting calibration coefficients were used to correct the $^{76}Se(n,p)^{76}As$ spectra at each spectrometer angle. The precise way in which this was done is discussed in the section on cross section calculations.

2.6 Energy Response and Calibration

The acceptance scan data were also used to determine the energy calibration of the spectrometer system. The ratio of magnetic field strength (NMR) to proton momentum (p) was fitted to a quadratic function with the H peak position (PP) at the focal plane in order to obtain the energy calibration coefficients, AK, BK, and CK such that

$$PP = AK + BK(\frac{NMR}{p}) + CK(\frac{NMR}{p})^2.$$
(2.2)

Given that the secondary proton energy is 198 MeV which corresponds to a momentum p of 640.9 MeV/c, the calculated calibration coefficients reproduced the incident neutron beam energy to be 198.1 MeV at the secondary target, which is consistent with the expected value. This assures that the calculation of the energy calibration coefficients is accurate. The peak position (PP) as a function of the magnetic field strength, and the resultant field curve is given in fig. 2.15.
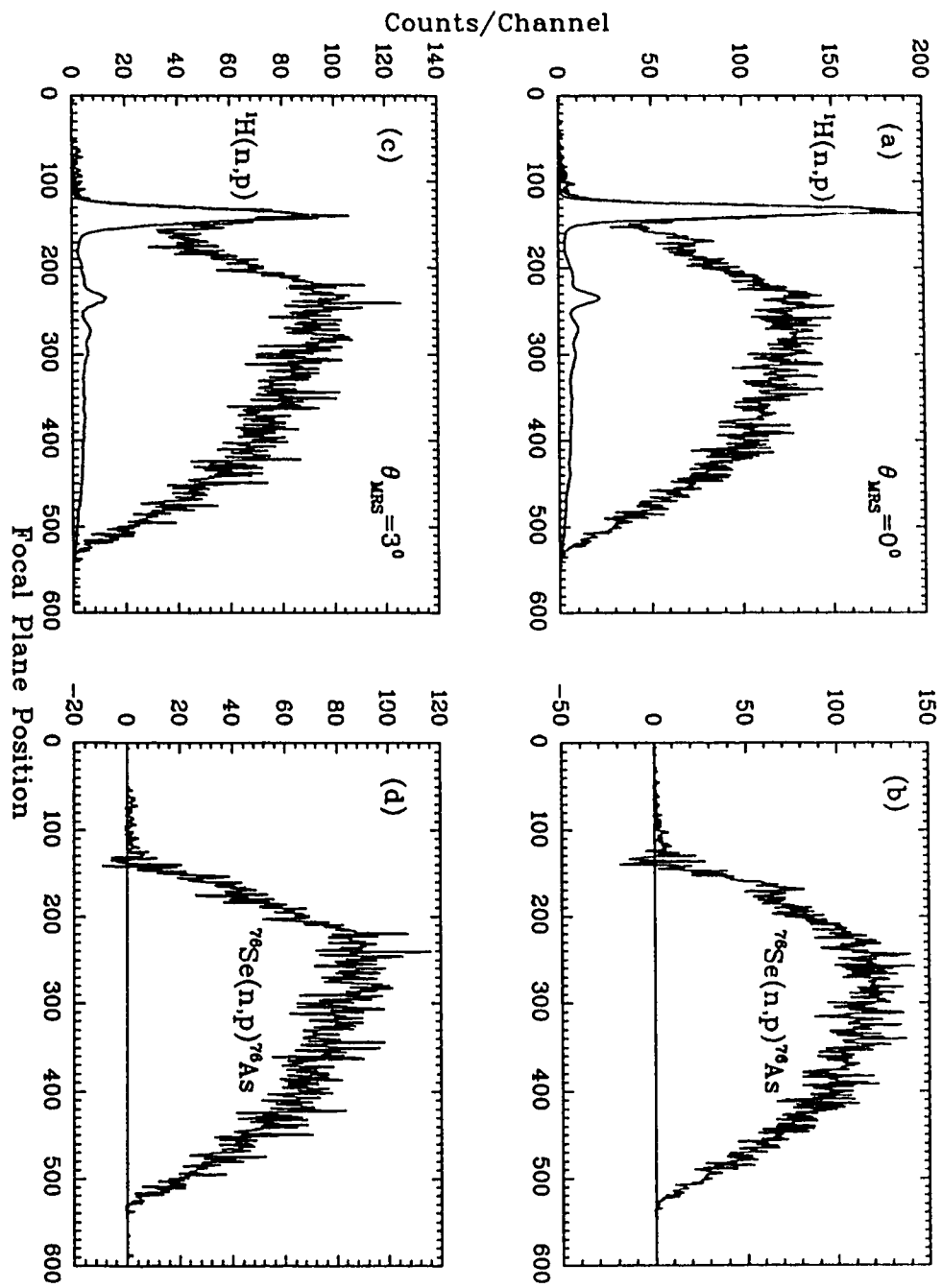
Figure 2.11: Summed raw spectra and the background subtraction for 0^0 and 3^0 MRS angles: (b) and (d) are the background-corrected spectra of (a) and (c), respectively.
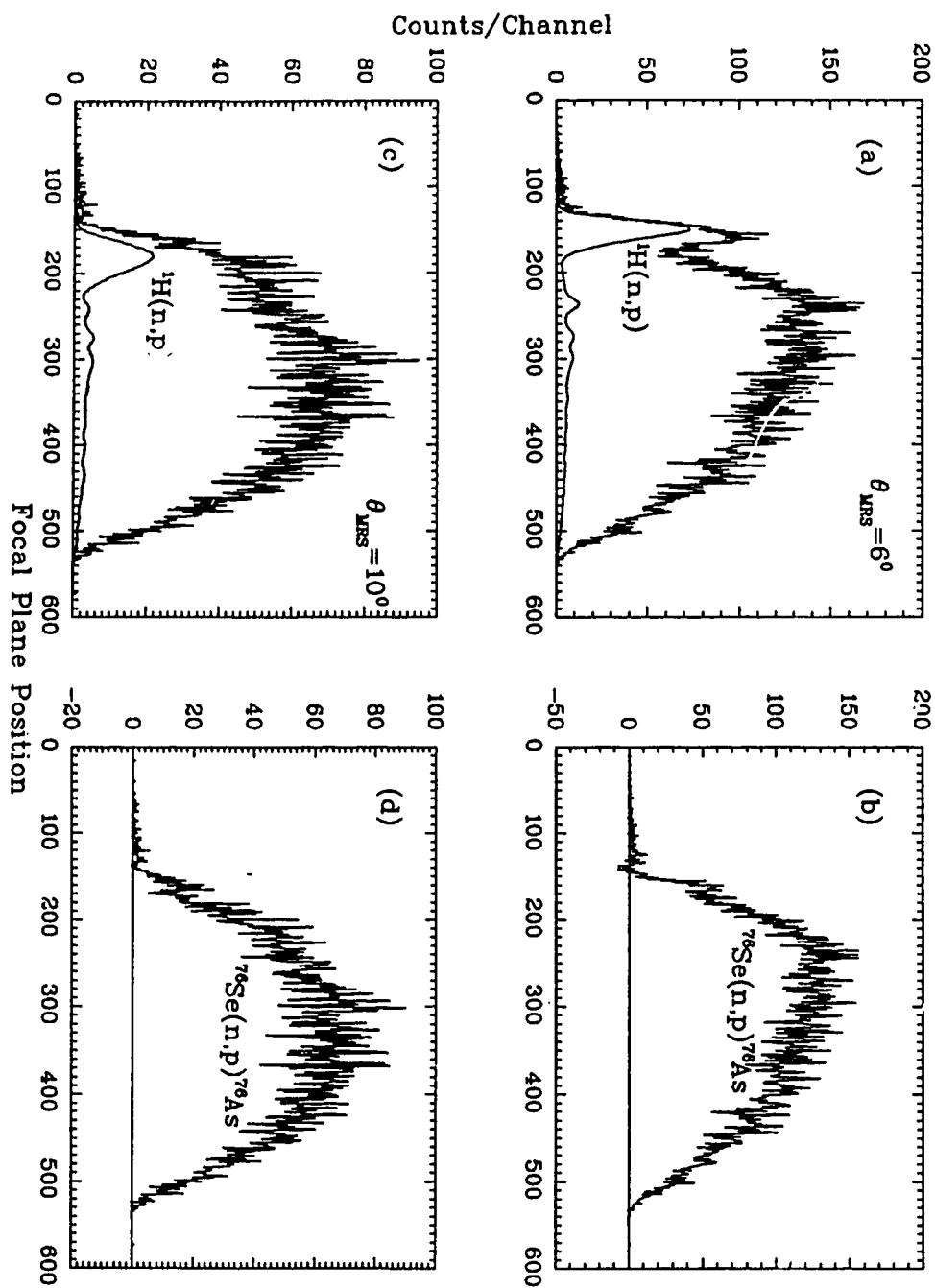
Figure 2.12: Summed raw spectra and the background subtraction for 6^0 and 10^0 MRS angles: (b) and (d) are the background-corrected spectra of (a) and (c), respectively.
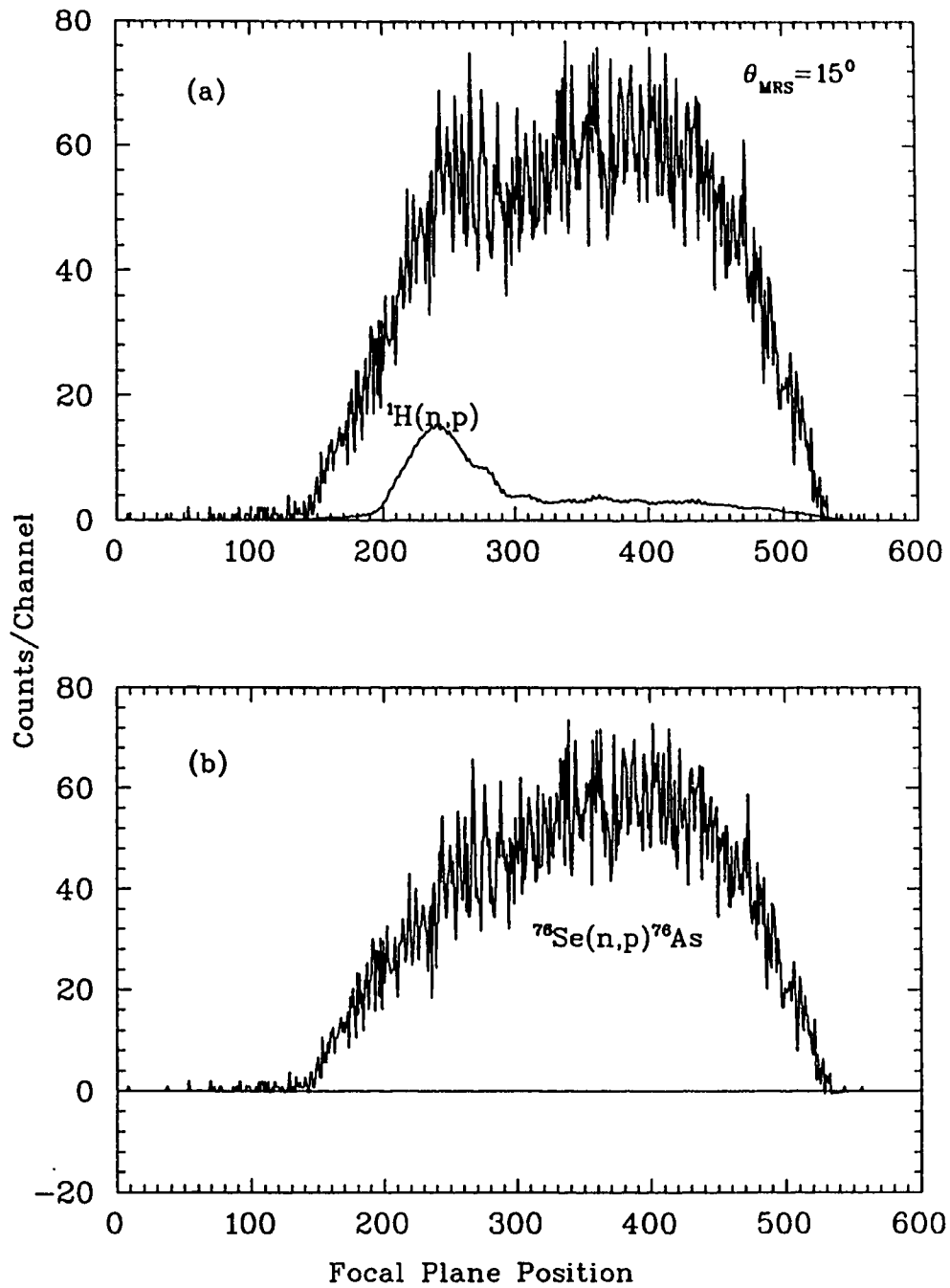
Figure 2.13: Summed raw spectrum and the background subtraction for 15^0 MRS angle: (b) is the background-corrected spectrum of (a).
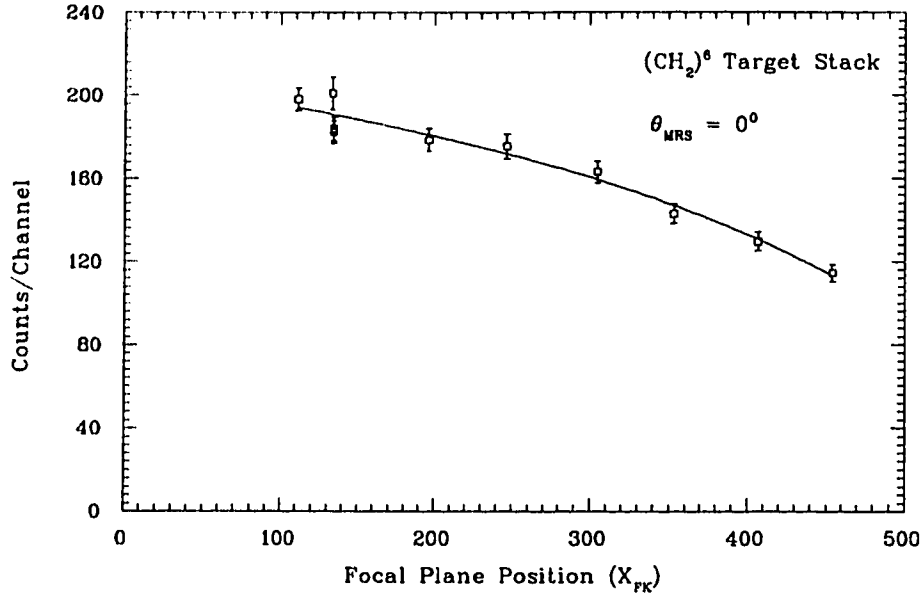
Figure 2.14: Acceptance calibration of the MRS spectrometer, obtained from the $^1H(n,p)$ reaction with the $(CH_2)^6$ secondary target stack. The measured yields for different NMR values are fitted to a cubic function of the peak position.
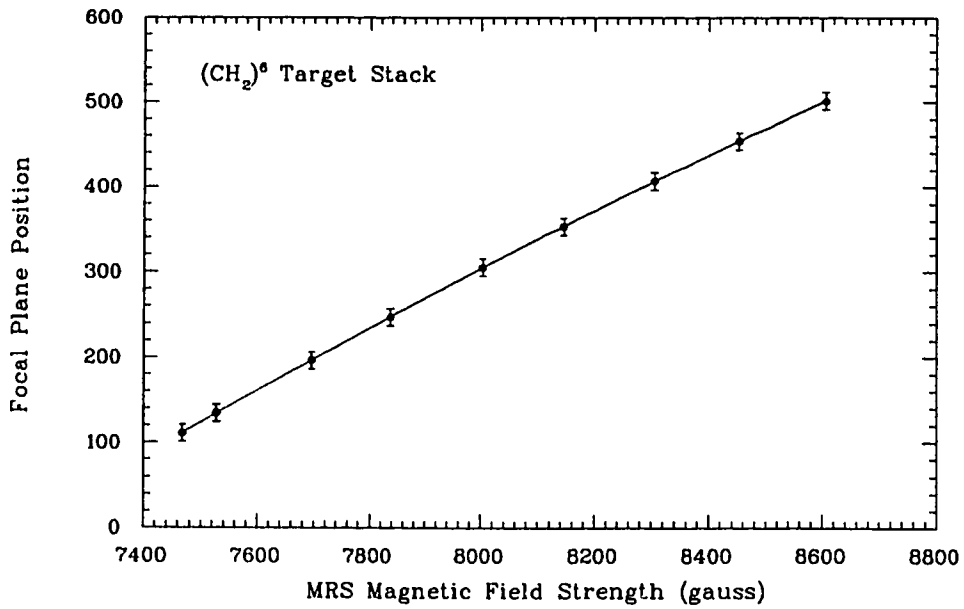
Figure 2.15: Energy calibration of the MRS spectrometer
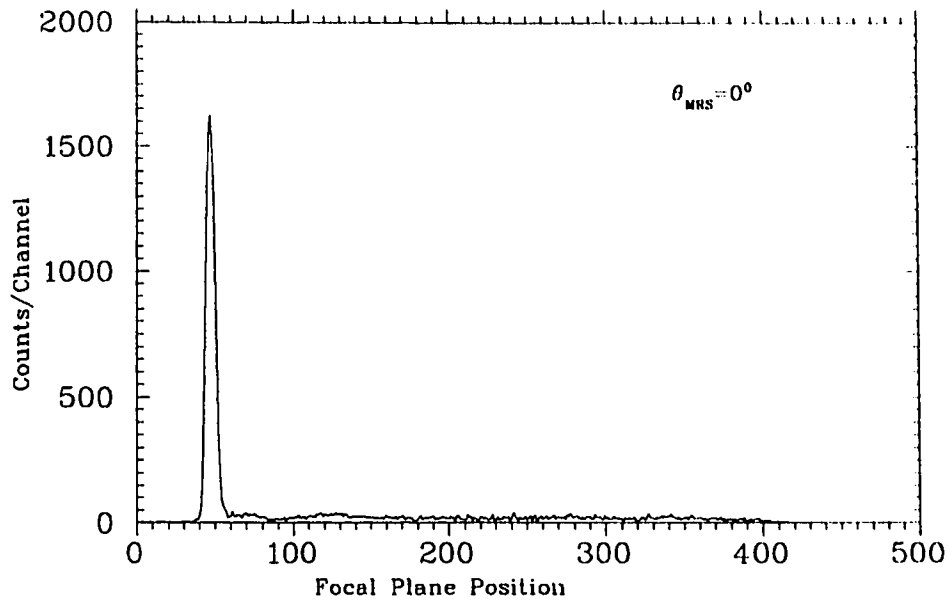
Figure 2.16: The proton spectrum that reflects the energy distribution of the secondary neutron beam from the primary target via the $^7Li(p,n)^7Be$ reaction. This spectrum was obtained with a CH_2 target from 200 MeV primary protons, and was corrected for the carbon peak.

2.7 Neutron Tail Deconvolution

Neutrons from the primary ^7Li target are not strictly monoenergetic, but have a low energy tail. This tail is reflected in the knock-out proton spectrum obtained with CH_2 target as shown in fig. 2.16. This spectrum was obtained previously by subtraction of a carbon spectrum from a CH_2 spectrum to remove the contribution from the $^{12}C(n,p)^{12}B$ reaction. The effect of the long tail of this energy distribution must be removed from the measured (n,p) spectra.

This was accomplished assuming that the cross section of the $^{76}Se(n,p)$ reaction is independent of neutron energy, and that there was no contribution from the neutron tail to the zero excitation part of the $^{76}Se(n,p)$ spectrum. The selenium spectrum and that shown in fig. 2.16 were rebinned into 1 MeV wide bins to improve the statistics. Then each succeeding bin of the $^{76}Se(n,p)$ spectrum, after the first, was corrected for events arising from neutrons in the tail corresponding to the appropriate lower excitation energy bins of the measured spectrum. An example of the result of this procedure is given in fig.

27

2.17, where fig. (a) shows the effect of the tail deconvolution to the selenium spectrum at 0^0 while fig. (b) gives the resultant cross sections for the two cases of (a). The small peak at 2 MeV could represent the Gamow-Teller strength.

2.8 Cross Section Calculations

The selenium target stack contained a CH_2 target in its last position (position f) which was used to normalize the $^{76}Se(n,p)^{76}As$ cross section by means of the $^1H(n,p)$ reaction. The $^1H(n,p)$ cross sections were obtained from the phase shift analysis program, SAID [36], and are tabulated in table (2.2). The cross section calculation takes into account the variation of the acceptance across the focal plane in the following way:

The yield of a nuclear reaction can be written as

$$Y = \frac{d\sigma}{d\Omega} \cdot N_{targ} \cdot accept \tag{2.3}$$

where N_{targ} = number of target atoms per unit area,

and $accept = N_{inc} \cdot eff \cdot d\Omega$

where N_{inc} is the number of incident particles and eff is the efficiency for the detection of outgoing particles into solid angle $d\Omega$.

For the acceptance scan data taken with the $(CH_2)^6$ stack, we then have for target f,

$$Y_f(X) = (\frac{d\sigma}{d\Omega})_H \cdot N_f \cdot accept_f(X) \tag{2.4}$$

and for targets $b \rightarrow e$,

$$Y_{b\rightarrow e}(X) = (\frac{d\sigma}{d\Omega})_H \cdot N_{b\rightarrow e} \cdot accept_{b\rightarrow e}(X) \tag{2.5}$$

where X is the position of the hydrogen peak on the focal plane. From these expressions, we find, for each spectrometer angle θ,

$$\frac{accept_{b\rightarrow e}(X)}{accept_f(X)} = \frac{Y_{b\rightarrow e}(X)}{Y_f(X)} \cdot \frac{N_f}{N_{b\rightarrow e}} \equiv \varepsilon(\theta). \tag{2.6}$$

This ratio then gives the acceptance for positions $b \rightarrow e$ (the positions in which the selenium targets were located) relative to position f, and takes into account the variation

28
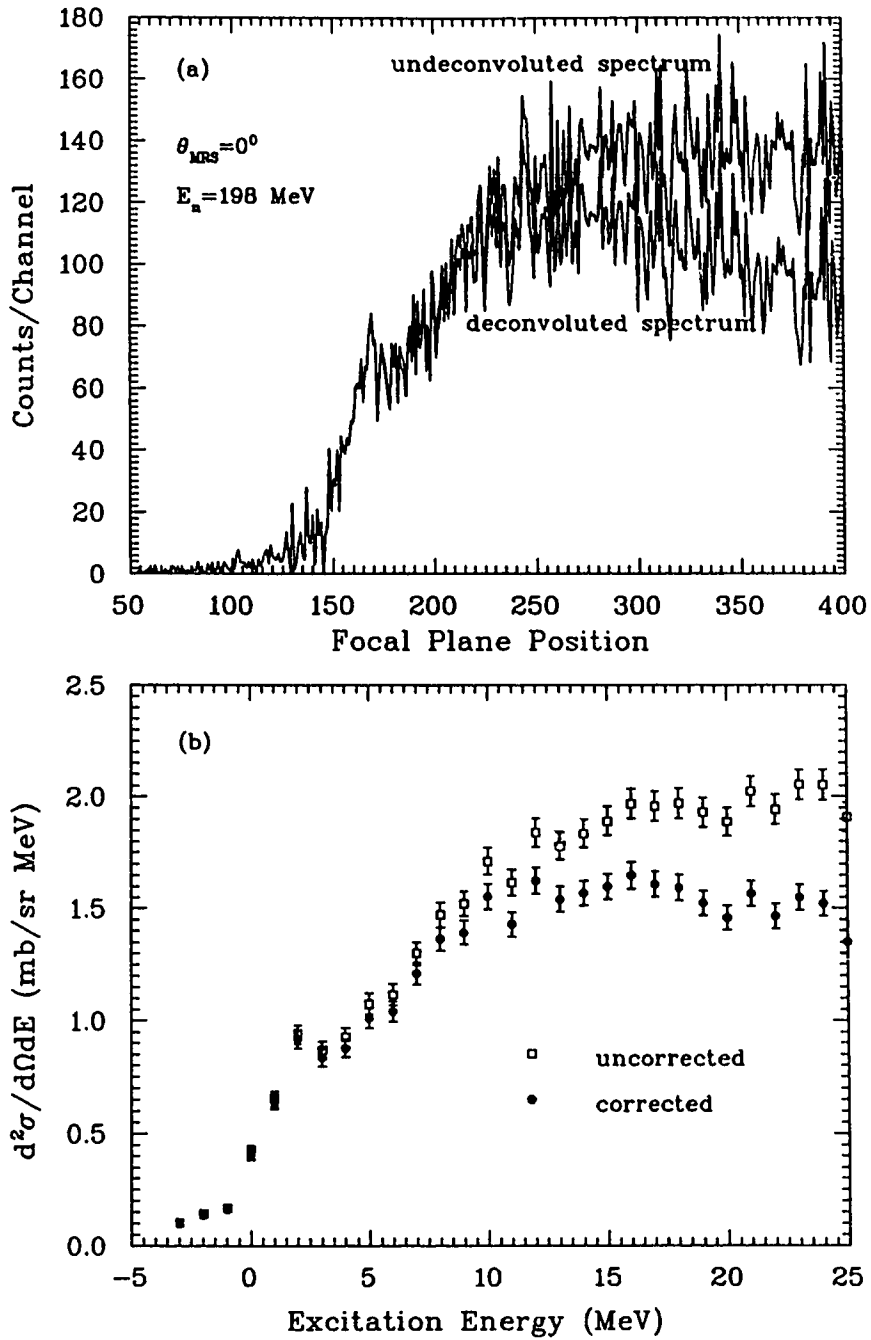
Figure 2.17: (a) shows the effect on the neutron tail deconvolution to the $^{76}Se(n,p)$ spectrum at $0°$, and (b) gives the resultant cross sections for the spectra in (a) with and without the deconvolution.

of neutron flux along the target stack and of the solid angle into the MRS. The values obtained for $1/\varepsilon(\theta)$ are tabulated in table (2.3).

For the selenium target stack, the yields are given as

$$Y_J(0) = (\frac{d\sigma}{d\Omega})_H \cdot N_J \cdot accept_J(0), \tag{2.7}$$

and

$$Y_{Se}(X) = (\frac{d\sigma(X)}{d\Omega})_{Se} \cdot N_{Se} \cdot accept_{b\to e}(X). \tag{2.8}$$

Here $Y_J(0)$ is the yield of the $^1H(n,p)$ reaction from the CH_2 target, N_J is the number of hydrogen atoms in the CH_2 target, and $accept_J(0)$ is the acceptance (as defined previously) for the $^1H(n,p)$ peak. $Y_{Se}(X)$ is the yield from the selenium targets in positions $b \to e$ as a function of focal plane position, N_{Se} is the number of selenium atoms and $accept_{b\to e}(X)$ is the acceptance for targets in positions b through e.

Dividing the above expressions gives

$$
\begin{aligned}
(\frac{d\sigma(X)}{d\Omega})_{Se} &= (\frac{d\sigma}{d\Omega})_H \cdot \frac{Y_{se}(X)}{Y_J(0)} \cdot \frac{N_J}{N_{Se}} \cdot \frac{accept_J(0)}{accept_{b\to e}(X)} \\
&= (\frac{d\sigma}{d\Omega})_H \cdot \frac{Y_{se}(X)}{Y_J(0)} \cdot \frac{N_J}{N_{Se}} \cdot \frac{accept_J(0)}{accept_J(X)} \cdot \frac{accept_J(X)}{accept_{b\to e}(X)}.
\end{aligned}
\tag{2.9}
$$

The term $\frac{accept_J(0)}{accept_J(X)}$ is the function plotted in fig. 2.14, while the term $\frac{accept_J(X)}{accept_{b\to e}(X)}$ has been defined above as $1/\varepsilon(\theta)$.

Upon dividing by the bin size of 1 MeV, the calculated cross sections are finally expressed as double differential cross sections, $d^2\sigma/d\Omega dE$. The results are given in figs. 2.18 and 2.19 for the five spectrometer angles.

30
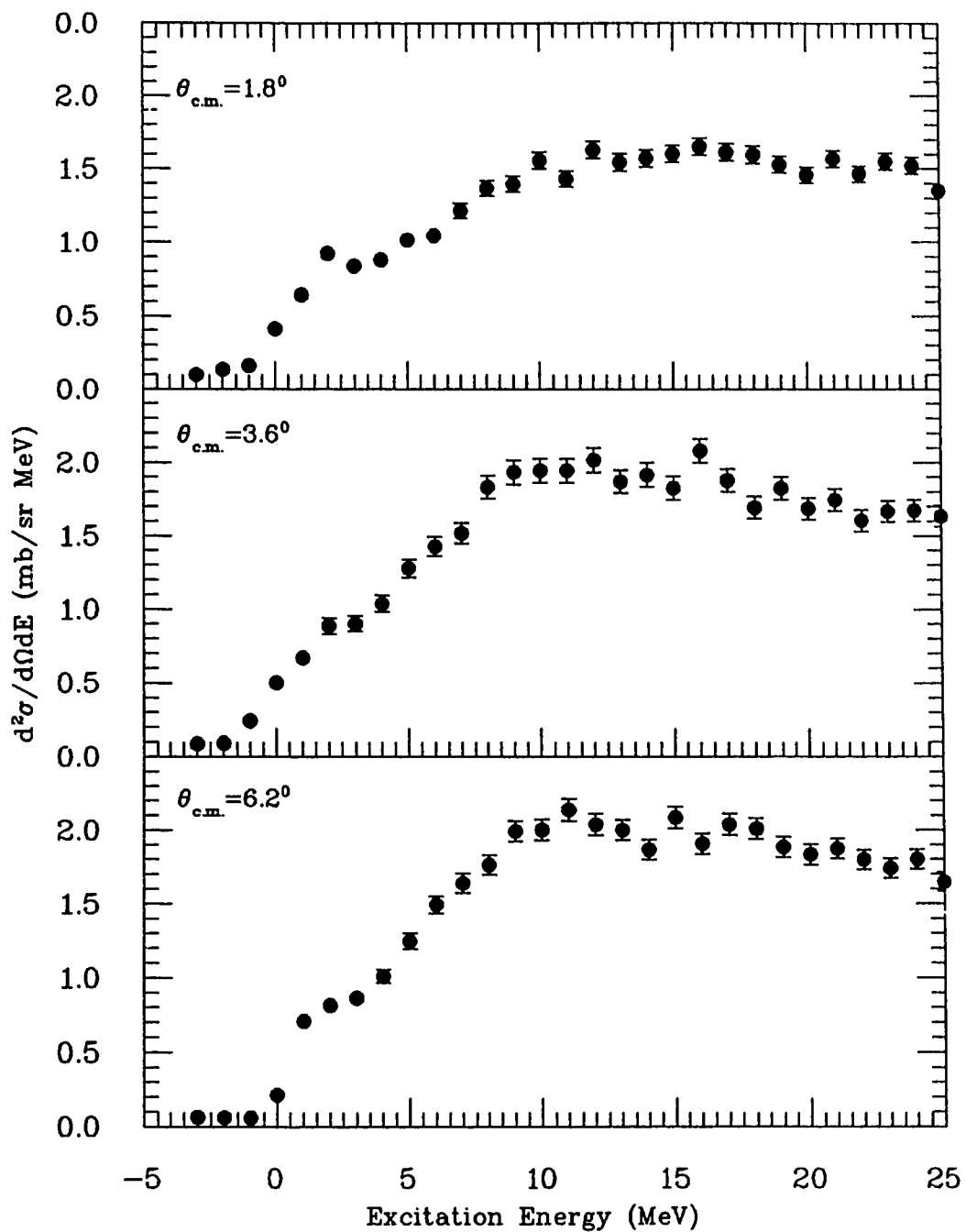
Figure 2.18: Cross section distributions for the reaction $^{76}Se(n,p)^{76}As$ at center-of-mass angles $1.8^0, 3.6^0$ and 6.2^0. Data were taken at 200 MeV using the TRIUMF CHARGEX facility.
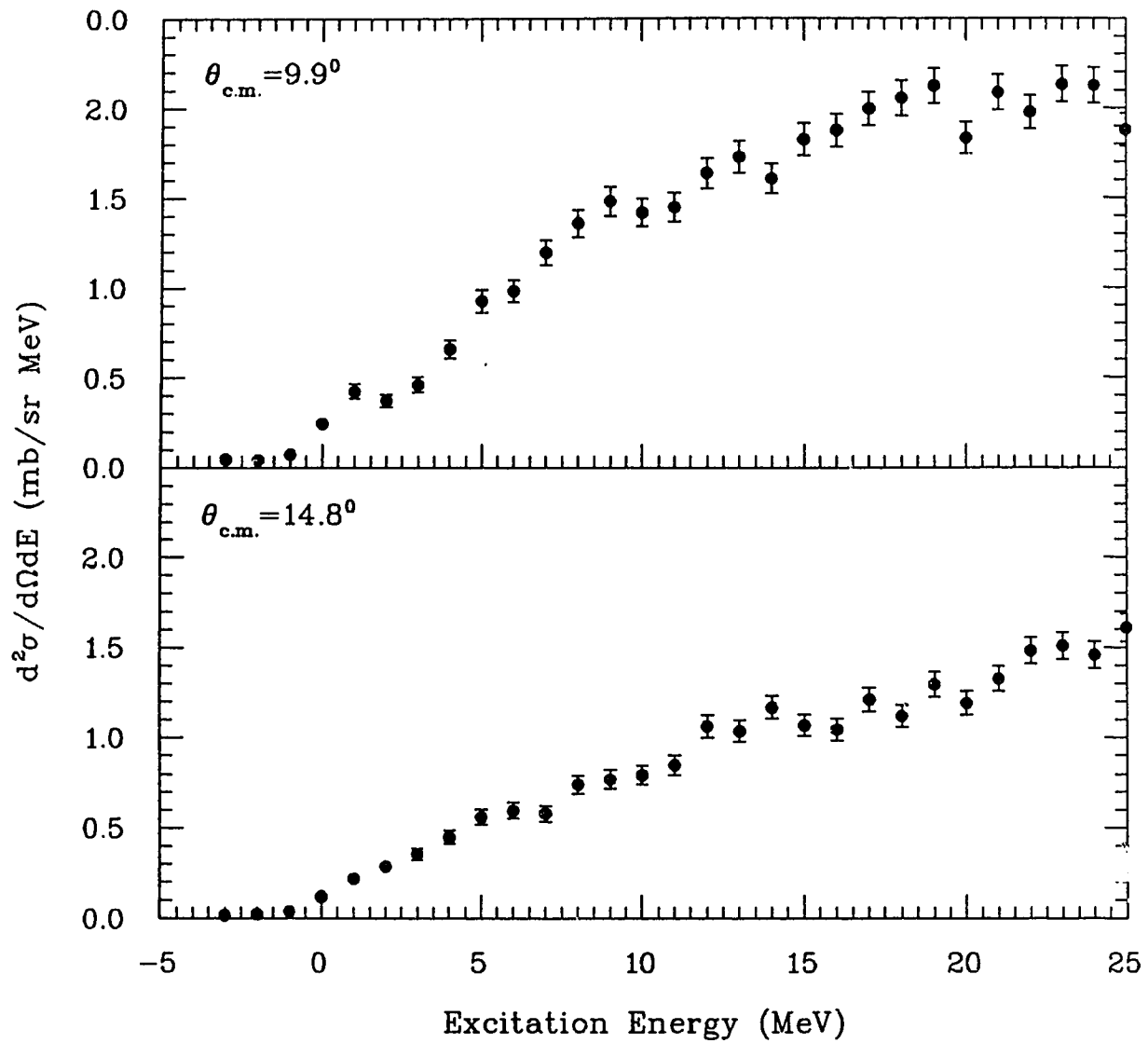
Figure 2.19: Cross section distributions for the reaction $^{76}Se(n,p)^{76}As$ at center-of-mass-angles 9.9^0 and 14.8^0. Data were taken at 200 MeV using the TRIUMF CHARGEX facility.

θ_{MRS}	θ_{lab}^{scatt}	$\theta_{c.m.}^{scatt}$	$\sigma_{c.m.}(H(n,p))$	$\sigma_{lab}(H(n,p))$
(deg.)	(deg.)	(deg.)	(mb/sr)	(mb/sr)
0	1.76	1.79	11.72	51.83
3	3.49	3.55	10.81	47.75
6	6.06	6.16	9.10	39.97
10	9.75	9.90	7.15	31.09
15	14.58	14.81	5.75	24.31

Table 2.2: $^1H(n,p)$ cross section predictions from the phase shift analysis program SAID program [36].

$\theta_{c.m.}^{scatt}$	$\frac{Y_F}{Y_{B\to E}}$	$\frac{1}{\epsilon(\theta)}$
(deg.)		
1.79	0.2615	0.9560
3.55	0.2568	0.9735
6.16	0.2571	0.9724
9.90	0.2484	1.0064
14.81	0.2513	0.9948

Table 2.3: The detection efficiency of the spectrometer for each angle, calculated using the analysed spectra for $(CH_2)^6$ stack as the secondary target.

Chapter 3

Multipole Decomposition

In order to separate the Gamow-Teller strength from other contributions to the measured spectra and to obtain quantitative estimates of its distribution, a multipole decomposition was carried out by fitting the measured spectra to a sum of shapes obtained by DWIA calculations (program DW81 [37]) for the L and J transfers expected to be significant in the data. It is assumed, in this method, that the contribution from each L and J transfer is independent so that there is no significant interference between the various multipole transitions. Thus, the incoherent sum of the cross section angular distributions for different values of the total angular momentum transfer and parity change ΔJ^π was fitted to the experimental cross section in each 1 MeV energy bin such that,

$$\sigma_{expt}(E) = \sum_{\Delta J^\pi} a_{\Delta J^\pi}(E)\, \sigma_{DW}(\Delta J^\pi, E), \tag{3.1}$$

where the coefficients $a_{\Delta J^\pi}(E)$ were obtained by carrying out a least-squares fit of the above expression to the data. DWIA calculations were carried out to obtain the theoretical cross section angular distributions, σ_{DW}, for each transition of a given ΔJ^π.

3.1   Selection of Particle-Hole Transitions

Shown in fig. 3.1 is a shell model representation of the ^{76}Se ground state configuration based on a ^{40}Ca core. The decomposition procedure consists of finding the $a_{\Delta J^\pi}$ coefficients of eq. (3.1) in each 1 MeV energy bin. Because data were taken at only five angles, it was possible to include at most four values of ΔJ^π in the fits. Therefore, it was
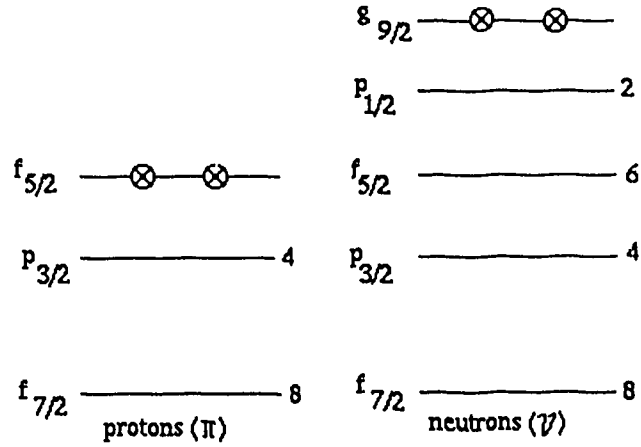
Figure 3.1: Ground state configuration of ^{76}Se, which is based on a ^{40}Ca core.

necessary to be quite selective in deciding which particle-hole excitations to use. Previous analyses [38-40] have shown that the extracted $L = 0$ strength is not terribly sensitive to any of the choices provided that it is the dominant component. Once an excitation energy is reached where other multipolarities become dominant, the extracted $L = 0$ strength becomes much more sensitive to the detailed shapes of these other components, and hence much more uncertain.

For the present fits, the following choices were made for the various multipolarities:

$$\Delta L = 0 : \quad [\pi(p_{3/2})^3, \ \nu(p_{1/2})]_{J^\pi=1+},$$

$$\Delta L = 1 : \quad [\pi(f_{7/2})^7, \ \nu(g_{9/2})]_{J^\pi=1-},$$

$$\Delta L = 2 : \quad [\pi(p_{3/2})^3, \ \nu(p_{1/2})]_{J^\pi=2+},$$

$$\Delta L = 3 : \quad [\pi(f_{5/2})^1, \ \nu(g_{9/2})]_{J^\pi=3-}.$$

The shapes for these transitions were calculated in DWIA (program DW81) using the Franey-Love interaction at 200 MeV with SP84 phase shift data [41]. The optical

potentials for the distortions in DW81 were generated using $MAINX8$ [42], and were phenomenological Woods-Saxon potentials fitted to elastic scattering data. A three parameter Fermi distribution (see eqn. (3.2)) with parameters W=0, R=4.409, and Z=0.583 taken from electron scattering on ^{70}Zn [43] was applied.

$$\rho(r) = \frac{\rho_0(1 + Wr^2/R^2)}{1 + \exp^{(\frac{r-R}{Z})}}$$ (3.2)

In eqn. (3.2), W is the deformation parameter, R the mean nuclear radius ($R = R_0 A^{\frac{1}{3}}$), and Z the diffuseness parameter. The calculated angular distributions for the transitions are illustrated in fig. 3.2 for extraction energies from -5 MeV to 35 MeV in 10 MeV steps. During the fitting procedure, angular distribution shapes were interpolated for energies between these calculated distributions.

3.2 Decomposition Results

The results of the multipole decomposition are shown in figs. 3.3 and 3.4 for the five angles involved. In these figures, the cross-hatched region is the $\Delta L = 0$ component, the left- and right-hatched regions are $\Delta L = 1$ and $\Delta L = 2$ components, while the horizontally-hatched region is the $\Delta L = 3$ component, respectively.

Contributions from each multipole to the total cross section angular distribution were extracted from the multipole results for different energy bins. Those at 2, 5, and 9 MeV excitation energies (the appropriate energies where $L = 0, 1, 2$ peak, approximately) are plotted against the center-of-mass angle in fig. 3.5. Also shown in each case is the incoherent sum which is fitted to the experimental data at the three energy bins.

The facts that the multipole decomposition was carried out independently in each energy bin, and that the results shown in figs. 3.3 and 3.4 are fairly smooth functions of energy give confidence that the procedure is a reasonable one.
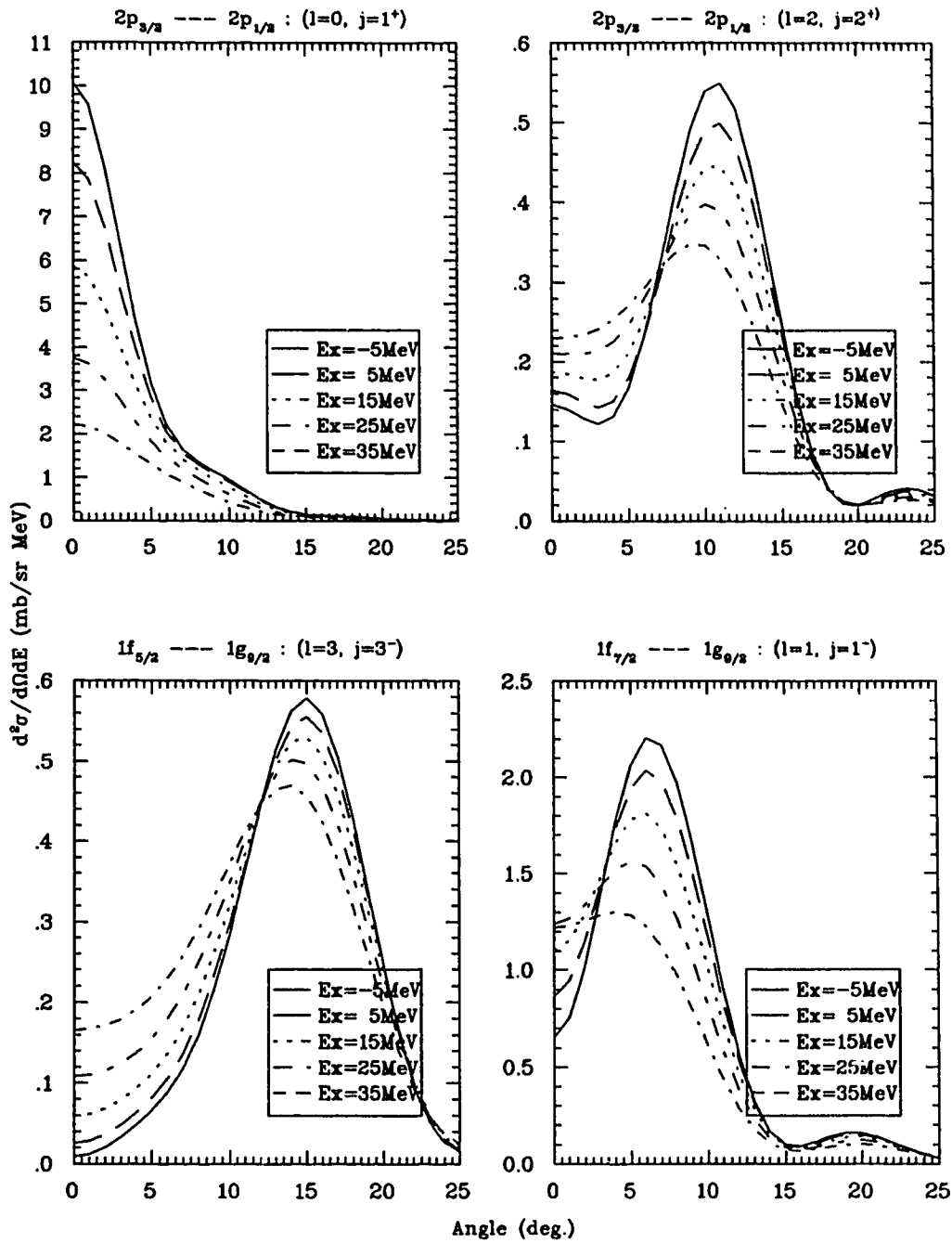
Figure 3.2: Theoretical cross section angular distributions calculated for each transition using the DWIA are shown for five excitation energies (-5, 5,15,25, and 35 MeV).
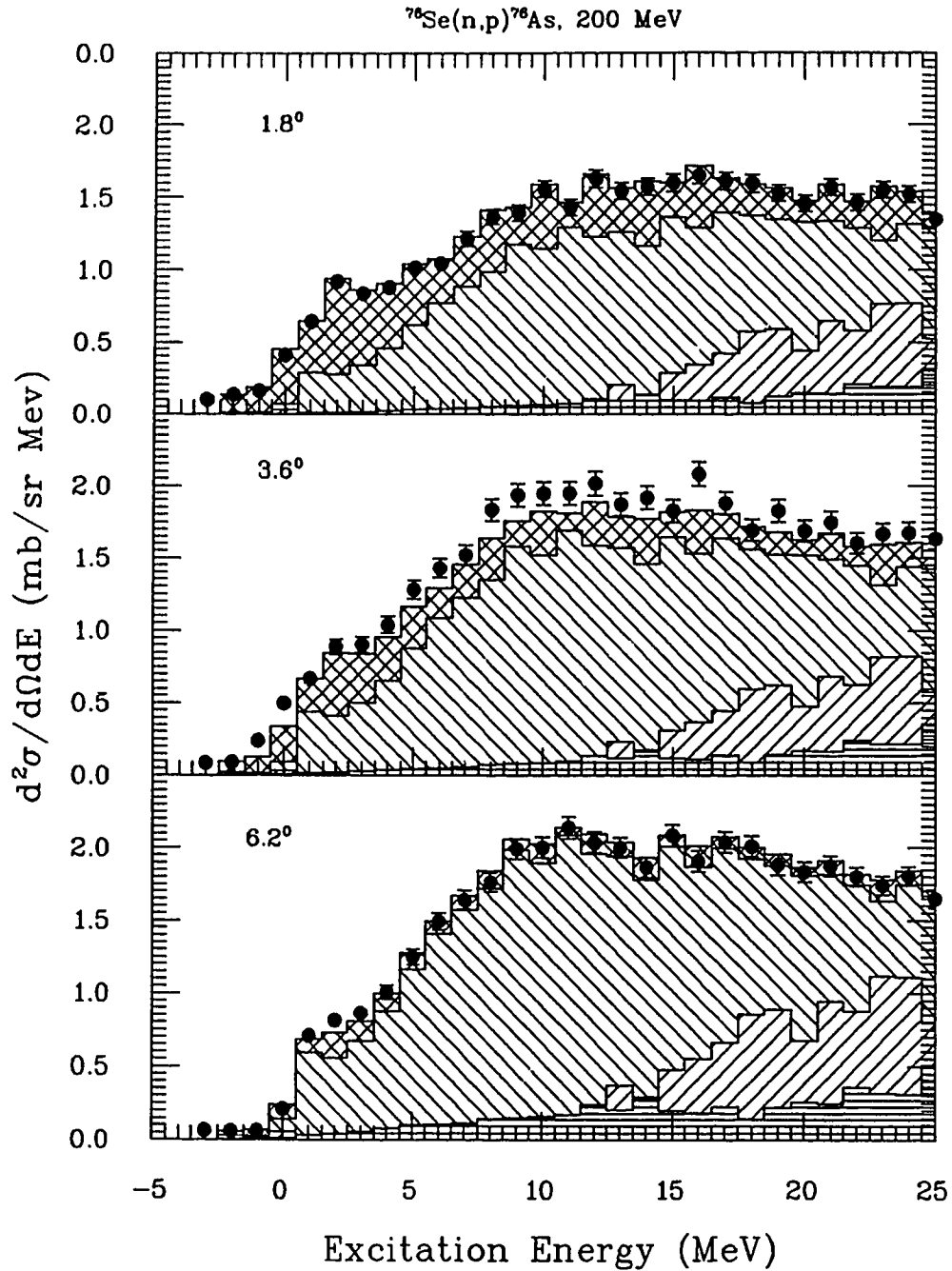
Figure 3.3: Multipole decomposition of the $^{76}Se(n,p)^{76}As$ cross sections at angles, $1.8°, 3.6°$, and $6.2°$. The cross-hatched region is the $\Delta L = 0$ component, the left- and right-hatched regions are $\Delta L = 1$ and $\Delta L = 2$ while the horizontally-hatched region is $\Delta L = 3$.
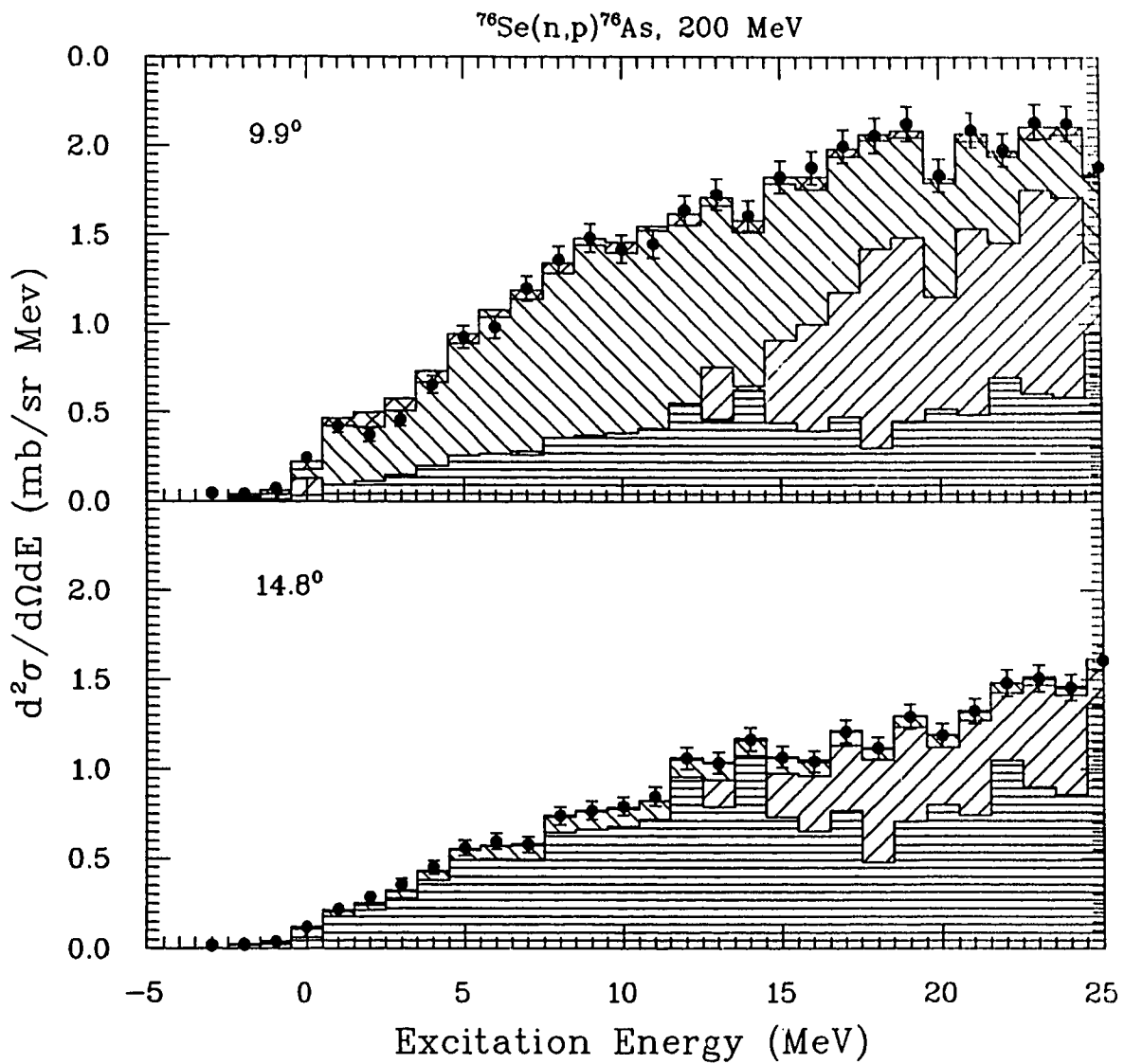
Figure 3.4: Multipole decomposition of the $^{76}Se(n,p)^{76}As$ cross sections at angles, 9.9° and 14.8°. The cross-hatched region is the $\Delta L = 0$ component, the left- and right-hatched regions are $\Delta L = 1$ and $\Delta L = 2$ while the horizontally-hatched region is $\Delta L = 3$.
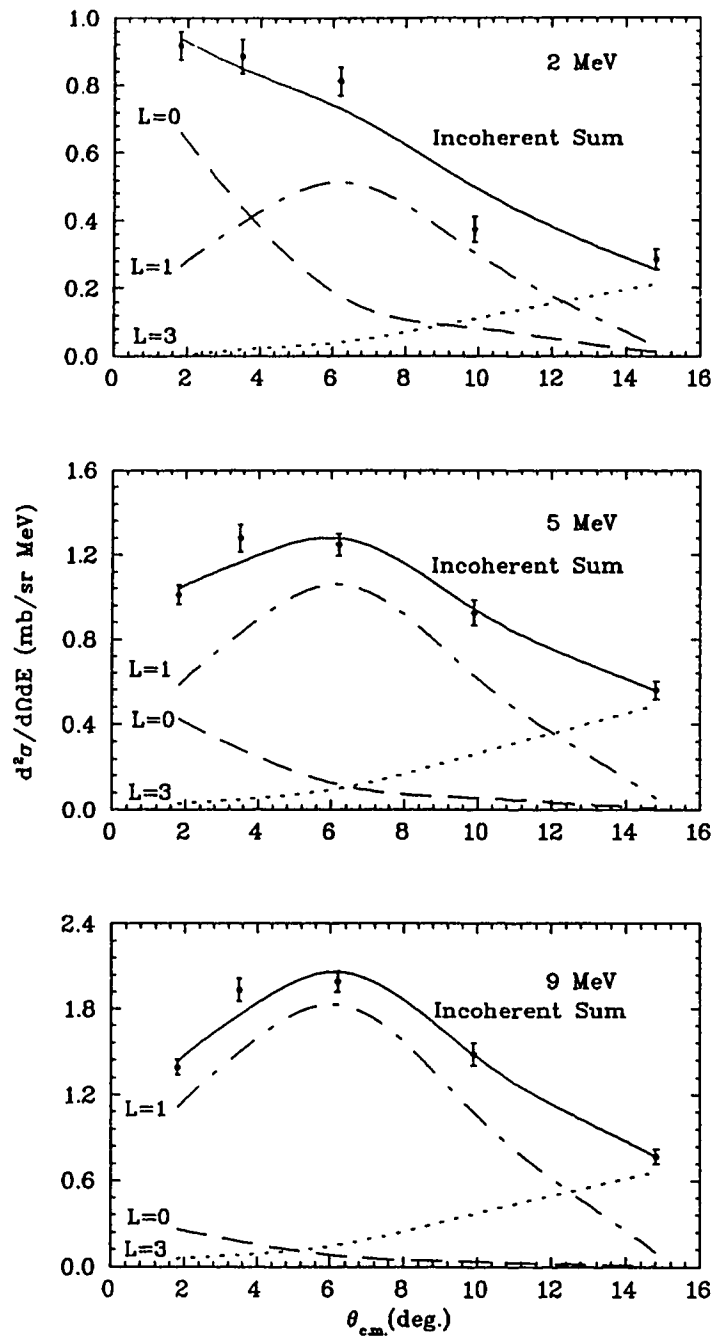
Figure 3.5: Contributions of multipole components to the total cross section at three different energy bins are shown. The incoherently summed total cross section is fitted to the experimental data in each case.

Chapter 4

Results and Conclusions

4.1 Gamow-Teller Strength

The relationship between (p,n) cross sections at small angles and the corresponding β-decay transition strengths has been studied in detail [13], and the result for $L = 0$ spin-flip transitions is given within the framework of the DWIA by,

$$\sigma_{pn}(q,\omega,A,\alpha) = \hat{\sigma}_{GT\text{-}}(A)F(q,\omega)B_{GT\text{-}}(A,\alpha), \tag{4.1}$$

where q and ω are the momentum and energy transfers, respectively. The final state of the recoil nucleus is denoted by α. The factor $F(q,\omega)$ describes the shape of the cross section distribution and goes to unity as $(q,\omega) \to (0,0)$. A similar relationship holds for the (n,p) cross sections and the corresponding B_{GT+} strengths with the proportionality constant $\hat{\sigma}_{GT+}$. To extract the GT strength from $^{76}Se(n,p)$ data, we use the proportionality constant, $\hat{\sigma}_{GT+}$, obtained from the charge exchange cross sections calibrated at 200 MeV against known β-decay [9,13].

The GT strength corresponding to the measured cross sections was obtained using the relation [13],

$$\hat{\sigma}_{GT+} = \frac{\sigma(q=\omega=0)}{B(GT^+)} = 4.6 \; mb/sr, \tag{4.2}$$

in this mass region. In order to use this value determined for $q = \omega = 0$, it was necessary to extrapolate the experimental data obtained at the centre-of-mass angle 1.8^0 to 0^0. This was accomplished with the DWIA and the corresponding correction factor,

41

$$[\sigma_{q=\omega=0}(0^0)/\sigma_{c.m.}(\theta = 1.8^0, \omega \neq 0)],$$

calculated for each energy bin between -2.0 to 10.0 MeV.

The Gamow-Teller strength was deduced from the $\Delta J^\pi = 1^+(\Delta L = 0, \Delta S = \Delta T = 1)$ component of the multipole decomposition, and is given in table 4.1. The second column indicates the extracted total cross section for each energy bin. The extracted $\Delta L = 0$ component at 1.8^0 is shown in the third column. Correction factors for the effective scattering angle and the energy transfer determined from the DWIA are given in the fourth column, and the resulting extracted cross sections in the fifth. The final column gives the $B(GT^+)$ strength.

E_x (MeV)	$\sigma_{c.m.}$ (mb/sr)	$\sigma_{L=0}(1.8^0)$ (mb/sr)	Correction Factor	$\sigma_{q=\omega=0}$ (mb/sr)	$B(GT^+)$
-2.0	0.136 ± 0.015	0.120 ± 0.017	1.188	0.143 ± 0.020	0.031 ± 0.004
-1.0	0.160 ± 0.017	0.171 ± 0.019	1.208	0.207 ± 0.023	0.045 ± 0.005
0.0	0.409 ± 0.027	0.378 ± 0.032	1.230	0.465 ± 0.040	0.101 ± 0.009
1.0	0.640 ± 0.034	0.351 ± 0.043	1.255	0.440 ± 0.054	0.096 ± 0.012
2.0	0.918 ± 0.042	0.663 ± 0.051	1.282	0.850 ± 0.065	0.185 ± 0.014
3.0	0.834 ± 0.040	0.518 ± 0.051	1.311	0.679 ± 0.067	0.148 ± 0.015
4.0	0.876 ± 0.041	0.448 ± 0.054	1.343	0.602 ± 0.055	0.131 ± 0.012
5.0	1.011 ± 0.044	0.426 ± 0.060	1.376	0.586 ± 0.061	0.127 ± 0.013
6.0	1.040 ± 0.045	0.306 ± 0.064	1.414	0.433 ± 0.090	0.094 ± 0.019
7.0	1.209 ± 0.049	0.342 ± 0.071	1.454	0.497 ± 0.103	0.108 ± 0.022
8.0	1.363 ± 0.053	0.426 ± 0.076	1.497	0.638 ± 0.114	0.139 ± 0.031
9.0	1.391 ± 0.053	0.261 ± 0.080	1.543	0.403 ± 0.123	0.088 ± 0.027
10.0	1.553 ± 0.057	0.444 ± 0.085	1.593	0.707 ± 0.135	0.154 ± 0.029

Table 4.1: Cross sections and Gamow-Teller strength for the $^{76}Se(n,p)^{76}As$ reaction at 200 MeV. $\Delta L = 0$ component of the total cross section was extracted by a full multipole decomposition of data at 1.8^0.

The Gamow-Teller strength was extracted only up to $E_x = 10$ MeV. In fact, above $E_x = 5$ MeV it is clear from fig. 3.5 that the $\Delta L = 1$ component is dominant, so as

mentioned previously, extraction of the $\Delta L = 0$ strength becomes much more uncertain.

The integrated strength below 10 MeV excitation is $\sum B(GT^+) = 1.4 \pm 0.2$.

4.2 Conclusions

The distribution of Gamow-Teller strength deduced from the experiment is compared with a QRPA calculation [44,31] in fig. 4.1. The calculation was carried out for the two values of particle-particle coupling strength. Case (a) in fig. 4.1 shows that for $g^{pp}=130$, a strong state is predicted at low excitation which is clearly not present in the data. For both cases, the total predicted strength [0.7 in case (a) and 0.2 in case (b)] is considerably less than the observed strength.

These results show that it would be difficult to have much confidence in a similar calculation that related a neutrino mass to a measured 0ν $\beta\beta$-decay lifetime. It may be that some simple modification to the calculation could result in improvement in the agreement between the calculated distribution and the measured one, and it is expected that a new calculation will be undertaken soon.
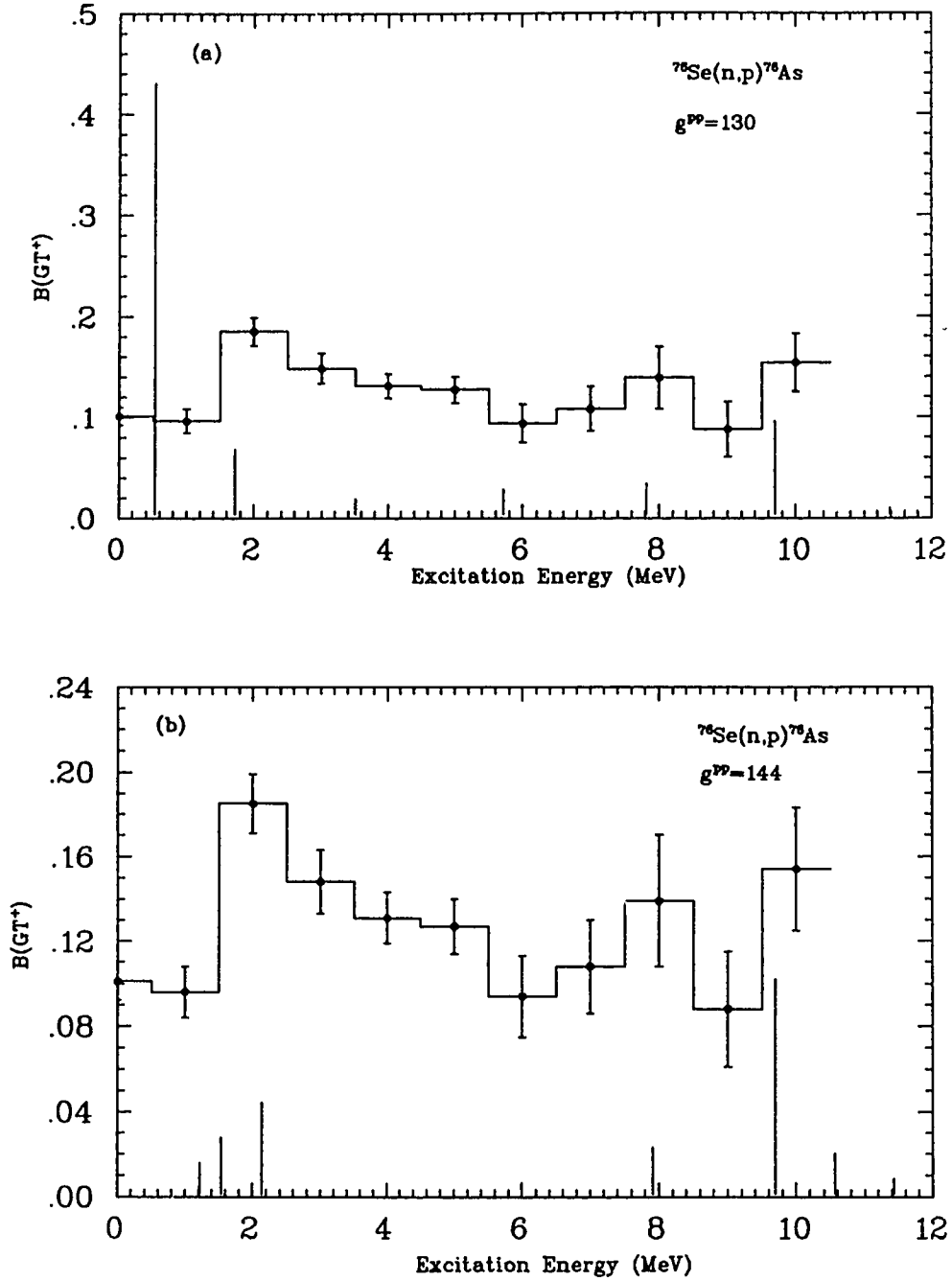
Figure 4.1: (a) and (b) illustrate two comparisons of the experimental results (Table 4.1) with theoretical predictions (the vertical lines) from a QRPA calculation at $g^{pp} = 130$ and 144, respectively.

REFERENCES

[1] J. D. Anderson and C. Wong, Phys. Rev. Lett. **7**, (1961) 250.

[2] R. R. Doering et. al., Phys. Rev. Lett. **35**, (1975) 1691.

[3] D. F. Measday and J. N. Palmieri, Phys. Rev. **161**, (1967) 1071.

[4] F. P. Brady, Can. J. Phys. **65**, (1987) 578.

[5] R. Helmer, Can. J. Phys. **65**, (1987) 588.

[6] R. S. Henderson et al., Nucl. Instr. and Meth. **A257**, (1987) 97.

[7] K. P. Jackson et al., Phys. Lett. **B201**, (1988) 25.

[8] M. C. Vetterli et. al., Phys. Rev. **40**, (1989) 559.

[9] M. C. Vetterli et al., Phys. Rev. Lett. **59**, (1987) 437.

[10] C. D. Goodman et al., Phys. Rev. Lett. **44**, (1980) 1755.

[11] D. E. Bainum et al., Phys. Rev. Lett. **44**, (1980) 1751.

[12] B. D. Anderson et al., Phys. Rev. **C31**, (1985) 1161.

[13] T. N. Taddeucci et al., Nucl. Phys. **A469**, (1987) 125.

[14] M. C. Vetterli et al., Phys. Rev. **45**, (1992) 997.

[15] P. Vogel, M. Ericson, and J. D. Vergados, Phys. Lett. **B212**, (1988) 259.

[16] W. P. Alford, et al., Nucl. Phys. **A514**, (1990) 49.

[17] P. Vogel and P. Fisher, Phys. Rev. **C32**, (1985) 1362.

[18] W. Pauli, Address to group on Radioactivity (Tubingen, December 4, 1930)
(unpublished); *Rappts. Septieme conseil Phys. Solvay, Bruxelles*, 1933
(Gautier-Villars, Paris, France, 1934).

[19] F. Reines and C. L. Cowan, Jr., Nature **178**, (1956) 446.
Cowan, Reines, Harrison, Kruse, and McGuire, Science, **124**, (1956) 103.

[20] J. A. Halbleib and R. A. Sorensen, Nucl. Phys. **A98**, (1967) 542.

[21] T. Kirsten, O. A. Schaeffer, E. Norton, and R. W. Stoenner, Phys. Rev. Lett. **20**,
(1968) 1300.

[22] S. R. Elliott, A. A. Hahn, and M. K. Moe, Phys. Rev. Lett. **59**, (1987) 2020.

[23] S. T. Belyaev et al., Zeitchrift fur Physik. **A343** (no.4), (1992) 397.

[24] H. S. Miley et al., Phys. Rev. Lett. **25**, (1990) 3092.

[25] F. T. Avignone et al., Phys. Lett. **B256**, (1991) 559.

[26] W. H. Furry, Phys. Rev. **56**, (1939) 1184.

[27] A. Halprin et al., Phys. Rev. **D13**, (1976) 2567.

[28] D. O. Caldwell et al., Phys. Rev. **D33**, (1986) 2737.

[29] S. Tremaine and J. E. Gunn, Phys. Rev. **42**, (1979) 407.

[30] C. S. Frenk et al., Astrophys. J. **271**, (1983) 417.

[31] J. Engel, P. Vogel, and M. R. Zirnbauer, Phys. Rev. **C37**, (1988) 731.

[32] H. V. Klapdor and K. Grotz, Phys. Lett. **B142**, (1984) 323.

[33] O. Civitarese, Amand Faessler, and T. Tomoda, Phys. Lett. **B914**, (1987) 11.

[34] MRS manual, TRIUMF (unpublished).

[35] List Mode Analysis program (LISA), TRIUMF, (unpublished).

[36] R. A. Arndt and L. D. Soper, scattering analysis interactive dial-in (SAID) program, Phys. Rev. **D35**, (1987) 128.

[37] J. R. Comfort, computer code DW81, Arisona State University.

[38] K. J. Raywood et al., Phys. Rev. **C41**, (1990) 2836.

[39] A. Celler et al., Phys. Rev. **C43**, (1991) 639.

[40] A. Celler et al., Phys. Rev. **C47**, (1993) 1563.

[41] M. A. Franey and W. G. Love, Phys. Rev. **C31**, (1985) 488.

[42] Computer code MAINX8, modification by R. G. Jeppesen, unpublished.

[43] C. W. de Jager, H. de Vries, and C. de Vries, At. Data Nucl. Data Tables **14**, (1974) 479.

[44] P. Vogel and M. R. Zirnbauer, Phys. Rev. Lett. **57**, (1986) 3148.

Appendix A

Hall Probe Calibration for Beamline 4B

A.1 Beamline 4B at TRIUMF

Beamline 4B is one of the three major external beamlines from the TRIUMF accelerator, the cyclotron that accelerates H^- ions to produce beams of protons at intermediate energies (180-520 MeV). The particle beam is kept collimated throughout the beamline using the various magnetic transport elements, such as quadrupoles, bending magnets, solenoids, etc. It is very important to have a precise updated calibration for each Hall probe installed in quadrupole magnets in order to tune beam line 4B. Since 4B is one of the two legs of beamline 4, 4B line tuning also requires the calibration of Hall probes that are installed in the beamline 4 quadrupoles located in the cyclotron vault area. There are three such quadrupoles in the vault that are common to the operation of both the 4A and 4B lines. Each is subjected to relatively high radiation levels. The fourteen quadrupoles in the full 4B beam line are labelled Q1 to Q14; those on beamline 4B are labelled 4BQn. Thus, Q1, Q2 and Q3 which are common to beam lines 4A and 4B are located in the vault, and 4BQ4 and 4BQ5 are located in the 4A tunnel. There is no 4BQ6 functioning on the beam line, and the rest of the quadrupoles are located in the 4B experimental hall where the magnetic spectrometer facilities reside.

The poletip magnetic field strengths of all these quadrupoles are measured by means of Hall probes positioned in aluminum jigs which sit in the quadrupole magnets. Figs. A.1 and A.2 illustrate the aluminum jig and how it is installed in the quadrupole. For low electronic noise, it is important that these aluminum jigs be insulated from ground,
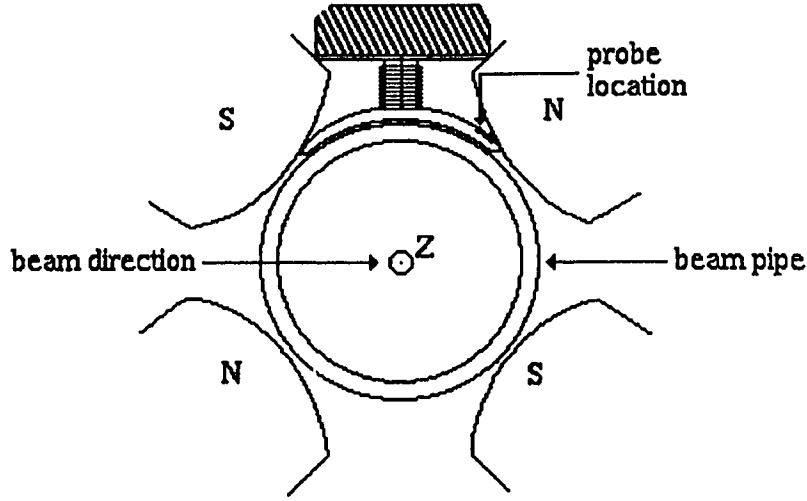
Figure A.1: Position of the Hall probe in a quadrupole.

and so the jigs are either anodized (those in Q1, Q2 and Q3 which suffer high radiation levels in the cyclotron vault) or wrapped with a single layer of yellow mylar tape. The jig is mounted right on the top of one of the poletips so that the Hall probe can read the magnetic field strength near the poletip radius. This arrangement leaves a small separation between the Hall probe and the poletip which will be taken into account later in calculating the actual magnetic field at the poletip.

The magnetic field of the quadrupole is measured by means of the Hall probe using the Hall effect. A known current I is sent through the probe, which is a semiconductor material. A uniform magnetic field is then applied perpendicular to the plane of the probe. The electrons in the Hall probe experience a Lorentz force, $\vec{F} = q\vec{V} \times \vec{B}$, which causes a voltage difference between points p and q on the probe (see fig. A.2).

The forces acting on the electron are

$$\vec{F}_e = (-e)(\vec{v}_e \times \vec{B}) \tag{A.1}$$

and,

$$\vec{F}_{Hall} = (-e)\vec{E}_{Hall}. \tag{A.2}$$

The Hall voltage across the probe (from $p \to q$) is established when $\vec{F}_e = \vec{F}_{Hall}$. Therefore,

$$E_{Hall} = v_e\,B = \frac{V_{Hall}}{d}, \tag{A.3}$$
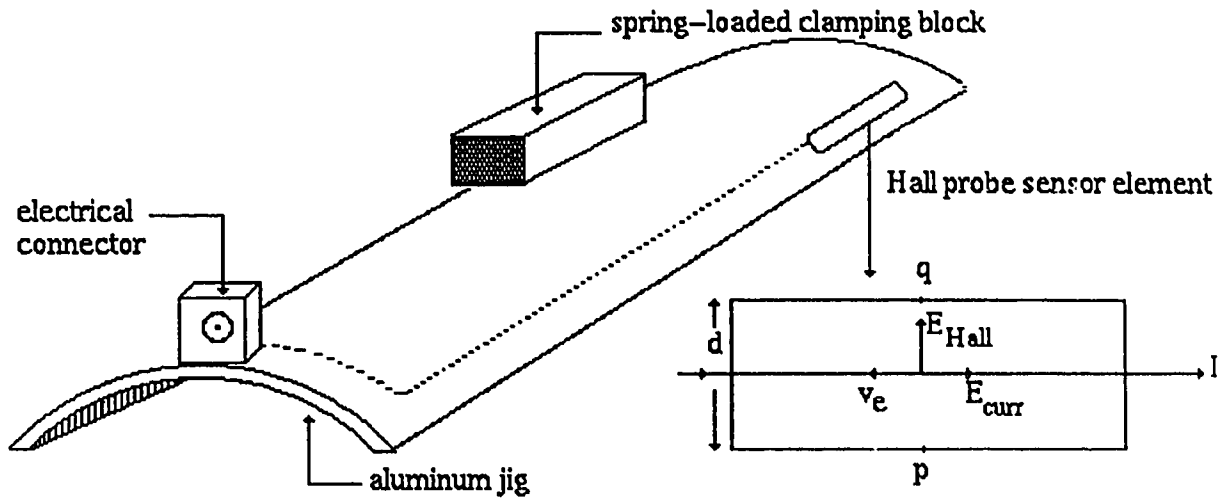
Figure A.2: Magnetic field measurement using the Hall effect.

and

$$V_{Hall} = d\, v_e\, B = \left(\frac{d}{neA}\right) I\, B = K\, B. \tag{A.4}$$

K is a constant for a given Hall probe with a constant current, I, which is given by,

$$I = nev_eA.$$

Here, A is the cross sectional area perpendicular to the current flow, d is the distance between p and q, n is the density of charge carriers (electrons), and v_e is their drift velocity in the medium, e is the electronic charge and V_{Hall} denotes the Hall voltage. The voltage thus generated is proportional to the magnetic field strength $\vec{B}$. In practical terms, for the Hall probes that are used in the beamline magnets, a field of a few kilogauss results in a Hall voltage of a few millivolts, for a Hall current of about 100 mA. The calibrations of these Hall probes have to be updated from time to time since the material of which the Hall probes are made is susceptible to radiation damage. The last calibration of this type was done in October 1986.

The new calibration was performed in the October, 1992 shutdown period. The radiation level at the front end of the beam line was about 50 mr/hr with the beam off, and at the site of the Hall probes removed from the front end quadrupole magnet, 4 mr/hr on contact. In the calibration process, the required homogeneous magnetic field was provided by a large dipole magnet (the BONNIE magnet in the proton hall). The absolute magnetic

field strength was accurately determined using the NMR (nuclear magnetic resonance) probe. The Hall voltage was measured for a given magnetic field and a known current, using the TELTERM remote-control system in the control room.

If the applied magnetic field is reversed, the generated Hall voltage is also reversed. The applied constant current, I, creates an electric field, E_{curr}, and the electric field, E_{Hall}, caused by the Hall effect is perpendicular to this. If the two sensor points p and q are not perfectly aligned with E_{Hall}, but have a component in the direction of E_{curr}, then when the applied magnetic field is reversed in sign, the voltage between p and q will change in magnitude. Therefore, it is essential to do this calibration with both polarities of the calibrating magnetic field.

All the Hall probes of beam line 4 are connected in series, and a constant current of 100.00 mA was applied. A shorting stub was used to maintain the electrical continuity in the circuit when one Hall probe was removed from a quadrupole for its calibration. The calibration between the magnetic field and the corresponding Hall voltage was found by fitting the data to a linear fit,

$$Y = M\,X + R = M\,(X - S), \tag{A.5}$$

and the constants M, R and S were found for the two polarities of each Hall probe. In this equation, Y gives the magnetic field strength in gauss that corresponds to the absolute value of the maximum Hall voltage X in microvolts. A detailed description on this calibration is found in reference [A1].

A.2   Calibration Results

The results of the calibration are given in table A.1. The new and the old calibrations of each Hall probe were compared with each other. Since the constant current in the previous calibration was 144.30 mA and that in the new calibration was 100.00 mA, the new results have been normalized by multiplying the coefficients M and R of eqn. (A.5) by the factor (100/144.3). These normalized results are given in table A.2 whereas the old calibration is found in table A.3. Comparison of the results reveals that the R and S constants for the present and earlier calibrations are different. This is expected because the error in R and S from the fitting process is large since they are very small compared

Table A.1: Hall probe calibration results in October 1992.

Quad	M(G/μV)		R(G)		S(μV)	
No.	-ve	+ve	-ve	+ve	-ve	+ve
Q1DB	1.2302	1.2267	4.2987	-1.7235	-3.4943	1.4049
Q1DT	1.2414	1.2422	-5.7478	12.9070	4.6301	-10.3904
Q2DT	1.2405	1.2408	-3.0852	17.3380	2.4871	-13.9732
Q3DT	1.2284	1.2264	7.6202	4.0323	-6.2033	-3.2879
Q4	1.0945	1.0949	3.8617	0.0446	-3.5283	-0.0407
Q5	1.0828	1.0819	-1.6724	-0.0647	1.5445	0.0598
Q7*†	1.3312	1.3300	-0.8301	-2.1554	0.6235	1.6206
Q8†	1.3313	1.3321	-1.0755	2.8122	0.8078	-2.1111
Q9†	1.3031	1.3032	-1.9843	0.0065	1.5227	-0.0050
Q10†	1.3267	1.3269	2.3055	-6.4935	-1.7377	4.8937
Q11†	1.3030	1.3014	-5.7317	2.9276	4.3988	-2.2496
Q12†	1.3231	1.3216	-10.3420	1.4614	7.8165	-1.1058

*No quadrupole has been labeled as Q6 on the beam line 4B.

†The set of six quadrupoles (Q7-Q12) constitutes the 4B twister [A2] between targets 4BT1 and 4BT2. DB and DT stand for the location of Hall probe in a quadrupole, namely the downstream bottom and downstream top with respect to the beamline.

Table A.2: 1992 calibration results normalized to a current of 144.3 mA.

Quad	$M(G/\mu V)$		$R(G)$		$S(\mu V)$	
No.	-ve	+ve	-ve	+ve	-ve	+ve
Q1DB	0.8525	0.8501	2.9790	-1.1944	-3.4943	1.4049
Q1DT	0.8603	0.8608	-3.9832	8.9446	4.6301	-10.3904
Q2DT	0.8597	0.8599	-2.1380	12.0152	2.4871	-13.9732
Q3DT	0.8513	0.8499	5.2808	2.7944	-6.2033	-3.2879
Q4		͘ 588	2.6761	0.0309	-3.5283	-0.0407
Q5		˙˙8	-1.1590	-0.0448	1.5445	0.0598
Q7		˙2.7	-0.5752	-1.4937	0.6235	1.6206
Q8		˙.9231	-0.7453	1.9489	0.8078	-2.1111
Q9	0.˙˙˙˙	0.9031	-1.˙751	0.0045	1.5227	-0.0050
Q10	0.9194	0.9195	1.5977	-4.5000	-1.7377	4.8937
Q11	0.9031	0.9019	-3.9721	2.0288	4.3988	-2.2496
Q12	0.9169	0.9159	-7.1670	1.0127	7.8165	-1.1058

to the $M X$ term of the fit where the Hall voltage, X, is in a range of 650 to 6400 μV [A1]. According to the theoretical explanation, constants R and S should be zero. But, the calibration was done by fitting the experimental data to a linear fit as shown in eqn. (A.5) for higher accuracy, which results in non-zero values for R and S.

It is only meaningful to compare the M values in the two calibrations. As a measure of the difference between the two calibrations, the quantity, [M(new)/M(old) - 1], has been calculated for both polarities of each Hall probe, and the results are given in table A.4. From this comparison it is clear that the calibrations of Hall probes installed in quadrupoles which are located in the cyclotron vault have changed significantly. Since the vault is a high radiation environment, this change is probably due to radiation damage in these probes. The calibrations of the rest of the Hall probes are considered to be unchanged.

The calibrations presented here relate the magnitude of the magnetic field measured at the location of the Hall probe, to the magnitude of the maximum Hall voltage. The actual quantity of interest in beam transport calculations is the poletip field strength of

52

Table A.3: Hall probe calibration done in November 1986.

Quad	M(G/μV)		R(G)		S(μV)	
No.	-ve	+ve	-ve	+ve	-ve	+ve
$Q1DB$	0.8302	0.8276	-3.2873	4.5241	3.9596	-5.4668
$Q1DT$	0.8429	0.8421	11.0397	14.6467	-13.0976	-17.3927
$Q2DT$	0.8567	0.8543	11.6580	-16.0630	-13.6086	-18.8031
$Q3DT$	0.8472	0.8455	-0.6536	6.1531	0.7716	-7.2778
$Q4$	0.7578	0.7572	-3.6074	2.6788	4.7605	-3.5377
$Q5$	0.7489	0.7481	0.8657	3.1065	-1.1559	-4.1527
$Q7$	0.9216	0.9205	1.1067	1.4722	-1.2009	-1.5994
$Q8$	0.9228	0.9224	2.1947	1.9105	-2.3782	-2.0713
$Q9$	0.9032	0.9020	2.5842	1.7516	-2.8612	-1.9419
$Q10$	0.9193	0.9189	-1.8323	-4.6096	1.9932	5.0166
$Q11$	0.9027	0.9013	5.4216	4.3508	-6.0060	-4.8270
$Q11$	0.9148	0.9144	8.2793	6.8910	-9.0508	-7.5359

the quadrupole. Since the Hall probe is not located exactly at the poletip in the practical setup, a small correction, which is explained later, has to be made for this geometric effect. Also, the sign of the field strength must be in agreement with standard beam transport notation, namely, that a horizontally-focusing quadrupole should have a positive field strength, and a horizontally-defocusing quadrupole should have a negative field strength. Geometric factors with corresponding sign coefficients for each quadrupole are given in table A.5.

The origin of the geometric factor is illustrated in fig. A.3. What we want is the field strength at point A (the poletip), but the Hall probe is actually located at point C. By moving the Hall probe on its mounting jig, between points C and D, it is empirically found that the magnetic field strengths at these two points are related by [A3]

$$B(D) = 0.8759 \times B(C).$$ (A.6)

For a standard TRIUMF 4-inch diameter quadrupole (4Q14/8), the actual radius of the pole-tip is 2.030" from the axis (distance OA). Point D is 0.070" away from the

Table A.4: The difference between the two Hall probe calibrations done in 1992 and 1986.

Quad No.	-ve polarity	+ve polarity
$Q1DB$	0.0269	0.0272
$Q1DT$	0.0207	0.0222
$Q2DT$	0.0035	0.0070
$Q3DT$	0.0048	0.0052
$Q4$	0.0009	0.0020
$Q5$	0.0019	0.0023
$Q7$	0.0010	0.0013
$Q8$	-0.0002	0.0008
$Q9$	-0.0002	0.0012
$Q10$	0.0001	0.0007
$Q11$	0.0003	0.0006
$Q12$	0.0023	0.0017

Note: The   dimensionless   quantities   given   in   this   table   are   calculated   as
$[M(new)/M(old) - 1]$

$AD = 0.1778$ cm

$OA = 5.1562$ cm
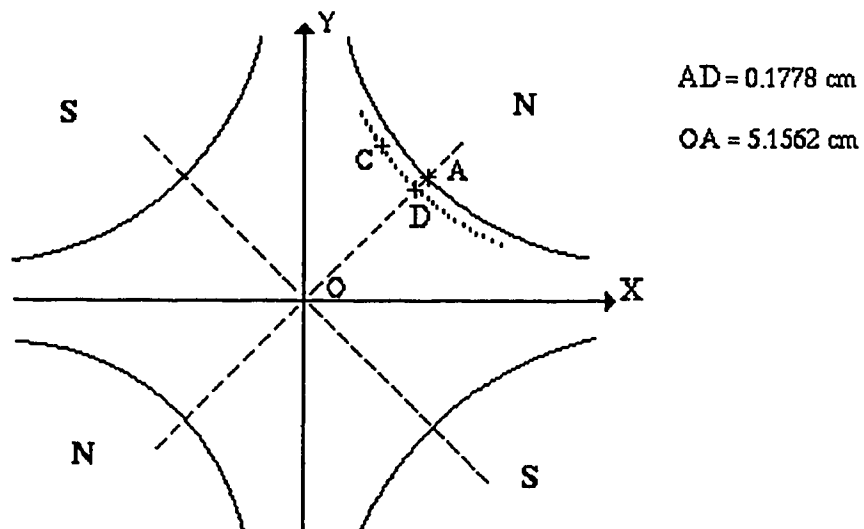
Figure A.3: Exact location of the Hall probe sensor element in the quadrupole.

Table A.5: Geometric factors for each quadrupole.

Quad	Geometric Factor (G)
$Q1DB$	-0.9072
$Q1DT$	-0.9072
$Q2$	-0.9072
$Q3$	-0.9072
$Q4$	-0.9083
$Q5$	-0.9083
$Q7$	-0.9083
$Q8$	+0.9083
$Q9$	+0.9083
$Q10$	+0.9083
$Q11$	-0.9083
$Q12$	+0.9083

poletip A, and thus experiences a field which is smaller than the pole-tip field by a factor of $(2.030 - 0.070)/2.030 = 0.9655$, so

$$B(A) = B(D)/0.9655 \qquad\qquad (A.7)$$

and thus, from equations (A.6) and (A.7),

$$B(A) = (0.8759/0.9655)\, B(C) = 0.9072 \times B(C) \qquad\qquad (A.8)$$

or, $\qquad\qquad B(poletip) = 0.9072 \times B(probe).$

This geometric factor is correct only for the quadrupoles in the vault (Q1, Q2 and Q3), whose Hall probe mounting jigs are anodized. The jigs on the other quadrupoles are not anodized and require mylar tape to insulate them from the ground. The thickness of this mylar tape is approximately 0.0023", and thus the factor in the eqn. (A.8) becomes (2.030-0.0723)/2.030=0.96438, and hence

$$B(A) = (0.8759/0.96438)\, B(C) = 0.9083 \times B(C) \qquad\qquad (A.9)$$

or, $\qquad\qquad B(poletip) = 0.9083 \times B(probe).$

The following algorithm is used for determining the pole-tip field strength of the quadrupoles located on the beam line 4B.

1. Let V be the Hall voltage in microvolts (the quantity displayed as raw data on the TELTERM screen).

2. Let M(+) and M(-) be the appropriate M coefficients for positive and negative polarities, respectively, from table A.1.

3. Let R(+) and R(-) be the appropriate R coefficients for positive and negative polarities, respectively, from table A.1.

4. Let G be the appropriate geometric coefficient from table A.5.

5. Let S be the sign coefficient from table A.5, to make the polarity of the quadrupole field strength agree with TRANSPORT convention.

A program computes the poletip magnetic field strength BFIELD for all the quadrupoles except Q1 using the following algorithm:

56

```
IF V<0 THEN
    VABS = ABS(V)              ! absolute value of voltage
    Z = M(-) * VABS + B(-)     ! absolute value of mag field
    BFIELD = -Z * G * S        ! signed value of mag field
ELSE
    VABS = ABS(V)              ! absolute value of voltage
    Z = M(+) * VABS + B(+)     ! absolute value of mag field
    BFIELD = Z * G * S         ! signed value of mag field
ENDIF
```

The new calibrations (1992) and this algorithm are incorporated on TELTERM page 4K. The corresponding old page 4P retains the 1986 calibrations. The quadrupole Q1 contains of two Hall probes. The reason is that Q1 also has a built-in vertical steerer 4VSM0; the two top poles have a different pole-tip field strength than the two bottom poles in order to produce a dipole field in the horizontal direction. The quadrupole field strength is determined by taking the arithmetic mean of the BFIELD values of the two Hall probes, which measure the field at one top and one bottom pole. The calibration of the MRS quadrupole is found elsewhere [A1].

Appendix B

Rawson-Lush Gaussmeter for Magnetic Fields

B.1 The Aim of Project

The spectrometer system in the proton hall at TRIUMF has become well equipped with the newly constructed second arm spectrometer (SASP) [B1]. This is pivoted at the T2 location on beamline 4B so that it can operate in conjunction with the existing medium resolution spectrometer (MRS), forming the dual arm spectrometer (DASS). SASP can also be used as a single arm spectrometer.

A separate project was carried out in order to use a Rawson-Lush gaussmeter for measuring the magnetic field of the SASP dipole. In this project, a program was developed in VAX/FORTRAN to check the value of this field from time to time to ensure that the magnetic field remains constant in the course of an experiment. A Slo-Syn stepping motor indexer is utilized to move the measuring probe to a standard position in the magnetic field. This probe is a Rawson-Lush rotating coil gaussmeter (RL probe). The system was installed on the dipole in such a way that the RL probe could be driven into the dipole field with an inclination of 45 degrees to the vertical in its bend plane. The RL probe carries a small rotatable coil at its end which is rotated at a known frequency by an electric motor attached to the opposite end of the probe. When this coil is rotated at a point in the magnetic field, the rate of change of magnetic flux through the coil is read as an electrical

signal by a digital voltmeter according to Faraday's law,

$$V = -\frac{d\Phi}{dt}$$

(B.1)

where V is the induced voltage and Φ is the magnetic flux in the coil. The medium resolution spectrometer (MRS) at TRIUMF has a homogeneous magnetic field so that the magnetic field can be monitored by means of an NMR (nuclear magnetic resonance) probe system with greater precision. Since the SASP dipole magnetic field is nonhomogeneous, the NMR probe method cannot be applied in this case. Consequently, the present convenient method (RL probe method) has been sought to overcome this difficulty. A CAMAC system is used to operate the instrument remotely from the data counting room which is well outside the nuclear experimental area. This is basically the procedure which will be used by the experimenter to check the SASP dipole magnetic field in the course of an experiment.

The whole instrument is entirely operated by a special software program enabling the experimenter to monitor the magnetic field of the dipole at any moment during the experiment. The RL probe can be driven into the magnetic field along a straight line in the bend plane through a distance of up to 40 cm with bellows installed, and another 40 cm in the same direction without bellows. The bellows is essential to preserve the vacuum inside the SASP dipole. Using this experimental setup along with the software program developed, we have commissioned the system and measured the field variation along a straight line in the bend plane of the SASP dipole magnetic field as a function of linear travel distance of the RL magnetic probe.

B.2   User Facilities

The normal data acquisition system must be stopped while the magnetic probe is being driven into the dipole field, otherwise bad data will be collected due to the scattering of particles by the probe itself. Thus, the zero reference point where the probe starts moving also must lie well outside the beam envelope. The experimenter is given an option to re-index the magnetic probe to its zero position. This is actually necessary only if there has been a power failure which causes the indexer to "forget" its position. Otherwise the probe always returns to its zero point at the end of each measurement.

B.3 Operational Procedure of the System

The RL probe is fixed to the Slo-Syn stepping motor indexer which is operated by a computer controlling system. The position of the probe is determined in two ways: using the Slo-Syn stepping motor indexer system and an optical shaft encoder device, and these two values are expected to be equal for a precise measurement. Three different CAMAC modules, namely a Four Channel RS232 Communication Interface and two 6 Decade BCD Display Scalers are utilized for reading the Slo-Syn indexer , optical shaft encoder, and the field sensing digital voltmeter readout, respectively. Thus it is possible to read both the magnetic field and the location of the RL probe position at the same time. Fig. B.1 represents the experimental set-up which is used to measure the magnetic field at a particular point. The hardware indexer basically consists of a pulse-stepping motor which is activated by the pulse signals sent through RS232 computer device with the Slo-Syn computer controlling system. The movable carriage through the ball screw holds the probe which is to be driven into the magnetic field. Consequently, the RL probe could be moved back and forth according to the experimenter's requirements with certain types of parameters defined in the Slo-Syn software program.

The RS232 parameters and commands used in the afformentioned Slo-Syn software package can be grouped into three general categories: L Codes, H Codes, and Line Data Codes. L Codes are used to set parameters for each indexer. These commands do not cause motion of the probe, but simply establish the motion parameters. H Codes are used to set indexer modes, to control manual motion and program execution, and to transmit parameters and indexer status via the serial communications port. The third category is Line Data Codes that define the motion that will be made when a cycle start is executed and sets the speed at which it will be done.

B.4 Coupling to Data Acquisition System

The program developed is used to couple the operation of the RL probe system to the data acquisition system which runs the experiment. In this way, the experimenter in the counting room can read the dipole magnetic field by invoking the program (see figs. B.1 and B.2). The detailed program is found in Appendix C. This program is able to control the entire Slo-Syn index system through CAMAC where three different CAMAC

60
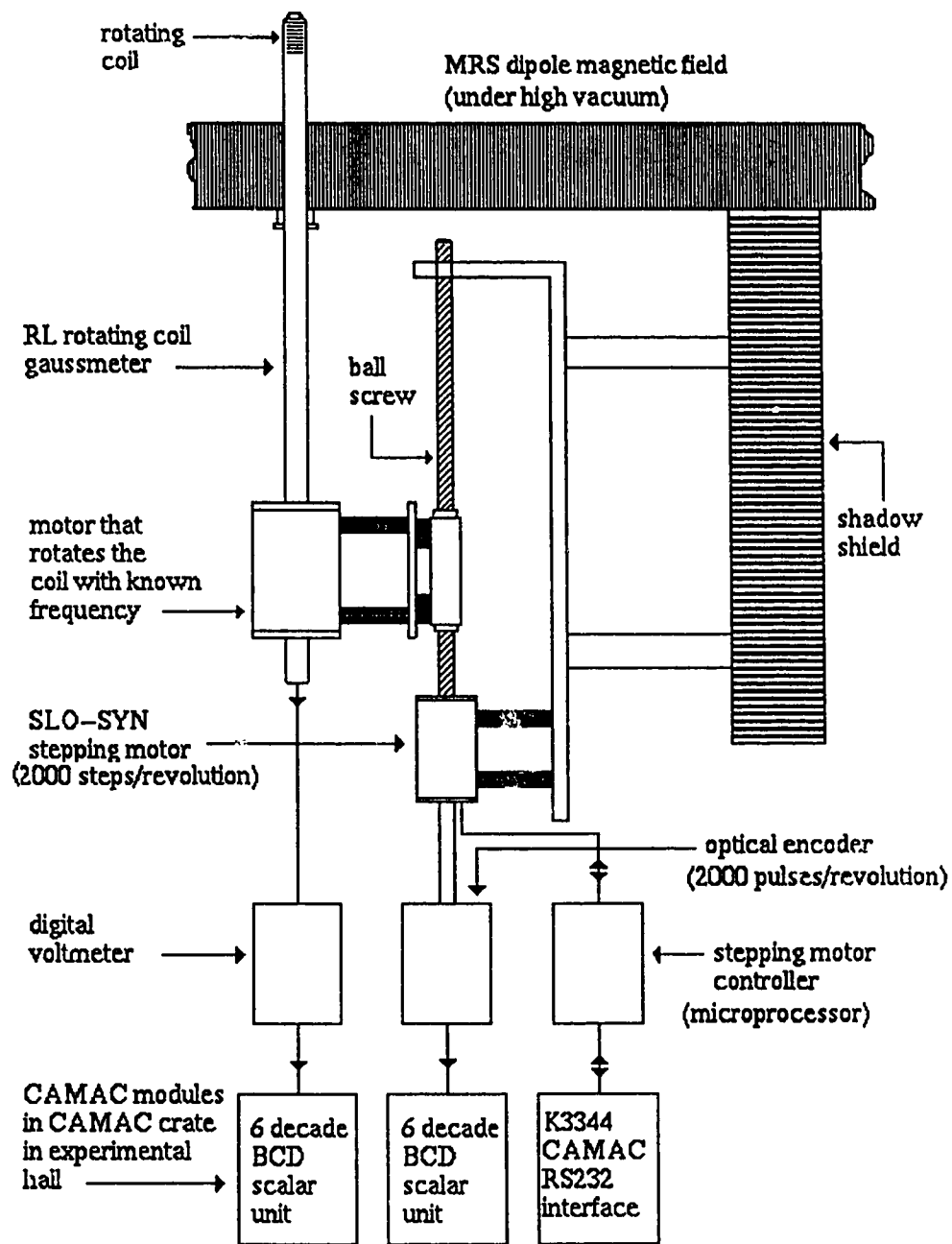
Figure B.1: A schematic diagram of the RL probe system.

61

modules are addressed, and to display the magnetic field of the SASP dipole on the host computer terminal in the counting room.

This program has been developed in such a way that when it is executed, it will drive the RL probe from a zero reference point which is outside the beam envelope up to 40 cm inside the dipole along a straight line in the bend plane. The probe then stays at this position until the user tells the program that no more measurements are desired, and returns back to its initial position. We have also developed a second program which could be used to modify the above mentioned measuring procedure, and is to be executed only by the experts. This second program allows experts to have access to L Codes, H Codes, and Line Data Codes, which can be changed to alter the measuring procedure according to their requirements. For example, one can alter the dynamic characteristics of the probe system such as the moving speed of the magnetic probe, moving distance and the acceleration and deceleration and so on. As a result, we have measured the variation of the magnetic field of the SASP dipole clam shell along the straight line in the bend plane starting from zero reference with zero magnetic field up to 80 cm, and recorded the results.

B.5   Four-Channel Communication Interface (K3344)

The Kinetics model 3344 is a single-width CAMAC module that interfaces the CAMAC dataway to as many as four separate RS-232 serial ports. Out of the sixteen data rates available in this module, we have used 9600 baud rate in our program to set up the configuration word #2 with eight data bits, one stop bit and no parity. Two buffers are provided for each channel with capacities of 1024 characters, one for input and one for output. Communications between the dataway and remote devices are provided by these buffers. As a diagnostic aid, input can be echoed back to the output as well as sent to the computer. This echo feature is programmable. On output block transfers, the buffer is filled by performing write commands until a Q=0 response is detected which indicates that the buffer is full. We are not using the LAM capability of the module, instead the program issues CAMAC read commands to read one word at a time from the output buffer until the buffer is empty (see appendix C). A Q=0 response means that either the input buffer is empty or that the End-of-Block character has been read. In our program, we have specified a single bit pattern using this software-selectable End-of-Block

62
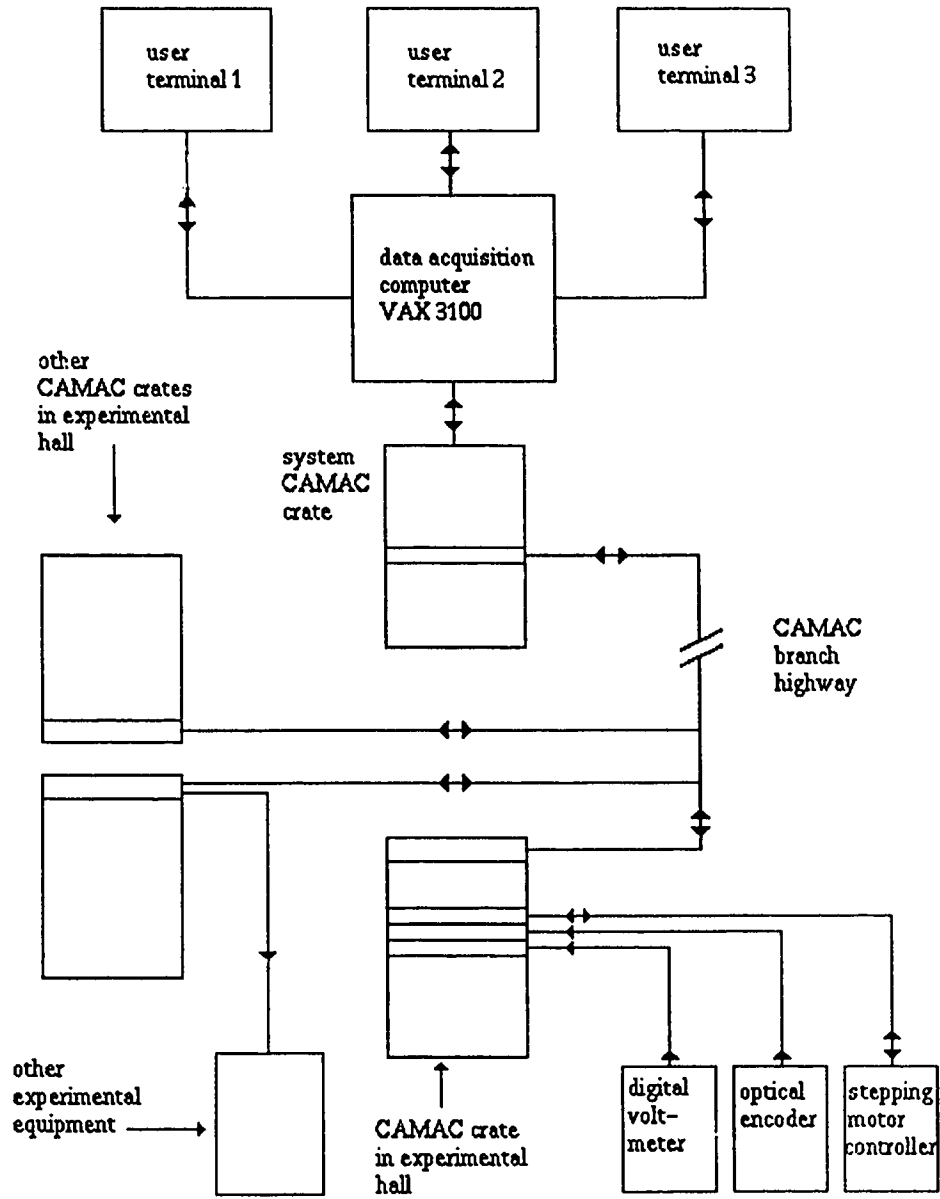
Figure B.2: The RL probe readout after coupling to the data acquisition system.

63

EMITTER   CODE WHEEL   PHASE ENCODER   MOUNTING
END PLATE   ASSEMBLY   PLATE   BODY   SURFACE
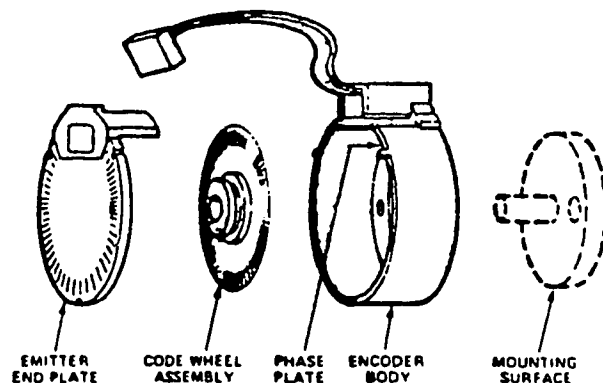
Figure B.3: Major parts of the optical shaft encoder device.

character such that if the bit fifteen is 1 then End-of-Block character is encountered. The
XON/XOFF protocol can be enabled and disabled from the dataway, and once enabled,
this protocol performs a software handshake with the remote RS-232 device. For this
reason, the configuration word #1 has been set in the program such that bit fifteen is ON,
and it clears UART, buffers, and etc [B2]. This CAMAC module is used to interface the
Slo-Syn RS-232 remote device to the data acquisition system so that the host computer
terminal can be used directly to talk to the Slo-Syn indexer.

B.6 Optical Shaft Encoder Device

The optical shaft encoder device has been rigidly connected to the rotating shaft
of the pulse-stepping motor, is a 56 mm diameter package consisting of three major parts,
namely; an encoder body, a metal code wheel, and an emitter end plate (see fig. B.5).

An LED source and lens transmit collimated light from the emitter module through
a precision metal code wheel and phase plate into a bifurcated detector lens. The light
is focused onto pairs of closely spaced integrated detectors which output two square wave
signals in quadrature, and an index pulse. Collimated light and a custom photodetector
configuration increase long life reliability by reducing sensitivity to shaft end play, shaft
eccentricity, and LED degradation. The output and the 5V supply input are accessed

64
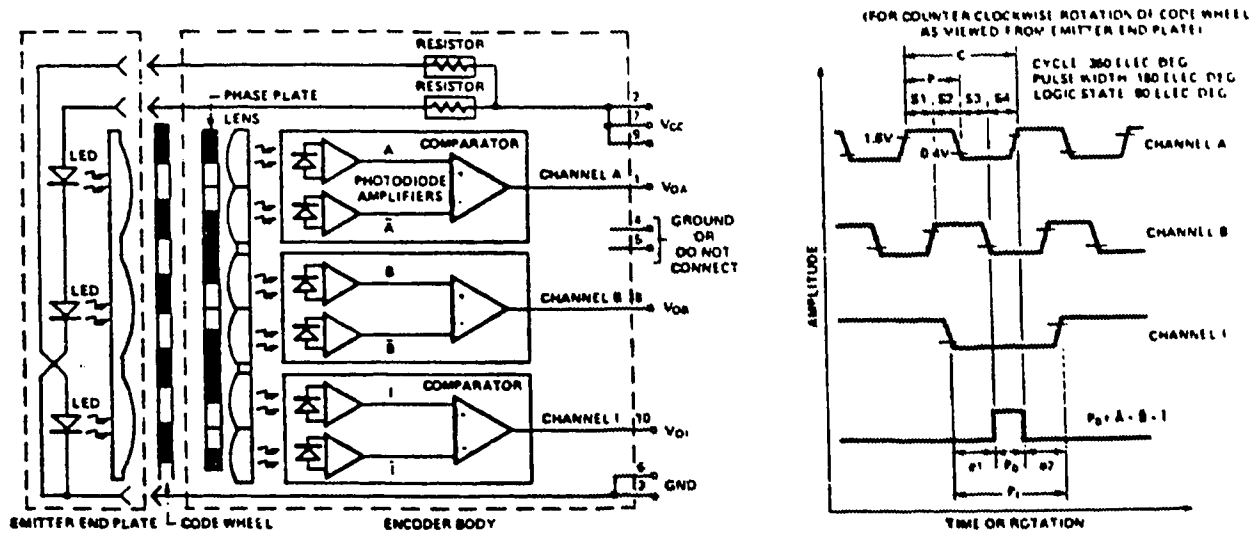
Figure B.4: Block diagram of the encoder electronic circuitry and output waveforms.

through a 10 pin connector mounted on a 0.6 metre ribbon cable.

B.7 Operation of the Encoder

The incremental shaft encoder operates by translating the rotation of a shaft into light beam pulses which are then converted to electrical pulses. In this device, the light source is a light-emitting diode collimated by a molded lens into a parallel beam of light. The emitter end plate is functioning with three light sources, one for each channel in this configuration.

The standard code wheel is a metal disc which has 1000 equally spaced slits around its circumference. An aperture with a matching pattern is positioned on the stationary phase plate. The light beam is transmitted only when the slits in the code wheel and the aperture line up; therefore, during a complete shaft revolution, there will be 1000 alternating light and dark periods. This modulated light is focussed into a silicon detector by a molded lens beneath the phase plate. The detection system and the phase plate are contained in the encoder body. The detection element for each channel consists of an integrated circuit with two photodiodes and amplifiers, a comparator, and output circuitry. See fig. B.4.

65

The apertures for the two photodiodes are positioned so that a light period on one detector corresponds to a dark period on the other. The photodiode signals are amplified and fed to the comparator whose output changes state when the difference of the two photo currents changes sign ("push-pull"). The second channel has a similar configuration but the location of its aperture pair provides an output which is in quadrature to the first channel (phase difference of 90 degrees). Direction of rotation is determined by observing which of the channels is the leading wave form. The outputs are TTL logic level signals. An index pulse of typically 1 cycle width is generated for each rotation of the code wheel, and thus a unique logic state (p) could be identified using a logic interface.

B.8 Position in the Magnetic Field

In this magnetic probe system, two measuring devices have been used (the Slo-Syn indexer itself and the optical encoder) to make two independent precise measurements of the shaft rotation. The probe itself is an aluminium metal rod which is 185 cm long with a diameter of 1.5 cm. The magnetic field sensing coil, which is 3 cm in length inside the probe at its end. This inner rod is protected by another cylindrical metal tube of the same length. The opposite end of the probe is fixed to an electric motor which rotates the coil with a known frequency so that the rate of change of magnetic flux is directly converted to an electric current signal which is read by means of a digital voltmeter. The digital Voltmeter is calibrated to give a BCD (binary code decimal) output of the magnetic field in Kilogauss. Thus a separate CAMAC scalar module is used to read the BCD output of the digital Voltmeter.

The pulse stepping motor completes one shaft revolution with 2000 Slo-Syn pulses, and drives the probe up to one fifth of an inch in its linear travel in either direction. The optical encoder operates simultaneously to measure the travel distance of the probe using a BCD scalar. The travel distance from both devices should be equal for a precise operation of the system. These two independent measurements of the probe position are required to agree with each other to within 0.004 inches, or an error message is output by the program. This is acceptable since there can be a very slight backlash of the Slo-Syn motor rotation. The program feeds this information to the data acquisition system of the experiment so that the magnetic field of the spectrometer can be monitored in the counting room.
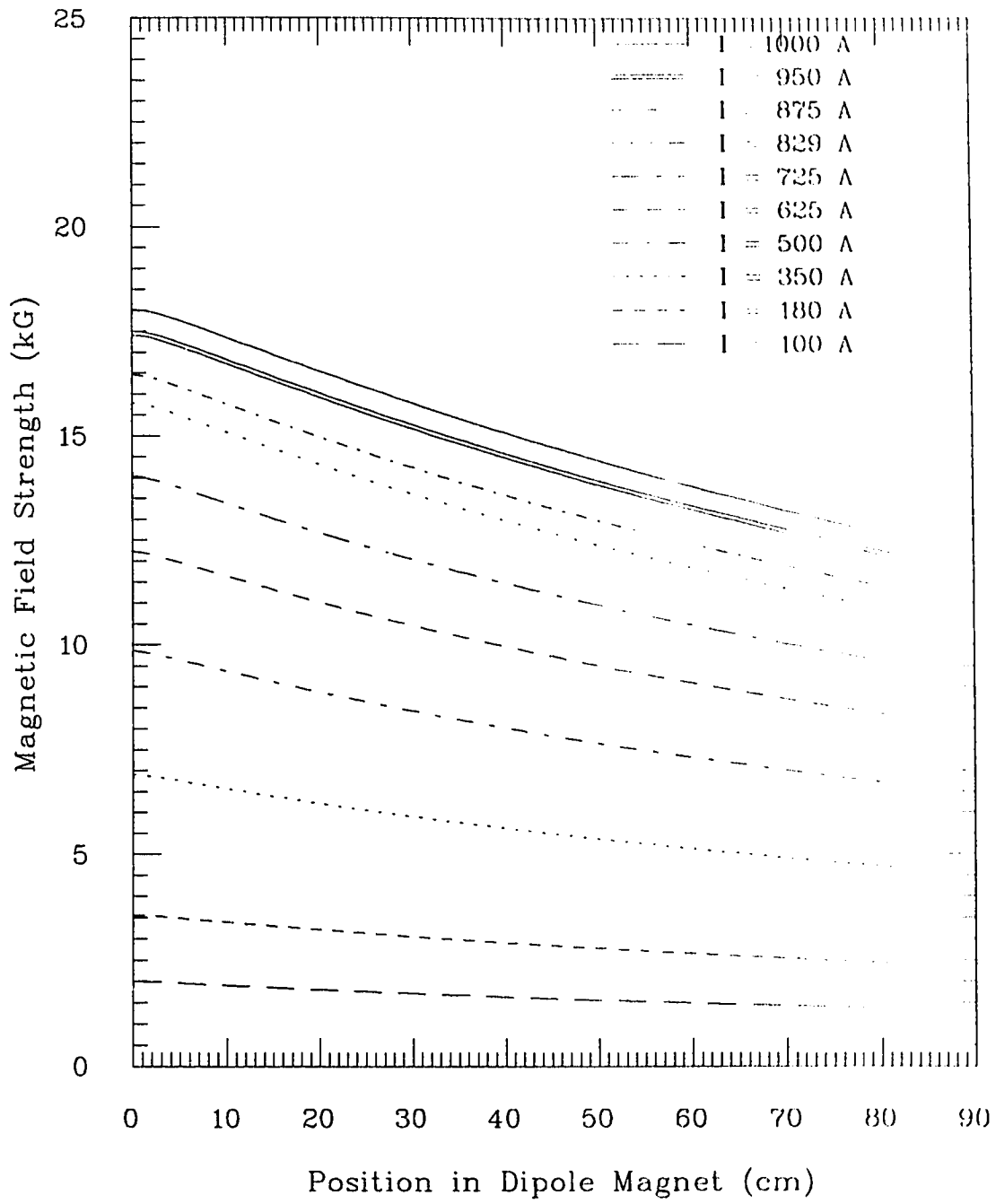
Figure B.5: Field variation in the SASP dipole magnet for different current values in the coil. Field is measured as a function of linear travel of the RL probe.

The magnetic field was measured as a function of the probe position inside the SASP dipole. These measurements were taken for different currents in the coil of the main magnet. Variation of the magnetic field strength is shown in fig. B.5. These measurements were taken using the computer code (see Appendix C) that operates the whole system in reading the magnetic field.

Appendix C

Computer Code for RL-Gaussmeter

```
C       file  RL_STAN.FOR
C       modified version of RL_SENA.FOR.
C       Authors:  Munasinghe Punyasena and Stanley Yen
C       Last update: June 23, 1993
C
C       compile:  FOR RL_STAN
C       link:     LINK RL_STAN,KOST$DIR:LIB/LIB
C
C       This program is used to read the SASP dipole magnetic
C       field  strength  at  a  given  reference  point.  The
C       Rawson-Lush rotating coil gaussmeter ('RL probe')  is
C       initially positioned out of the dipole  field, at the
C       'mechanical home'  position  of  the Slo-syn stepping
C       motor.  When  the   dipole  field  is  to  be   read,
C       the Slo-syn stepping  motor  moves the RL probe in to
C       the reference position.
C
C       There are two independent measures of the position of
C       the RL probe. (1) The  Slo-syn  stepping motor counts
C       the  number  of  steps  from  the  'electrical  home'
C       position,  which  is  set  to  be  the    same  as the
C       'mechanical  home'  position.  The  'electrical home'
```

```
C       is just a software 'home'. The 'mechanical  home' is
C       defined  by the logical AND of the upper  microswitch
C       and  the  zero  point  of  the optical  encoder.  The
C       Slo-syn steps 2000 steps for each turn  of the shaft.
C       (2)  The optical encoder also outputs 2000 pulses for
C       each  turn of the  shaft, and the scaler which counts
C       these pulses is zeroed by the 'mechanical home' pulse.
C       Thus, both  devices  should  read  the  same position
C       unless  there  is some backlash or unless the Slo-syn
C       misses steps. We take the maximum tolerable difference
C       between X and XPOS
C       to be 0.005 inches, where
C               X=SLOSYN POSITION
C               XPOS=OPTICAL ENCODER POSITION.
C       ----------------------------------------------------
C       This  set  of  L  parameters  has  been found to wor'
C       These  may  be  viewed, and changed, with the progra..
C       TESTK3344.
C
C       L06 1              L07 0000          L08 +
C       L09 0008000        L11 00003000      L12 0000020
C       L13 00000009       L14 0001000       L16 00000000
C       L17 +00000000      L18 +12000        L19 -153000
C       L20 0              L21 01            L22 9600
C       L23 8              L25 1             L26 0
C       L42 2000           L43 0000          L44 0050
C       L47 00000000       L49 00            L50 00
C       L52 000            L55 000           L56 000
C       L57 004            L66 -00001000     L67 0
C       L70 010            L71 00115000      L72 2
C       L73 00000100       L98 100
C       ----------------------------------------------------
        PROGRAM SASP_DIPOLE_FIELD
C
```

```fortran
      IMPLICIT     NONE
      LOGICAL      START,IERR,CHR_PRESENT,FINISHED
      CHARACTER*1  ICHR,STRING2,ANS
      CHARACTER*3  CBACKSTEPS,CREFSTEPS,CCORR
      CHARACTER*14 COMMANDSTRING
      INTEGER      COUNT,IERRCON,ERRCON1,ERRCON2,ERRCON3,TIME,
      INTEGER      ICORR, BK, CK, NK, AK, BO, CO,NO,BM,CM, NM,
      INTEGER      IBACKSTEPS, IREFSTEPS
      REAL         X,XPOS,Y,k,K1,XREF,BFIELD,TOLDIFF,XCORR
C
C      Common block for address of K3344 RS-232 interface unit
      COMMON/K3344/BK,CK,NK,AK
C      Common block for address of SCALER for optical encoder
      COMMON/OPTIC/BO,CO,NO
C      Common block for  address of SCALER for  magnetic field
C      readout
      COMMON/MAG/BM,CM,NM
C      ---------------------------------------------------------
C      This  section  is  for  changes in   device  addresses,
C      reference positions,  and  tolerances. This is the only
C      location in the program  where such changes need to  be
C      made.
C      Now  assign CAMAC  addresses  for  the various  devices
C      This is the only  place  where the changes in addresses
C      need to be made
C      ADDRESS FOR K3344
      BK=7   ! BRANCH 7
      CK=6   ! CRATE  6
      NK=15  ! SLOT    15
      AK=0   ! SUBADDRESS 3
C
C      Address for SCALER for optical encoder
      BO=7   ! BRANCH 7
      CO=6   ! CRATE  6
```

71

```
       NO=17 ! SLOT    17
C
C      Address for SCALER for magnetic field
       BM=7   ! BRANCH 7
       CM=6   ! CRATE  0
       NM=18  ! SLOT    18
C
C      Reference position  where B-field needs to be measured;
C      this is the only place  in  the program where  it needs
C      to be changed if  a  different  value  of the reference
C      point is adopted.
       XREF=15.00000  ! in inches
C      Tolerable  difference   between   Slo-Syn  and optical
C      encoder positions
       TOLDIFF=0.005  ! inches
C      ---------------------------------------------------------
C      Number of Slo-syn pulses need to move prob to reference
C      point; the  Slo-syn  takes  2000 steps per revolution of
C      the shaft, and the shaft  has a screw pitch of 5 threads
C      per inch,  so 10000 Slo-syn steps results in one inch of
C      travel for the RL-probe
C      Number of  Slo-Syn  steps to reference point in magnetic
C      field
       IREFSTEPS=IFIX(XREF*10000. + 0.5)
C      Number  of  Slo-Syn  steps for H06 command to retract RL
C      probe out of the magnetic field.
C      We  want to retract to within 0.5 inch of the mechanical
C      home  at  high  speed using the H06 command, and then go
C      the  remaining  inch  at  low speed using the mechanical
C      home cycle, for a precise relocation of mechanical home.
       IBACKSTEPS=IFIX((XREF-0.5)*10000. +0.5)
C      Initialize  the  CAMAC  module  for  the  SLO-SYN motor
C      controller
       CALL INIT_K3344
```

72

```fortran
C           Check that the SLO-SYN is ready to accept commands within
C           2 seconds
            CALL TEST_SLOSYN_READY(2,IERRCON)
            IF(IERRCON.NE.0)THEN
                  PRINT*
                  PRINT*,'SLO-SYN CONTROLLER NOT RESPONDING'
                  PRINT*,'CHECK POWER TO SLO-SYN'
                  CALL RINGER(6)
                  STOP
            ENDIF
C           We have received '=' response from the SLO-SYN
            PRINT*
            PRINT*,'               MAGNETIC FIELD OF THE SASP DIPOLE'
            PRINT*,'               =============================='
            PRINT*
            PRINT*,'After a power interruption,'
            PRINT*,' the RL probe must be re-indexed'
            FINISHED=.FALSE.
            DO WHILE(.NOT.FINISHED)
                PRINT*,'Do you want to re-index the RL probe [y/n]?'
                ACCEPT 1,ANS
1               FORMAT(A1)
                IF((ANS.EQ.'Y').OR.(ANS.EQ.'y'))THEN
C                           first move the RL probe out 1.5 inches
                            CALL OUTPUT_STRING('L13 15000')
                            CALL OUTPUT_STRING('H07')
                            CALL TEST_SLOSYN_READY(30,IERRCON)
C                           Then initiate mechanical home cycle
                            CALL MECHANICAL_HOME(IERRCON)
                            FINISHED= TRUE.
                ELSEIF((ANS.EQ.'N').OR.(ANS.EQ.'n'))THEN
                            FINISHED=.TRUE.
                ELSE
                            PRINT*,'????? - unknown response'
```

73

```
        ENDIF
      ENDDO
C
C     Read the current position of the RL probe
      CALL READ_POSITION(X,XPOS) !X = position by Slo-Syn
C                                !XPOS = position by Encoder
C     If  both  the  optical  encoder  and  the Slo-syn read
C     positions of zero, we assume that the probe is already
C     at  mechanical home.  Otherwise,  we   ask  the  probe
C     to  go   through the mechanical home cycle.
      IF ((X.NE.0).OR.(XPOS.NE.0))THEN
            PRINT*
            PRINT*,'Starting position of RL probe not zero'
            PRINT*,'RL probe reads to be re-indexed'
            PRINT*,'Mechanical home cycle initiated'
C     first move the RL probe out 1.5 inches
            CALL OUTPUT_STRING('L13 15000')
            CALL OUTPUT_STRING('H0?')
            CALL MECHANICAL_HOME(IERRCON)
      ENDIF
C     Set the distance that the probe must move into the
C     Slo-syn controller.
C     This distance is XREF inches(IREFSTEPS Slo-syn steps).
      CALL WRITE_CHR_STRING('L13',IREFSTEPS,COMMANDSTRING)
      CALL OUTPUT_STRING(COMMANDSTRING)
      PRINT*
      PRINT*
      PRINT*,'RL Probe is  NOW  being  inserted  into  the'
      PRINT*,' magnetic field'
      PRINT*
C     Tell  Slo-syn  to step CCW by the specified number of
C     steps to insert the RL probe.
C     'H37' enables current boost; the current to the motor
C     coils is boosted by 50% during the first 5 seconds of
```

```
C         acceleration and decceleration;   this has   been
C         observed to decrease the  amount of motor slippage
          CALL OUTPUT_STRING('H37')      ! enable current boost
C         TEST SLOSYN READY AND EMPTY K3344 OUTPUT BUFFER
          CALL TEST_SLOSYN_READY(10,IERRCON)
          CALL OUTPUT_STRING('H07')               ! CCW Direction
C         Allow maximum 60 seconds delay for the probe movement
          CALL TEST_SLOSYN_READY(60,IERRCON)
          IF(IERRCON.NE.0)THEN
              PRINT 200,'INSERTION',60
200           FORMAT(/' ****ERROR****'/
          1   ' RL PROBE ',A10,' NOT CUMPLETED AFTER',I3,' SECONDS'/
          2   ' RL PROBE MAY BE STUCK'/
          3   ' DO NOT RESUME DATA ACQUISITION'/
          3   ' TRY RE-STARTING PROGRAM AND RE-INDEXING, OR'/
          4   ' CONSULT GASP COORDINATOR')
                  CALL RINGER(18)
                  STOP
          ENDIF
C         Read absolute position w.r.t. zero point
          CALL READ_POSITION(X,XPOS)
          Y=XPOS-X
          IF(ABS(Y).LT.TOLDIFF)THEN
            PRINT 230,XPOS
230         FORMAT(//' RL PROBE POSITION =',F8.4,' INCHES')
          ELSE
            PRINT*
            PRINT*,'**** WARNING ****'
            PRINT*,'Optical encoder position=',XPOS,' inches'
            PRINT*,'SLO-SYN position        =',X,' inches'
            PRINT 240,Y,TOLDIFF
240         FORMAT(' Difference =',F8.4,' exceeds ',f8.4,' inches')
            PRINT*,'We will index probe position with optical encoder'
          ENDIF
```

```
Cnow correct  for  the  difference between the position
C        according to  the  optical  encoder  'XPOS'  and   the
C        desired  position  'XREF'  do  this  iteratively until
C        optical encoder position agrees with 'XREF'.
         FINISHED=.FALSE.
         DO WHILE (.NOT.FINISHED)
          XCORR=XPOS-XREF
          ICORR=ABS(XCORR)*10000.+0.5  ! number cf motor steps
            IF(ABS(XCORR).GT.TOLDIFF)THEN
               CALL WRITE_CHR_STRING('L13',ICORR,COMMANDSTRING)
               CALL OUTPUT_STRING(COMMANDSTRING)
               IF(XPOS.GT.XREF)THEN !we've already gone too far
                 CALL TEST_SLOSYN_READY(10,IERRCON)
                 CALL OUTPUT_STRING('H06') :CW motion,
C                                          !retract probe
            ELSE
               CALL TEST_SLOSYN_READY(10,IERRCON)
               CALL OUTPUT_STRING('H07') !CCW motion,
C                                          !insert probe
            ENDIF
            CALL TEST_SLOSYN_READY(30,IERRCON)
            IF(IERRCON.NE.0)THEN
               PRINT 200,'INCREMENT',30
               CALL RINGER(18)
               STOP
            ENDIF
            CALL READ_POSITION(X,XPOS)
            ELSE
               FINISHED=.TRUE.
            ENDIF
         ENDDO  ! end of do loop to correct positions
         CALL READ_POSITION(X,XPOS)
         PRINT*,'POSITION FROM OPTICAL ENCODER=',XPOS,' INCHES'
C        Read the magnetic field strength from the CAMAC scaler
```

76

```fortran
250        CALL READ_MAGNETIC_FIELD(BFIELD,IERRCON)
        IF(IERRCON.NE.0)THEN
          PRINT*,' '
          PRINT*,'**** ERROR ****'
          PRINT*,'WHILE READING B-FIELD, IERRCON=',IERRCON
          PRINT*,'NO VALID READ OF B-FIELD SCALER AFTER 100 TRIES'
          CALL RINGER(6)
        ENDIF
C       Print the magnetic field
           PRINT 255,BFIELD
255     FORMAT(/' SASP DIPOLE FIELD =',F10.4,' kG'/)
C       Give the opportunity to adjust the magnetic field if
C       necessary
        PRINT*
        PRINT*
        PRINT*,'Adjust the dipole current if necessary'
        PRINT*
260     PRINT*,'Do you want to read the magnetic field again '
        PRINT*,'  keeping RL probe at the same position [Y/N]?'
        ACCEPT 2,ANS
2       FORMAT(A1)
        PRINT*
         IF((ANS.EQ.'Y').OR.(ANS.EQ.'y'))THEN
                GOTO 250
         ELSEIF((ANS.EQ.'N').OR.(ANS.EQ.'n'))THEN
                GOTO 300
         ELSE
                PRINT*,'   ????? - unknown response'
                GOTO 260
         ENDIF
C       Probe returns to the original position which should
C       be its mechanical home
300     PRINT*
        PRINT*,'RL Probe is NOW being retracted'
```

```
C          First retract probe to 1 inch from mechanical home,
C          at high speed,          by using the H06 command
           CALL WRITE_CHR_STRING('L13',IBACKSTEPS,COMMANDSTRING)
           CALL OUTPUT_STRING(COMMANDSTRING)
           CALL OUTPUT_STRING('H06')
           CALL TEST_SLOSYN_READY(60,IERRCON)
           IF(IERRCON.NE.0)THEN
                   PRINT 200,'RETRACTION',60
                   CALL RINGER(18)
                   STOP
           ENDIF
C          Now retract the remaining one inch to mechanical home
           CALL MECHANICAL_HOME(IERRCON)
           PRINT*,' '
           PRINT*,'RL probe now retracted to zero position'
           PRINT*,'Resume data acquisition'
           CALL RINGER(1)
           STOP
           END
C          -----------------------------------------------------
C          *    MECHANICAL_HOME      *
C
           SUBROUTINE MECHANICAL_HOME(IERRCON)
C
C          This subroutine makes the SLO-SYN stepping motor go
C          through a mechanical home cycle.  That is, it
C          re-indexes itself by searching  for the 'mechanical
C          home' which is  defined  by the logical AND of the
C          upper microswitch and  the  index  point  on  the
C          optical encoder wheel.
C          Any failure to  complete  the mechanical home cycle
C          will result in the program  stopping, since this is
C          a fatal error.
C          OUTPUT:
```

78

```
C          -------
C          IERRCON        INTEGER*4        RETURN 0 if no error
C

           IMPLICIT NONE
           INTEGER CYCLE,IERRCON
           REAL X,XPOS
           CHARACTER*1 ANS
C          Give  H10 command  to  make  RL  probe  return   to
C          mechanical home
C

           IERRCON=1 ! set error flag unless explicitly cleared
C                    ! later
           CYCLE=0   ! counter  for  iterations  of attempted
C                    ! mechanical home cycle
C
C          First ensure that the L17 parameter (Mechanical home
C          offset)        parameter is 0,      that the mechanical and
C          electrical  homes  will  be  defined  to be the same
C          location.
           CALL OUTPUT_STRING('L17 000000')
           DO WHILE(CYCLE.LE.2)      ! try mechanical home cycle
C                                    ! 3 times
C          First make sure SLO-SYN is  ready  and  K3344 output
C          buffer is empty
  195      CALL TEST_SLOSYN_READY(5,IERRCON)
C          Send 'H10' string to SLO-SYN controller to  activate
C          mechanical home cycle.
           CALL OUTPUT_STRING('H10')
C          Wait until the SLO-SYN finishes its mechanical
C          home cycle, and responds with '='
C
  200      CALL TEST_SLOSYN_READY(150,IERRCON) !wait maximum 150
C                                              !seconds
           IF(IERRCON.NE.0)THEN
```

79

```fortran
      PRINT*
      PRINT*,'****ERROR****'
      PRINT*,'FAILURE TO COMPLETE MECHANICAL HOME CYCLE'
      PRINT*,'AFTER WAITING 150 SECONDS'
      PRINT*,'RL PROBE MAY BE STUCK'
      PRINT*,'PLEASE CONSULT SASP COORDINATOR'
      CALL RINGER(18)
      STOP
      ENDIF
      PRINT*
      PRINT*
C     Read the position of the SLO-SYN and the optical
C     encoder, and check that they both read zero at the
C     end of the mechanical home cycle.
210   CALL READ_POSITION(X,XPOS)
      IF ((X.EQ.0).AND.(XPOS.EQ.0))THEN
C     Successful completion of mechanical home cycle
      PRINT*,'SUCCESSFUL COMPLETION OF MECHANICAL HOME CYCLE'
      IERRCON=0
      RETURN
      ELSE
C     One of Slo-Syn and optical encoder not reading zero
      IERRCON=1
      PRINT*
      PRINT*,'**** ERROR ****'
      PRINT*,'Error on termination of mechanical home cycle'
      PRINT*,'Probe position is not zero'
      PRINT 205,X,XPOS
205   FORMAT(/' Stepping motor position =',F10.4,' inches'/
     2       ' Optical encoder postion =',F10.4,' inches')
      TYPE *,'TRY READING POSITION ENCODERS AGAIN?'
      ACCEPT 215,ANS
215   FORMAT(A1)
      IF(ANS.EQ.'Y'.OR.ANS.EQ.'y')GOTO 210
```

```
              PRINT*,'Program will try to reset mechanical home again'
C        Move the RL probe 1.5 inches away from mechanical home
            CALL OUTPUT_STRING('L13 15000')
            CALL OUTPUT_STRING('H07')
         ENDIF
         CYCLE=CYCLE+1
         ENDDO  ! END OF DO WHILE (CYCLE.LE.2)
C        Failure to set both position counters to zero after 3
C        mechanical home attempts
         PRINT*
         PRINT*,'Failure in mechanical home cycle'
         PRINT*,'Cannot find zero position after',CYCLE,' tries'
         PRINT*,'Please consult the SASP coordinator'
         STOP
         END
C        -------------------------------------------------------


C        *        INIT_K3344        *
C
         SUBROUTINE INIT_K3344
C        Subroutine to initialize the KINETICS 3344 RS-232 CAMAC
C        INTERFACE
         IMPLICIT NONE
         LOGICAL               Q
         CALL GEC$INTENT ()
C        Initialize the model 3344 unit
C        F(0)A(i) FOR i=0,1,2,3 TO clear UART, FIFO buffers,
C        error
C        status
C        register, and resets  XON/XOFF circuitry for channel i.
         CALL ACCESS_K3344 (0, 9, 0, Q) !Clear UART, buffers, etc.
         CALL ACCESS_K3344 (1, 9, 0, Q)        !Clear UART, buffers, etc.
         CALL ACCESS_K3344 (2, 9, 0, Q)        !Clear UART, buffers, etc.
         CALL ACCESS_K3344 (3, 9, 0, Q)        !Clear UART, buffers, etc.
```

```
C                             A   F  IDAT  Q
C      F(17).A(i) writes configuration word 1 for channel i,
C      i=0,1,2,3
C      Set Config Word #1 to the following:
C      Bit15 = ON (Xon/Xoff protocol ON)
       CALL ACCESS_K3344 (0, 17, '4000'x, Q)
       CALL ACCESS_K3344 (1, 17, '4000'x, Q)
       CALL ACCESS_K3344 (2, 17, '4000'x, Q)
       CALL ACCESS_K3344 (3, 17, '4000'x, Q)
C                                 F    IDATA   Q
C      F(17).A(i+4) writes configuration word 2 for channel i,
C      i=0,1,2,3
C      Set config word #2 to:
C        9600 baud rate
C        8 data bits
C        1 stop bit
C        No parity
       CALL ACCESS_K3344 (4, 17, '00BE'X, Q)
       CALL ACCESS_K3344 (5, 17, '00BE'X, Q)
       CALL ACCESS_K3344 (6, 17, '00BE'X, Q)
       CALL ACCESS_K3344 (7, 17, '00BE'X, Q)
       RETURN
       END
C      -------------------------------------------------------
C      *   TEST_SLOSYN_READY   *
C
       SUBROUTINE TEST_SLOSYN_READY(NSECONDS,IERRCON)
C      Subroutine to test SLO-SYN and see that it is not busy
C      and ready to accept more commands
C      Input:
C      NSECONDS  INTEGER*4   The number of seconds the program
C                            should continue querying the K3344
C                            before giving up
C      Output:
```

```
C       IERRCON            INTEGER*4   IERRCON=0 If SLO-SYN is ready
C                          IERRCON=1   If SLO-SYN not ready within
C                                      the specified waiting time period
        IMPLICIT    NONE
        INTEGER*4   NSECONDS,IERRCON,LIMIT,COUNT,IDEC,COLON
        LOGICAL     MORE,IEOB,CHR_PRESENT
        CHARACTER*1 ICHR,ANS
C       First empty the output buffer of the k3344
        CALL READ3344_UNTIL_EMPTY
C       Send "<1" to the SLO-SYN
  100   CALL OUTPUT_STRING('<1')
C       Repeatedly search for a  '=' response
C       Each cycle of the DO WHILE has a built-in  wait  of 0.1
C       seconds, so we execute a maximum of NSECONDS*10. cycles
C       of the DO WHILE.
        LIMIT=10*NSECONDS
        COUNT=0
        COLON=0
        MORE=.TRUE.
        DO WHILE(MORE)
                CALL READ3344(ICHR,IEOB,CHR_PRESENT)
                IF(IEOB.OR.(.NOT.CHR_PRESENT))THEN
                        IERRCON=2
                        COUNT=COUNT+1
                        IF(COUNT.GT.LIMIT)THEN
                                MORE=.FALSE.
                        ENDIF
                ELSE IF(ICHR.EQ.'=')THEN ! Ready
                        MORE=.FALSE.
                        IERRCON=0
                ELSE IF(ICHR.EQ.':')THEN ! STILL BUSY
                        IERRCON=1
                        COUNT=COUNT+1
                        COLON=COLON+1
```

```fortran
                     IF(COUNT.GT.LIMIT)then
                              MORE=.FALSE.
                     ELSE
C        If we find ':', the SLO-SYN is busy, so we
C        send another '<1' and try again
                         CALL OUTPUT_STRING('<1')
                     ENDIF
                ELSE ! Some character other than '=' or ':'
                     IERRCON=2
                ENDIF  ! End of checking what character we've read
                CALL LIB$WAIT(0.1)  ! Wait 0.1 Seconds
                IF(MOD(COUNT,60).EQ.0)THEN
                     PRINT*,'wait...'
                END IF
        ENDDO  ! end of do while (more) loop
C               Empty the K3344 output buffer
        CALL READ3344_UNTIL_EMPTY
        IF(IERRCON.NE.0)THEN
                PRINT*
                PRINT *,'**** ERROR ****'
                PRINT *,'AFTER WAITING ',NSECONDS,' SECONDS'
                PRINT*,'SLO-SYN STILL NOT READY TO ACCEPT COMMANDS'
                PRINT*,'SLO-SYN MAY BE HUNG'
                print*,'Please consult the SASP coordinator'
                CALL RINGER(18)
        ENDIF
        RETURN
        END
C       --------------------------------------------------------
C       *        LENGTH        *
C
        FUNCTION LENGTH (STRING)
C       Function to find logical length of character string
C       excluding trailing blanks
```

```
C        Input:
C        STRING          CHARACTER*1 ARRAY
         CHARACTER*(*) STRING
         INTEGER         I, L
         L = LEN (STRING)
         DO I = L,1,-1
            IF (STRING (I:I) .EQ. ' ') THEN
               L=L-1
            ELSE
               LENGTH=L
               RETURN
               ENDIF
         ENDDO
         END
C        ------------------------------------------------------------
C        *         READ3344_UNTIL_EMPTY   *
C
         SUBROUTINE READ3344_UNTIL_EMPTY
C        Subroutine to repeatedly read one characterfrom the K3344
C        output buffer and display it on the terminal, until the
C        buffer is empty
         IMPLICIT        NONE
         CHARACTER*20   OUTSTRING
         CHARACTER*1    ICHR
         LOGICAL                 BAD_READ, CHR_PRESENT, Q
         LOGICAL                 IEOB ! END OF BLOCK CHARACTER
         INTEGER                 NO_CHAR_COUNT
         BAD_READ = .FALSE.
         NO_CHAR_COUNT = 0
         DO WHILE (.NOT. BAD_READ)
            CALL LIB$WAIT (0.015)        ! Wait for 15 milliseconds
            CALL READ3344 (ICHR, IEOB, CHR_PRESENT)
            IF (CHR_PRESENT.AND.(.NOT.IEOB)) THEN
               WRITE (*,999) ICHR
```

```
999            FORMAT('+',A1,$)
               NO_CHAR_COUNT = 0
         ELSE   ! either no character, or end-of-block character
               NO_CHAR_COUNT = NO_CHAR_COUNT + 1
         ENDIF
C        Terminate if we fail to get a valid character 5 times
C        in succession.
         IF(NO_CHAR_COUNT.GT.5)THEN
               BAD_READ=.TRUE.
         ENDIF
         ENDDO ! DO WHILE (.NOT. BAD_READ)
         RETURN
         END
C        ------------------------------------------------------
C        *         OUTPUT STRING  *
C
         SUBROUTINE OUTPUT_STRING (STRING)
C        Subroutine to output a character string to the k3344
C        Input: STRING    A CHARACTER*1 ARRAY
         CHARACTER*(*)        STRING
         CHARACTER*1     CHR,CR,LF
         INTEGER              LOUT, I
         BYTE            BCR, BLF
         EQUIVALENCE     (CR, BCR)
         EQUIVALENCE     (LF, BLF)
         DATA            BCR /13/
         DATA            BLF /10/
C        Find the actual length of outstring, excluding trailing
C        blanks
         LOUT = LENGTH (STRING)
         IF (LOUT .EQ. 0) THEN
               RETURN
         ENDIF
C        Output this string  to  the  teletype interface, one
```

86

```
C         character at a time, terminated by a carriage return
          DO I = 1, LOUT
             CHR = STRING (I:I)
             CALL WRITE3344 (CHR)
          ENDDO
          CALL WRITE3344(CR)  ! Carriage return
          RETURN
          END
C         ----------------------------------------------------
C         *  ACCESS_K3344 *
C
          SUBROUTINE  ACCESS_K3344(A, F, IDATA, Q)
C         Send a camac command to the K3344 module
          IMPLICIT    NONE
          INTEGER     A, F, IEXT, B, C, N, DUMMY
          INTEGER*2   IDATA
          LOGICAL     Q, X
          COMMON      /K3344/B,C,N,DUMMY
          CALL CDREG (IEXT, B, C, N, A)
          CALL CFSA  (F, IEXT, IDATA, Q, X)
          END
C         -----------------------------------------------------------
C         *   READ3344   *
C
          SUBROUTINE READ3344 (ICHR, IEOB, CHR_PRESENT)
C         Subroutine  to  make  the  K3344  read  and return a single
C         character from the SLO-SYN  motor controller; return IEOB=1
C         if End-Of-Block        character is found.
C         OUTPUT:
C         ICHR        CHARACTER*1 character read
C         IEOB        LOGICAL     .TRUE. if End-Of-Block character found
C                                 .FALSE. otherwise
C         CHR_PRESENT LOGICAL     .TRUE. if character present to be read
C                                 .FALSE. if no character present
```

87

```fortran
      IMPLICIT NONE
      CHARACTER*1       ICHR
      LOGICAL           IEOB        ! end of block character found
      LOGICAL           CHR_PRESENT
      INTEGER    B,C,N,A
      COMMON     /K3344/B,C,N,A
      INTEGER*2  IDATA
C     F(0).A(I) reads from character buffer for channel I of K3344
      CALL ACCESS_X3344 (A,  0, IDATA, CHR_PRESENT)
C                       A   F   IDATA   Q
C     Form chacter from lower 8 bits of the data word by
C     taking bitwise AND of IDATA and 11111111(binary)='FF'
C     Hexadecimal
      IF(CHR_PRESENT)THEN
          ICHR = CHAR (IAND (IDATA, 'FF'X))
      ENDIF
C     Test bit 15 of the data word
C     BIT 15 = 1 indicates that we  just  readn an END-OF-BLOCK
C     character. See  Kinetics  3344 manual, Pg. 4, for details
      IF (BTEST (IDATA, 15)) THEN
          IEOB = .TRUE.
      ELSE
          IEOB=.FALSE.
      ENDIF
      RETURN
      END
C     ----------------------------------------------------------
C     *         WRITE3344       *
C
      SUBROUTINE WRITE3344 (CHR)
C     Subroutine to make the K3344 output a single character
C     to the SLO-SYN motor controller.
C     Use output mode of Ne7061, i.e. subaddress 2
      IMPLICIT   NONE
```

```
        CHARACTER   CHR
        EXTERNAL    ACCESS_K3344
        INTEGER*2   CHR_DATA
        LOGICAL        Q,X
        INTEGER     B,C,N,A
        COMMON      /K3344/B,C,N,A
        CHR_DATA = ICHAR (CHR)
C       F(16).A(I) writes the character buffer for channel I
        CALL ACCESS_K3344 (A, 16, CHR_DATA, Q)
C                        A    F    IDATA    Q
        END
C       ------------------------------------------------------------
C       *          READ_SLOSYN_POSITION   *
C

        SUBROUTINE READ_SLOSYN_POSITION(X,IERRCON)
C       Subroutine to perform an 'H17' and return the absolute
C       position of  the stepping motor relative to electrical
C       home, in inches
C       OUTPUT
C       ------
C       X        REAL*4     RL Probe position(Inches)
C       IERRCON  INTEGER*4  Error condition number
C                IERRCON=0  No Error
C                IERRCON=1  Cannot find '+' or '-' sign  in
C                           100 reads
C                IERRCON=2  Error in reading 11 chars after
C                           + or -
C                IERRCON=3  NO CHAR PRESENT during  reading
C                           11 Characters after + or -
        IMPLICIT     NONE
        INTEGER*4    I,IPULSES,IERRCON,ITERATION
        CHARACTER*1  IDIGIT(12),ICHR
        CHARACTER*11 ISTRING
        LOGICAL      IEOB,CHR_PRESENT,FINISHED
```

```
        REAL*4          WAIT, X
        DATA            WAIT/.015/ ! empirically,    at  least
C                                  0.015 sec wait is needed
C                                  to avoid
C                                  "no character present" error
        IERRCON=0
C       First read and diaplay output from SLO-SYN until output
C       buffer is empty
        CALL READ3344_UNTIL_EMPTY
C       Give H17 to SLO-SYN
        CALL OUTPUT_STRING('H17')
C       Read and display all characters in output buffer of K3344
C       until we encounter a '+' or '-' sign, which is the first
C       valid output character in response to a H17 command
        FINISHED=.FALSE.
        ITERATION=0
        DO WHILE(.NOT.FINISHED)
            ITERATION=ITERATION+1
            CALL LIB$WAIT(WAIT)
            CALL READ3344(ICHR,IEOB,CHR_PRESENT)
            IF(ICHR.EQ.'+'.OR.ICHR.EQ.'-')THEN
                FINISHED=.TRUE.
            ELSE IF(ITERATION.GT.100)THEN
                FINISHED=.TRUE.
                IERRCON=1
            ENDIF
        ENDDO  ! END OF DO WHILE (.NOT.FINISHED)
        IF(IERRCON.NE.0)RETURN
C       Read the absolute position of the RL Probe relative to
C       ELECTRICAL HOME
C       electrical home
C       We are expecting sign+10 digits+CRLF = 12 characters in all
        IDIGIT(1)=ICHR
        DO I=2,12
```

```fortran
            CALL LIB$WAIT(WAIT)
            CALL READ3344(ICHR,IEOB,CHR_PRESENT)
            IF(IEOB)THEN
                IERRCON=2  ! Read END-OF-BLOCK character
            ELSE IF(.NOT.CHR_PRESENT)THEN
                IERRCON=3  ! CHARACTER NOT PRESENT
            ELSE
                IDIGIT(I)=ICHR
            ENDIF
        ENDDO
C       Now convert the first 11 digits to an integer
        ISTRING=IDIGIT(1)//IDIGIT(2)//IDIGIT(3)//IDIGIT(4)//IDIGIT(5)//
       1 IDIGIT(6)//IDIGIT(7)//IDIGIT(8)//IDIGIT(9)//IDIGIT(10)//
       2 IDIGIT(11)
        READ(ISTRING,2)IPULSES
    2   FORMAT(I11)
C       IPULSES is the position in pulses, where 10,000
C       pulses = 1 Inch
        X=IPULSES/10000.
        RETURN
        END
C       ----------------------------------------------------------
C       *     READ_POSITION     *
C
        SUBROUTINE READ_POSITION(X,XPOS)
C       Subroutine that reads  the absolute position
C       of the RL probe
C       OUTPUT
C       ------
C       X       SLO-SYN stepping motor position (inches)
C       XPOS    OPTICAL ENCODER position (inches)
        REAL*4    X,XPOS,XNEWPOS
        INTEGER*4 IERRCON1,IERRCON2,COUNT1,COUNT2,COUNTER
        LOGICAL   POS1,POS2,FINISHED
```

```
C          Read absolute position of the RL probe
C          using the SLO-SYN
           CALL READ_SLOSYN_POSITION(X,IERRCON1)
           IF(IERRCON1.EQ.1)THEN
             PRINT*,'  Cannot find ''+'' or ''-'' sign in 100 reads'
           ELSEIF(IERRCON1.EQ.2)THEN
             PRINT*,'   Error in reading 11 characters'
             PRINT*,'   after ''+'' or ''-'' sign'
           ELSEIF(IERRCON1.EQ.3)THEN
             PRINT*,'   No character present during reading'
             PRINT*,'   11 characters after  ''+'' or ''-'' sign'
           ENDIF
C          Read the psition of the RL probe
C          using the optical shaft encoder
C          We read until two successive values 0.5 seconds apart
C          are the same, to clear any garbage in the output
C          register of the scaler for the optical encoder.
C          Garbage has been observed immediately after a clear
C          pulse has been         applied to the scaler.
           CALL READ_OPTICAL_ENCODER(XPOS,IERRCON2)
           IF(IERRCON2.EQ.1)THEN
             PRINT*,'   Error occurred in reading the'
             PRINT*,'   optical shaft encoder '
             PRINT*,'   i.e. no valid data is read'
             PRINT*,'   after 10 seconds/100 tries'
             RETURN
           ENDIF
           FINISHED=.FALSE.
           COUNTER=1
           DO WHILE(.NOT.FINISHED)
             CALL LIB$WAIT(0.5)
             CALL READ_OPTICAL_ENCODER(XNEWPOS,IERRCON2)
             COUNTER=COUNTER+1
             IF(XNEWPOS.EQ.XPOS)THEN
```

```
                 FINISHED=.TRUE.
          ELSE
               XPOS=XNEWPOS
               IF(COUNTER.GT.10)THEN
                 PRINT*,'**ERROR**'
                 PRINT*,'10 SUCCESSIVE READS OF OPTICAL ENCODER'
                 PRINT*,'SEPARATED BY 0.5 SECONDS'
                 PRINT*,'CANNOT PRODUCE 2 SUCCESSIVE VALUES'
                 PRINT*,'WHICH AGREE WITH EACH OTHER'
                 PRINT*,'SCALER FOR OPTICAL ENCODER FAULTY'
                 PRINT*,'OR SHAFT STILL IN MOTION'
                 FINISHED=.TRUE.
               ENDIF
          ENDIF
        ENDDO
        X=ABS(X)   ! RETURN A POSITIVE VALUE ONLY
        RETURN
        END


C       ------------------------------------------------------
C       *  READ_OPTICAL_ENCODER *
C
        SUBROUTINE READ_OPTICAL_ENCODER(XPOS,IERRCON)
C       SUBROUTINE TO READ OPTICAL ENCODER
C       Output:
C       XPOS       REAL*4     Optical Encoder position in Inches
C       IERRCON    INTEGER*4  Error condition
C                  IERRCON=0  If no Error
C                             after 10 seconds/100 tries
        IMPLICIT  NONE
        INTEGER*4 I,IDATA,IPULSES,IERRCON,B,C,N,IEXT,A,F,ITERATIONS
        REAL*4    XPOS
        LOGICAL   Q,X,FINISHED
        COMMON    /OPTIC/B,C,N   ! CAMAC address B,C,N of SCALER
```

```
C                                        ! for Optical Encoder
C          Read is A(0) F(0)
           A=0
           F=0
           CALL CDREG(IEXT,B,C,N,A)
           FINISHED=.FALSE.
           ITERATIONS=0
           DO WHILE(.NOT.FINISHED)
              CALL CFSA(F,IEXT,IDATA,Q,X)
C          If bit 24 is 1, then the output is invalid because
C          the nmodule is still in the process of of digitizing
                IF(.NOT.BTEST(IDATA,24))THEN ! VALID DATA
                    IERRCON=0
                    FINISHED=.TRUE.
                ELSE  ! Invalid data
                    ITERATIONS=ITERATIONS+1
                    IERRCON=1
                    IF(ITERATIONS.GT.1000)FINISHED=.TRUE.
                    IF(.NOT.FINISHED)CALL LIB$WAIT(.1)  ! Wait 0.1 Sec
                ENDIF
           ENDDO
C          The Optical Encoder disk for the RL Probe outputs
C          2000 pulses per revolution, and the screw thread
C          pitch is 5 threads per inch, so the Encoder outputs
C          10,000 pulses per inch of linear travel.
C          The output of the CAMAC SCALER is BCD, which has
C          to be converted.
           IF(IERRCON.EQ.0)THEN     ! VALID DATA
               CALL BCD_TO_DECIMAL(IDATA,IPULSES)
               XPOS=IPULSES/10000.  ! POSITION IN INCHES
           ENDIF
           RETURN
           END
C          ------------------------------------------------------------
```

94

```fortran
C        *    BCD_TO_DECIMAL    *
C
         SUBROUTINE BCD_TO_DECIMAL(IBCD,IDECIMAL)
C        Subroutine to convert 24-bit BCD to decimal
C        Input:
C        IBCD             INTEGER*4 BCD with 24 bits
C        Output:
C        IDECIMAL         INTEGER*4 Decimal representation
         IMPLICIT  NONE
         INTEGER*4  I,IBCD,IDECIMAL,J,I4BITS
         IDECIMAL = 0
         J=IABS(IBCD)
         DO I=1,6
            I4BITS=IAND(J,'F'X)  ! EXTRACT LOWER 4 BITS OF J
            IDECIMAL=10**(I-1)*I4BITS + IDECIMAL
            J=J/16  ! SHIFT 4 BITS RIGHT
         ENDDO
         IF(IBCD.LT.0)IDECIMAL=-IDECIMAL
         RETURN
         END
C        ----------------------------------------------------------
C        *  READ_MAGNETIC_FIELD  *
C
         SUBROUTINE READ_MAGNETIC_FIELD(BFIELD,IERRCON)
C        SUBROUTINE TO READ OPTICAL ENCODER
C        Output:
C        BFIELD          REAL*4    Magnetic field in Kilogauss
C        IERRCON         INTEGER*4 Error condition
C                        IERRCON=0 If no error
C                        IERRCON=1 If no valid data is read
C                                  after 10 seconds/100 tries
         IMPLICIT  NONE
         INTEGER*4  I,IDATA,IVALUE,IERRCON,B,C,N,IEXT,A,F
         INTEGER*4  ITERATIONS
```

95

```fortran
      REAL*4      BFIELD,ARG,DELAY
      LOGICAL     Q,X,FINISHED
C     Remove the next two lines after the bit 24 test is
C     implemented
      REAL*4      BB(5),OLDBFIELD,DIFF
      INTEGER*4 ISUCCESS,IREADS
      COMMON      /MAG/B,C,N ! CAMAC address B,C,N of SCALER for
C                            ! magnetic field measured by RL Probe
C     Read is A(0) F(0)
      A=0
      F=0
      CALL CDREG(IEXT,B,C,N,A)
C     Remove the next 4 lines after the bit 24 test is implemented
      OLDBFIELD=-1000000.
      ISUCCESS=0
      IREADS=0
      DO WHILE(ISUCCESS.LT.2)
      FINISHED=.FALSE.
      ITERATIONS=0
      DO WHILE(.NOT.FINISHED)
            CALL CFSA(F,IEXT,IDATA,Q,X)
            IREADS=IREADS+1
C     If BIT 24 is 1, then the output is invalid because
C     the module is still in the process of digitizing
C     ***WARNING**
C     As of July 7, 1993, this feature has not been implemented
C     in the hardware of this scalar unit, but is on Randy's
C     list to check for read errors due to reading  during
C     the digitizing process, we demand 3 successive reads with
C     the same value
         IF(.NOT.BTEST(IDATA,24))THEN ! VALID DATA
               IERRCON=0
               FINISHED=.TRUE.
         ELSE   ! Invalid data
```

```
                         ITERATIONS=ITERATIONS+1
                         IERRCON=1
                         IF(ITERATIONS.GT.100)FINISHED=.TRUE.
                         IF(.NOT.FINISHED)CALL LIB$WAIT(.1)   ! Wait 0.1 Sec
                 ENDIF
             ENDDO
             IF(IERRCON.EQ.0)THEN              ! valid data
                         CALL BCD_TO_DECIMAL(IDATA,IVALUE)
                         BFIELD=IVALUE/1000.   ! Magnetic field in Kilogauss
             ELSE
                         BFIELD=0.0
             ENDIF
C        Remove all lines between here and the return statement
C        after the bit 24 test is implemented
C        TYPE *,' READ BFIELD=',BFIELD
             DIFF=ABS(BFIELD-OLDBFIELD)
             IF(DIFF.LE.0.010)THEN ! AGREEMENT OF 2 SUCCESSIVE
C                                            VALUES TO WITHIN 10 GAUSS
                         ISUCCESS=ISUCCESS+1
                         BB(ISUCCESS)=OLDBFIELD
                         BB(ISUCCESS+1)=BFIELD
             ELSE
                         ISUCCESS=0   ! set success counter to zero
C                                     ! after a failure
             ENDIF
             OLDBFIELD=BFIELD
             ARG=MOD(FLOAT(IREADS)*24.,360.)
             DELAY=0.2+0.1*ABS(SIND(ARG))
             CALL LIB$WAIT(DELAY)   ! Wait 0.3 seconds between
C                                     ! successive reads
             ENDDO
             BFIELD=(BB(1)+BB(2)+BB(3))/3.   ! Take BFIELD to be
C                                            ! average of the 3 values
C        Type *,'3 successive values in agreement after
```

```
C         ',IREADS,' READS'
C         Type 888,BB(1),BB(2),BB(3),BFIELD
 C888          FORMAT(' 3 VALUES OF ',3F8.4,' KG'/
C         1 ' AVERAGE IS ',F8.4,' KG')
          RETURN
          END
C         ----------------------------------------------------
          SUBROUTINE RINGER(N)
C         SUBROUTINE TO RING THE BELL I TIMES
          IMPLICIT NONE
          INTEGER I,N
          DO I=1,N
                  CALL BELL(1)
                  CALL LIB$WAIT(.20)
          ENDDO
          RETURN
          END
C         ---------------------------------------------------------
          SUBROUTINE WRITE_CHR_STRING(CFUNC,IVALUE,CSTRING)
C         Subroutine to create a character string with the correct
C         format for outputting to the SLO-SYN controller
C         For example, ERITE_CHR_STRING('L13',200,CSTRING) would
C         give CSTRING the value 'L13 200' and
C         WRITE_CHR_STRING('L13',9,CSTRING) would give CSTRING the
C         value 'L13 9' which is what the SLO-SYN controller wants.
C         Note that 'L13      9' which is the result of a fixed-format
C         write, does not work properly.
          IMPLICIT NONE
          CHARACTER*1 CDIGITS(6)
          CHARACTER CSTRING*14,CFUNC*3,CABSVALUE*9
          INTEGER IVALUE,IABSVALUE,I,IDIGITS
          IABSVALUE=ABS(IVALUE)
          IF(IABSVALUE.LE.9)THEN
                  WRITE(CABSVALUE,10)IABSVALUE
```

98

```
10              FORMAT(I1,'           ')
        ELSE IF(IABSVALUE.LE.99)THEN
                WRITE(CABSVALUE,20)IABSVALUE
20              FORMAT(I2,'          ' )
        ELSE IF(IABSVALUE.LE.999)THEN
                WRITE(CABSVALUE,30)IABSVALUE
30              FORMAT(I3,'         ' )
        ELSE IF(IABSVALUE.LE.9999)THEN
                WRITE(CABSVALUE,40)IABSVALUE
40              FORMAT(I4,'        ' )
        ELSE IF(IABSVALUE.LE.99999)THEN
                WRITE(CABSVALUE,50)IABSVALUE
50              FORMAT(I5,'       ' )
        ELSE IF(IABSVALUE.LE.999999)THEN
                WRITE(CABSVALUE,60)IABSVALUE
60              FORMAT(I6,'      ' )
        ELSE IF(IABSVALUE.LE.9999999)THEN
                WRITE(CABSVALUE,70)IABSVALUE
70              FORMAT(I7,'     ' )
        ELSE IF(IABSVALUE.LE.99999999)THEN
                WRITE(CABSVALUE,80)IABSVALUE
80              FORMAT(I8,' '        )
        ELSE
                WRITE(CABSVALUE,90)IABSVALUE
90              FORMAT(I9)
        ENDIF
        IF(IVALUE.GE.0)THEN
                CSTRING=CFUNC//' '//CABSVALUE
        ELSE
                CSTRING=CFUNC//' -'//CABSVALUE
        ENDIF
        RETURN
        END
```

REFERENCES

[A1] Munasinghe Punyasena, Pat Walden, Stanley Yen, TRIUMF Design Note, TRI-DN-93-3, Hall probe calibration for beamline 4B and MRS spectrometer.

[A2] MRS mannual, TRIUMF, 1988 (unpublished).

[A3] Private communications, Stanley Yen, TRIUMF.

[B1] P. L. Walden, The Annual Report of Scientific Activities, TRIUMF, 1990.

[B2] Instruction manual for model K3344 four-channel communication interface.

END

16-05-94

FIN